Finite element procedure for plastic flow of orthotropic composites with Hoffman yield criterion.

Krasnovskiy, Evgeny E

Department of Civil Engineering
University of Wales, Swansea

Finite element procedure for plastic flow of orthotropic composites with Hoffman yield criterion

Evgeny E. Krasnovskiy
Math.-Eng.-Res. (BMSTU)

Thesis submitted to the University of Wales in fulfilment of the requirements for the Degree of Master of Philosophy

March 2004

Summary

This thesis presents a finite element methodology for the numerical simulation for plastic flow of orthotropic composites governed by the Hoffman yield criterion.

All numerical procedures were developed for plane strain and axisymmetric states with infinitesimal strains. Thermal effects were ignored and the loading was assumed quasi-static. It was further assumed that no fracture or debonding occurred. The hardening behaviour was isotropic.

The strategy used for the numerical simulation was based on implicit displacement finite element procedures. An operator split methodology and fully implicit backward Euler elastic predictor / plastic corrector algorithm were used to find a stress state at the Gauss point. During the plastic corrector part the Newton-Raphson method was used. A line search algorithm based on dichotomy concept was developed to find an improved initial guess for the Newton-Raphson method in order to obtain a physically reasonable solution for materials with high degree of elastic anisotropy. The tangent modulus consistent to the state update algorithm was obtained to ensure a quadratic rate of convergence.

Attention was focused on elastically anisotropic composites.

The robustness and correctness of the proposed algorithms is illustrated by means of numerical examples and comparison with results obtained by other authors.

DECLARATION

This work has not previously been accepted in substance for any degree and is not being concurrently submitted in candidature for any degree

Signed .... (candidate)

Date..... March 19, 2004 .....

STATEMENT 1

This thesis is the result of my own investigation, except where otherwise stated. Other sources are acknowledged by footnotes giving explicit references. A bibliography is appended.

Signed ... . (candidate)

Date..... March 19, 2004 .....

STATEMENT 2

I hereby give consent for my thesis, if accepted, to be available for photocopying and for inter-library loan, and for the title and summary to be made available to outside organisations.

Signed .... (candidate)

Date..... March 19, 2004 .....

Contents

Acknowledgements

I would like to thank Professor D.R.J. Owen for his supervision, support and guidance as well as very careful and patient revision of this thesis. Many thanks are also due to Doctor E.A. de Souza Neto for numerous valuable discussions and many pieces of good advice on a variety of issues related to this work.

Thanks are also given to Professor D. Perić and Doctor R.D. Wood for their lectures I attended while working at this research.

I am grateful to the School of Engineering of the University of Wales Swansea for the excellent computer facilities and the hospitality shown.

I am obliged to Professor V.S. Zarubin for his efforts, patience and supervision at the Bauman Moscow State Technical University as well as his full support in my decision to pursue MPhil studies in Swansea.

I would like to acknowledge the grant of the President of the Russian Federation Vladimir V. Putin as the financial support allowed me to complete this thesis.

I am indebted to my parents who have always provided me with their support and encouragement.

Finally, I wish to thank my friends for their friendship, which has made my stay in Swansea enjoyable.

Chapter 1. Introduction

To gain an advantage over the competitors, modern engineers have not only to create sophisticated structural designs, but also use new materials with superior properties. In this context composites have become materials of paramount importance as they offer advantages such as low weight, improved strength, corrosion resistance, high fatigue strength, faster assembly, low thermal expansion coefficient, etc. They are used in different industries such as aerospace, underwater, automobile, chemical, electrical, leisure, to name but a few.

In many cases composites are more efficient than traditional materials such as metals. For example, in the highly competitive airline market there is a constant search for reductions in the overall mass of an aircraft without reducing the stiffness and strength of its components. Reducing 1 lb (0.453 kg) of mass of a commercial aircraft can save up to 360 gal (1360 l) of fuel per year. Hence, a company will become more profitable as fuel expenses are 25% of the operational expenses of a commercial airline (Kaw, 1997).

Composite materials are those that consist of two or more constituent materials that together produce required properties for a particular application. These materials are combined at a macroscopic level and do not penetrate into each over. One constituent is called the reinforcing phase (it can be in the form of fibres, particles or flakes) and the other is called the matrix (which is usually continuous). Fibre-reinforced composites are the most commonly used forms nowadays and they are composed of high strength and high modulus fibres in a matrix material. In these composites fibres are the principal load carrying components, and the matrix material simply keeps the fibres together, acts as a load transfer medium between them and protects them from the environment. Geometrically, fibres have near crystal-sized diameter and a very high length-to-diameter ratio (Kaw, 1997; Reddy and Miravete, 1995).

Composites have a long history. Significant examples include the use of reinforced mud walls in houses with bamboo shoots, glued laminated woods by the Egyptians (1500 BC), and laminated metals in forging swords (1800 AD). In the twentieth century fibreglass (where glass fibres are embedded in a resin) were first used in 1930. Later, in 1960-1970, new fibres such as carbon, boron and aramide and

new matrixes of metal and ceramics appeared (Kaw, 1997; Matthews and Rawlings, 1994).

Obviously, as more complicated materials appear, more sophisticated mathematical models and numerical methods are required to perform a stress analysis of structures made of these materials. It should be mentioned that the majority of problems of practical interest are nonlinear. For instance, taking into account the plastic response of a structure allows an increase in its performance and reduction in weight.

Consequently, two major problems arise:

1. creating a mathematical model capable of describing all essential material properties (for example, different elastic moduli and plastic anisotropy i.e. different yield stresses and / or hardening in different directions);
2. development of methods capable of solving engineering problems of practical interest for these material models.

This thesis is dedicated to the study of plastic behaviour of elastically and plastically orthotropic composite materials with a Hoffman yield criterion (Hoffman, 1967). This criterion is suitable if a composite has significantly different tensile and compressive yield stresses. Actually, many fibrous composites have such differences (Koh *et al.* 1995). In such cases the popular Hill yield criterion (Hill, 1947) is inadequate and a more general Hoffman yield criterion should be used. Needless to say, a flow theory will be used in this work as it allows calculations to be performed for a complicated deformation history.

Originally the Hoffman yield criterion was designed as a fracture condition for brittle anisotropic materials (Hoffman, 1967). The criterion itself is a modification of the criterion proposed by Hill (Hill, 1947) through inclusion of terms which are linear in the stress. This can overcome the restriction of the Hill criterion, according to which the tensile and the compression yield strength should be equal.

On the other hand, obtaining an analytical solution of mechanics problems requires integration of systems of partial differential equations over a domain, on the boundary of which unknown functions must satisfy given boundary conditions. As it is very difficult to find such a solution analytically especially in the case of nonlinear problems, numerical methods are widely used. Nowadays, the finite element method, which combines the variational formulation of a problem and special basis functions,

is one of the most universal and popular methods. Modern commercial finite element software allows the analysis of a complete structure or structural system. They also permit the incorporation of design simulation and virtual prototyping into a product development process in order to minimize costs and improve time-to-market. Such systems as ABAQUS, ANSYS, Elfen, NE/Nastran, etc. are widely used by engineers nowadays.

In this thesis the HYPLAS finite element code is dealt with. This program is supplied with a text book "Computational plasticity: small and large strain finite element analysis of elastic and inelastic solids" by de Souza Neto *et al.* (2003). HYPLAS is a finite element software for implicit small and large strain analysis of hyperelastic and elasto-plastic solids in plane stress, plane strain and axisymmetric states. Its main purpose is to illustrate the computational implementation of numerical procedures for material models described in the mentioned text book. HYPLAS source code is written in FORTRAN.

1.1. Scope of the thesis

The purpose of this work is to implement computational algorithms within the HYPLAS program for the numerical simulation of plastic flow for orthotropic composite material with the Hoffman yield criterion.

These numerical procedures will be developed for plane strain and axisymmetric states for infinitesimal strains. This loading is quasi-static (i.e. inertia effects are ignored) and thermal effects are also ignored. It was assumed that no fracture or debonding occurs. The hardening behaviour is assumed to be isotropic.

Both elastic and plastic anisotropy are taken into account. Appropriate numerical examples, together with an accuracy analysis via iso-error maps for the state update algorithm at the Gauss point level, are provided.

To the best of our knowledge, studying the influence of elastic anisotropy for the Hoffman material is a new issue. For instance, in surveyed articles by Hashagen and de Borst (2001), Schellekens and de Borst (1990), and Xikui Li *et al.* (1994) all numerical examples for the Hoffman material were provided for elastically isotropic cases only. An accuracy analysis using iso-error maps provided by the article by Schellekens and de Borst (1990) was also limited to the elastically isotropic case. On the whole, it must be said that an extremely limited number of references dealing with composite materials with the Hoffman yield criterion was found.

1.1.1. Numerical methods adopted

The full Newton-Raphson algorithm is used in HYPLAS to solve the nonlinear system of finite element equations for displacements during the global system iteration. This method was chosen due to its quadratic rate of convergence.

As for the Gauss point level, an operator split methodology and fully implicit backward Euler elastic predictor / plastic corrector algorithm were used to find a stress state satisfying the yield criterion. During the plastic corrector part of this algorithm the full Newton-Raphson method was used to solve the appropriate nonlinear equations. A line search algorithm based on dichotomy concept was developed to find an improved initial guess for the Newton-Raphson method in order to obtain a physically reasonable solution.

To ensure the quadratic rate of convergence of the global system iteration a tangent modulus consistent to the state update algorithm was also derived.

1.2. Thesis layout

This thesis is divided into six chapters.

After the introductory Chapter, Chapter 2 reviews the general strategy of the finite element method and its application to solving nonlinear problems of solid mechanics. The HYPLAS structure and subroutines are also described.

Chapter 3 is dedicated to a description of the Hoffman yield criterion for orthotropic composite materials. A corresponding elasto-plastic constitutive material model is also discussed.

Chapter 4 is dedicated to an explanation of the two main subroutines necessary for computational implementation of the Hoffman material model: state update for the Gauss point level and consistent tangent computation. All algorithms, appropriate numerical methods as well as accuracy verifying techniques are described in detail. Influence of the degree of elastic anisotropy at the accuracy of the state update procedure is discussed.

In Chapter 5 test examples are provided.

Chapter 6 contains a short summary and the conclusions of this work along with the suggestions for future research.

1.3. Notations and conventions

In this work the following conventions were adopted:

- Tensors are written in greek or capital latin letters with italic bold font, i.e. $\boldsymbol{\varepsilon}$ or $\boldsymbol{W}$;
- Vectors are written in small latin letters with italic bold font, i.e. $\boldsymbol{u}$;
- Matrices and finite element arrays are written in greek or latin letters with upright bold font, i.e. $\boldsymbol{\varepsilon}$ or $\mathbf{S}$;
- Components of tensors or vectors are written with italic font, i.e. ε_{ij} or u_i.

The main notations are as follows:

$\boldsymbol{u}$ is the displacement vector and u_i $(i=1,2,3)$ are its components;

$\boldsymbol{\varepsilon}$ is the Cauchy full strain tensor and ε_{ij} $(i,j=1,2,3)$ are its components;

$\boldsymbol{\varepsilon}^e$ is the Cauchy elastic strain tensor and ε_{ij}^e $(i,j=1,2,3)$ are its components;

$\boldsymbol{\varepsilon}^p$ is the Cauchy plastic strain tensor and ε_{ij}^p $(i,j=1,2,3)$ are its components;

$\dot{\boldsymbol{\varepsilon}}^p$ is the plastic strain rate tensor;

$\bar{\boldsymbol{\varepsilon}}^p$ is the accumulated plastic strain;

$\boldsymbol{\sigma}$ is the Cauchy stress tensor and σ_{ij} $(i,j=1,2,3)$ are its components;

$\boldsymbol{\alpha}$ is the set of internal variables;

$\dot{\lambda}$ is the plastic multiplier;

E is the Young's modulus for an anisotropic material;

ν is the Poisson ratio for an anisotropic material;

E_1, E_2, E_3 are Young's moduli in corresponding directions for an orthotropic material;

G_{12}, G_{23}, G_{31} are shear moduli in corresponding directions for an orthotropic material;

$\nu_{12}, \nu_{23}, \nu_{31}, \nu_{21}, \nu_{32}, \nu_{13}$ are Poisson ratios in corresponding directions for an orthotropic material;

$\boldsymbol{C}$ is the elasticity tensor;

$F(\boldsymbol{\sigma}, k)$ is the yield function;

k is the hardening variable;

$c_1,\ldots c_9$ are nine independent material parameters of the Hoffman material model;

σ_Y is the reference yield stress;

σ_{iiT_0}, σ_{iiC_0} are the yield stresses in the direction i in tensile and compressive tests respectively and subscript "0" means that the corresponding yield stresses are initial;

σ_{ijS_0} is the yield in shear tests in the direction ij and subscript "0" means that the corresponding yield stresses is initial;

$\boldsymbol{n}$ and $\boldsymbol{t}$ are respectively the unit (in Euclidian norm) normal and tangent vectors to the yield surface;

n_{dim} is the number of spatial dimensions;

n_{node} is the number of nodes of the finite element;

N_i^e is an element shape function associated with a node i;

n_{elem} is the total number of elements;

n_{poin} is the total number of nodal points in the mesh;

N_i^g is the global shape function associated with a node i;

η is the virtual displacement vector and η_i $(i=1,2,3)$ are its components;

$\mathbf{u_f}$ is the global array of nodal displacements;

$\boldsymbol{\eta}_\mathbf{f}$ is the global array of nodal virtual displacements.

$\boldsymbol{b}$ is a vector of the body loads;

$\boldsymbol{w}$ is a vector of the surface loads;

$\bar{\boldsymbol{u}}$ is a vector of the boundary conditions on the displacements;

$\mathbf{K_T}$ is the global tangent stiffness matrix;

$\hat{\mathbf{D}}$ is a consistent tangent matrix;

$\mathbf{B^g}$ is the matrix of the global strain displacement operator;

$\mathbf{B^e}$ is the matrix of the element strain displacement operator;

$\mathbf{N^e}$ is the element interpolation matrix;

$\mathbf{N}^g$ is the global interpolation matrix;

$\mathbf{f}^{\text{int}}$ is the internal force vector;

$\mathbf{f}^{ext}$ is the external force vectors;

W and V are the tensors used in the yield function;

$\mathbf{P}$ is a matrix used in the yield function;

$\mathbf{q}$ is a vector used in the yield function;

$\boldsymbol{\sigma}$ is a finite element array of stresses;

$\boldsymbol{\varepsilon}^{e}$ is a finite element array of elastic strains;

$\Delta\boldsymbol{\varepsilon}^{p}$ is a finite element array of increments of plastic strains;

$\varepsilon^{e\ trial}$ is the elastic trial strain;

σ^{trial} is the elastic trial stress;

$\boldsymbol{\varepsilon}^{e\ trial}$ is a finite element array of elastic trial strains;

$\mathbf{e}_{n+1}^{trial}$ is a finite element array of elastic trial strains where the shear component is multiplied by 2 (engineering shear strain)

$\boldsymbol{\sigma}^{trial}$ is a finite element array of trial stresses;

$\mathbf{D}$ is the finite element array corresponding to the elasticity tensor

$\mathbf{S}$ is the finite element array used in the derivative of the yield function;

I is identity fourth order tensor;

$\mathbf{I}$ is the identity matrix of the 4th order (a finite element array corresponding to the identity fourth order tensor);

D^{ep} is the tensor of the consistent tangent modulus;

$\mathbf{D}^{ep}$ is the finite element array corresponding to the tensor of the consistent tangent modulus;

$$\mathbf{Z}=\begin{pmatrix}1&0&0&0\\0&1&0&0\\0&0&2&0\\0&0&0&1\end{pmatrix};$$

: denotes the double contraction operator, i.e. $\boldsymbol{A}:\boldsymbol{B}=A_{ij}B_{ij}$; $\boldsymbol{C}:\boldsymbol{B}=C_{ijkl}B_{kl}$.

Chapter 2. The finite element method and an overview of the HYPLAS program

In this Chapter the general strategy of the finite element method and its application to solving nonlinear problems of solid mechanics is discussed briefly. Hence the goal of the given work is implementation of the Hoffman material model into the HYPLAS program (de Souza Neto *et al.* 2003), the HYPLAS structure and subroutines is also described.

2.1. General concepts of the finite element method

The finite element method is the most powerful general technique for the numerical solution of applied engineering problems. Although the method was initially developed for analysis in structural mechanics, a large amount of research devoted to it made it possible to solve many other classes of problems. For example, the method can be applied to stress analysis of solids, solving acoustical, neutron physics and field problems such as heat transfer, and analysis of fluid flows (Hinton and Owen 1977; Bathe 1996; Zienkiewicz and Taylor 2000a).

The main idea of the method is discretisation, i.e. approximating a continuous mechanical problem with infinite number of degrees of freedom by a discrete problem having a finite number of degrees of freedom. Such substitution can be performed by dividing (meshing) a model by a finite number of components. The second step is choosing the type and number of degrees of freedom and making an assumption how an approximate solution depends on them. The final step is finding the values of the degrees of freedom by solving a system of linear algebraic equations.

The benefit of the finite element method is that a discrete problem can be solved on a computer easily even if the number of elements is very large. On the other hand, the exact solution of a continuous problem can be obtained only via mathematical manipulations, which can be extremely difficult or even impossible to perform.

At the beginning, in the 1940s, in articles by McHenry (1943), Hrenikoff (1941), Nemark (1949) it was shown that reasonably good solutions to an elastic problem can be obtained by replacing the small portions of the continuum by an arrangement of simple elastic bars. Later, in 1950s, original articles by Argyris

and Kelsey (1955) as well as by Turner *et al.* (1956) appeared. The name 'finite element' first appeared in an article by Clough (1960). There was a very important early article by Zienkiewicz and Cheung (1964) showing an application of the method. Since 1960, a very large number of publications have appeared - a historical development of the subject was presented by Zienkiewicz and Taylor (2000a). There are also the compilation of references made by Noor (1991) and the Finite Element Handbook edited by Kardestuncer and Norrie (1987).

Finite element techniques used to obtain a solution of a quasi-static plasticity problem with infinitesimal strains are presented below following the definitions and description given in the text book by de Souza Neto *et al.* (2003).

2.1.1. Problem statement

Let the body X occupy the region Ω with a boundary $\partial\Omega$ in space. There are volumetric and surface loads affecting the body as well as some constraints on the displacements. The loading is assumed to be quasi-static (i.e. inertia effects are ignored), thermal effects are ignored and strains are infinitesimal. The material model is path-dependant, i.e. the stress tensor is not a function of the current value of strain tensor only, it depends on the whole history of deformations.

So, the initial boundary value problem can be stated as follows:

Given the initial values $\boldsymbol{\alpha}(t_0)$ of the internal variables $\boldsymbol{\alpha}$ and the history of volumetric loads $\boldsymbol{b}(t)$ and surface loads $\boldsymbol{w}(t)$ (pseudo-time increment $t \in [t_0, \bar{t}]$) for each point of the body X, find the functions $\boldsymbol{\sigma}(t)$, $\boldsymbol{\alpha}(t)$, $\boldsymbol{u}(t)$ and $\boldsymbol{\varepsilon}(t)$ which satisfy the following equations at each point of the body X:

$$\frac{\partial \sigma_{ij}(t)}{\partial x_j} + b_i(t) = 0, \tag{2.1}$$

$$2\varepsilon_{ij}(t) = \frac{\partial u_i(t)}{\partial x_j} + \frac{\partial u_j(t)}{\partial x_i}, \tag{2.2}$$

$$\dot{\boldsymbol{\alpha}}(t) = f(\boldsymbol{\varepsilon}(t), \boldsymbol{\alpha}(t)) \tag{2.3}$$

relations between $\boldsymbol{\sigma}(t)$, $\boldsymbol{\alpha}(t)$ and $\boldsymbol{\varepsilon}(t)$ defined by a material model (2.4)

and boundary conditions

$$\sigma_{ij} n_j = w_i(t) \text{ on } S_t \subset \partial\Omega, \tag{2.5}$$

$$u_i = \bar{u}_i \text{ on } S_u = \partial\Omega \setminus S_t, \tag{2.6}$$

where

σ is the Cauchy stress tensor and σ_{ij} $(i,j=1,2,3)$ are its components;

ε is the Cauchy full strain tensor and ε_{ij} $(i,j=1,2,3)$ are its components;

u_i $(i=1,2,3)$ are the components of the displacement vector;

f is a function defined by a material model;

n_i $(i=1,2,3)$ are components of the normal vector $\boldsymbol{n}$ to the surface S_1;

$\bar{u}_i$ $(i=1,2,3)$ are boundary conditions on the displacements.

Expression (2.1) is an equilibrium equation, expression (2.2) is a definition of the Cauchy strain tensor, expression (2.3) shows the rate of the internal variables, and expressions (2.4) are defined by a constitutive material model (see Chapter 3 for an example).

The numerical solution of problem (2.1)-(2.6) by the finite element method will be shown below in Section 2.1.3. However, in order to find this solution the principle of virtual work has to be obtained (Section 2.1.2).

2.1.2. The principle of virtual work

Expression (2.1) is an equation of equilibrium in a certain point of the continuum. In this section the corresponding weak (global or integral) form of this expression will be derived.

The space Ψ of virtual displacements η on body X consists of sufficiently regular arbitrary displacements which satisfy the following condition:

$$\eta_i \equiv 0 \text{ on } S_u.$$

The principle of virtual work states that "the body X is in equilibrium if and only if its stress field $\sigma(t)$ satisfies the following equation:

$$\int_\Omega \sigma_{ij}(t)\varepsilon_{ij}^{\eta} dV - \int_\Omega b_i(t)\eta_i dV - \int_{S_t} w_i(t)\eta_i dS = 0, \quad \forall \eta \in \Psi, \tag{2.7}$$

where

$$2\varepsilon_{ij}^{\eta} = \frac{\partial \eta_i}{\partial x_j} + \frac{\partial \eta_j}{\partial x_i}.$$

When the stress field is sufficiently smooth, virtual work expression (2.7) is equivalent to equilibrium expression (2.1). In order to prove this the following calculations must be performed.

First of all, as the stress tensor is symmetric the following expression is valid (pseudo-time dependence is omitted):

$$\int_{\Omega}\sigma_{ij}\varepsilon_{ij}dV=\frac{1}{2}\int_{\Omega}\sigma_{ij}\left(\frac{\partial u_i}{\partial x_j}+\frac{\partial u_j}{\partial x_i}\right)dV= \\ =\frac{1}{2}\int_{\Omega}\sigma_{ij}\left(\frac{\partial u_i}{\partial x_j}+\frac{\partial u_i}{\partial x_j}\right)dV+\frac{1}{2}\int_{\Omega}\sigma_{ij}\left(\frac{\partial u_j}{\partial x_i}-\frac{\partial u_i}{\partial x_j}\right)dV=\int_{\Omega}\sigma_{ij}\frac{\partial u_i}{\partial x_j}dV. \tag{2.8}$$

Expression (2.7) can be rearranged using expression (2.8) and the divergence theorem:

$$\int_{\Omega}\sigma_{ij}\varepsilon_{ij}^{\eta}dV-\int_{\Omega}b_i\eta_i dV-\int_{S_t}w_i\eta_i dS=\int_{\Omega}\sigma_{ij}\frac{\partial\eta_i}{\partial x_j}dV-\int_{\Omega}b_i\eta_i dV-\int_{S_t}w_i\eta_i dS= \\ =\int_{\Omega}\frac{\partial\left(\sigma_{ij}\eta_i\right)}{\partial x_j}dV-\int_{\Omega}\eta_i\frac{\partial\sigma_{ij}}{\partial x_j}dV-\int_{\Omega}b_i\eta_i dV-\int_{S_t}w_i\eta_i dS= \\ =-\int_{\Omega}\eta_i\left(\frac{\partial\sigma_{ij}}{\partial x_j}+b_i\right)dV+\int_{S_t}\eta_i\left(\sigma_{ij}n_j-w_i\right)dS=0. \tag{2.9}$$

Finally, since expression (2.9) is valid for any virtual displacement η then it follows that each bracketed term in the last line of expression (2.9) is equal to zero at every point within their respective domains.

Since the principle of virtual work has been proved, the finite element procedure can be described now.

2.1.3. The finite element method

The material presented in this Section covers the basic procedures that are necessary for computational implementation of the displacement finite element method. From here on in this Section the material will be presented according to the text book by de Souza Neto *et al.* (2003).

Two major numerical approximations are necessary for obtaining a finite element solution of the problem stated in Section 2.1.1:

1. Pseudo-time discretisation. A numerical integration scheme will be used to solve the problem which requires history of deformations to

calculate stresses. So, the original problem is transformed into an incremental (time-discrete) one.

2. A finite element discretisation i.e. a finite element approximation of the virtual work statement where the domain of the body and associated functional are replaced with finite-dimensional counterparts generated by finite element interpolation functions.

After applying these two approximations, the original problem is transformed into a set of incremental (generally nonlinear) algebraic finite element equations to be solved at the end of each time interval. In this section the solution of the associated nonlinear algebraic system using the quadratically convergent Newton-Raphson algorithm will be given.

Finite element interpolation

Let $a(x)$ be a generic field defined over the domain Ω^e of a finite element. In this case the finite element interpolation $\mathbf{a}^{\mathbf{h}}(x)$ of this field within a finite element is defined as follows:

$$\mathbf{a}^{\mathbf{h}}(x) = \sum_{i=1}^{n_{node}} a^i N_i^e(x),$$

where

n_{node} is the number of nodes of the finite element;

$N_i^e(x)$ is an element shape function associated with a node i whose coordinate is x^i ($N_i^e(x^i) \equiv 1$; $N_i^e(x^j) \equiv 0 \quad i \neq j$) and

a^i is the value of $a(x)$ at node i: $a^i = a(x^i)$.

An interpolation of $a(x)$ over the whole domain $h_\Omega = \bigcup_{e=1}^{n_{elem}} \Omega^e$ (where n_{elem} is the total number of elements) is defined as follows:

$$\mathbf{a}^{\mathbf{h}}(x) = \sum_{i=1}^{n_{poin}} a^i N_i^g(x)$$

where

n_{poin} is the total number of nodal points in the mesh;

$N_i^g(x)$ is the global shape function associated with a node i.

Finite element interpolation in matrix notation

The global array of nodal displacements is defined as follows:

$$\mathbf{u_f} = \left(u_1^1, \ldots u_{n_{\text{dim}}}^1, \ldots\ldots, u_1^{n_{poin}}, \ldots u_{n_{\text{dim}}}^{n_{poin}}\right)^T, \tag{2.10}$$

where

n_{dim} is the number of spatial dimensions;

u_i^j is the i-th component of the displacement vector at node j.

The global interpolation matrix can be defined as follows

$$\mathbf{N^g}(x) = \left(diag\left[N_1^g(x)\right], \ldots\ldots diag\left[N_{n_{poin}}^g(x)\right]\right)_{n_{\text{dim}} \times n_{\text{dim}} n_{poin}},$$

where

$$diag\left[N_i^g(x)\right] = \begin{pmatrix} N_i^g & 0 & \cdots & 0 \\ 0 & N_i^g & \cdots & 0 \\ & & \ddots & \\ 0 & 0 & \cdots & N_i^g \end{pmatrix}_{n_{\text{dim}} \times n_{\text{dim}}}$$ is the $n_{\text{dim}} \times n_{\text{dim}}$ diagonal matrix.

An array expression corresponding to the displacements' finite-dimensional set $\mathbf{u^h}(x) = \sum_{i=1}^{n_{poin}} diag\left[N_i^g(x)\right]\boldsymbol{u}^i$, $\boldsymbol{u}^i = \bar{\boldsymbol{u}}^i\left(x^i\right)$ *if* $x^i \in \partial\Omega_u$ ($\boldsymbol{u}^i$ is the displacement vector at node i) appears as follows:

$$\mathbf{u^h}(x) = \mathbf{N^g}(x)\mathbf{u_f} = \begin{pmatrix} N_1^g(x)u_1^1 + \ldots + N_{n_{poin}}^g(x)u_1^{n_{poin}} \\ \vdots \\ N_1^g(x)u_{n_{dim}}^1 + \ldots + N_{n_{poin}}^g(x)u_{n_{dim}}^{n_{poin}} \end{pmatrix}.$$

An array expression corresponding to the following virtual displacements' finite-dimensional set $\boldsymbol{\eta}^{\mathbf{h}}(x) = \sum_{i=1}^{n_{poin}} diag\left[N_i^g(x)\right]\boldsymbol{\eta}^i$, $\boldsymbol{\eta}^i = 0$ *if* $x^i \in \partial\Omega_u$, can be obtained in similar way:

$$\boldsymbol{\eta}^{\mathbf{h}}(x) = \mathbf{N^g}(x)\boldsymbol{\eta}_{\mathbf{f}},$$

where

$\boldsymbol{\eta}_{\mathbf{f}} = \left(\eta_1^1, \ldots \eta_{n_{\text{dim}}}^1, \ldots\ldots, \eta_1^{n_{poin}}, \ldots \eta_{n_{\text{dim}}}^{n_{poin}}\right)^T$ is the global array of nodal virtual displacements.

It must be mentioned that each global array of nodal virtual displacements $\boldsymbol{\eta}_{\mathbf{f}}$ on body X consists of nodal virtual displacements which are equal to zero on the

part of border of the body on which boundary conditions on displacements are assigned. All these arrays belong to the space Ψ_f.

As strains are used in expression (2.7) of the principle of virtual work, a strain vector and the global strain displacement operator should be introduced. For example, for a three dimensional problem the strain finite element array appears as follows:

$$\boldsymbol{\varepsilon} = \left(\varepsilon_{11} \quad \varepsilon_{22} \quad \varepsilon_{33} \quad \gamma_{12} = 2\varepsilon_{12} \quad \gamma_{23} = 2\varepsilon_{23} \quad \gamma_{13} = 2\varepsilon_{13}\right)^T.$$

For an axisymmetric case this array has to be ammended as follows:

$$\boldsymbol{\varepsilon} = \left(\varepsilon_{11} \quad \varepsilon_{22} \quad \gamma_{12} \quad \varepsilon_{33}\right)^T.$$

The global strain displacement operator B^g is defined as follows:

$$\boldsymbol{\varepsilon} = \mathbf{B}^{\mathbf{g}}\mathbf{u}_{\mathbf{f}}.$$

For example, in the two dimensional case this operator appears as follows:

$$\mathbf{B}^{\mathbf{g}} = \begin{pmatrix} \frac{\partial N_1^g}{\partial x} & 0 & \frac{\partial N_2^g}{\partial x} & 0 & \cdots & \frac{\partial N_{n_{poin}}^g}{\partial x} & 0 \\ 0 & \frac{\partial N_1^g}{\partial y} & 0 & \frac{\partial N_2^g}{\partial y} & \cdots & 0 & \frac{\partial N_{n_{poin}}^g}{\partial y} \\ \frac{\partial N_1^g}{\partial y} & \frac{\partial N_1^g}{\partial x} & \frac{\partial N_2^g}{\partial y} & \frac{\partial N_2^g}{\partial x} & \cdots & \frac{\partial N_{n_{poin}}^g}{\partial y} & \frac{\partial N_{n_{poin}}^g}{\partial x} \end{pmatrix}.$$

It is reasonable now to introduce a stress array for a three dimensional problem:

$$\boldsymbol{\sigma} = \left(\sigma_{11} \quad \sigma_{22} \quad \sigma_{33} \quad \sigma_{12} \quad \sigma_{23} \quad \sigma_{13}\right)^T.$$

Analogously, for the plane strain or axisymmetric cases this array has to be ammended as follows:

$$\boldsymbol{\sigma} = \left(\sigma_{11} \quad \sigma_{22} \quad \sigma_{12} \quad \sigma_{33}\right)^T.$$

The finite element equations

Virtual work expression (2.7) can be rewritten using the appropriate matrix notations:

$$\int_{\Omega} \boldsymbol{\sigma}(t)\mathbf{B}^{\mathbf{g}}\boldsymbol{\eta}_{\mathbf{f}}\,dV - \int_{\Omega} \mathbf{b}(t)\mathbf{N}^{\mathbf{g}}\boldsymbol{\eta}_{\mathbf{f}}\,dV - \int_{S_t} \mathbf{w}(t)\mathbf{N}^{\mathbf{g}}\boldsymbol{\eta}_{\mathbf{f}}\,dS = 0, \quad \forall \boldsymbol{\eta}_{\mathbf{f}} \in \Psi_{\mathbf{f}}. \tag{2.11}$$

Having rearranged expression (2.11) one gets

$$\left[\int_{\Omega} \left(\mathbf{B}^{\mathbf{g}}\right)^{\mathrm{T}} \boldsymbol{\sigma}(t)\,dV - \int_{\Omega} \left(\mathbf{N}^{\mathbf{g}}\right)^{\mathrm{T}} \mathbf{b}(t)\,dV - \int_{S_t} \left(\mathbf{N}^{\mathbf{g}}\right)^{\mathrm{T}} \mathbf{w}(t)\,dS\right]\boldsymbol{\eta}_{\mathbf{f}} = 0, \quad \forall \boldsymbol{\eta}_{\mathbf{f}} \in \Psi_{\mathbf{f}}. \tag{2.12}$$

As expression (2.12) is satisfied $\forall \eta_f \in \Psi_f$, it follows that the expression in brackets is equal to zero.

It should be pointed out that the material is path-dependant. Usually numerical algorithms for integration of such problems are obtained by implementing a pseudo-time discretisation of the loads and deformation path.

A pseudo-time increment $[t_n, t_{n+1}]$ is considered below and it is assumed that both the set α_n of internal variables of the converged state at t_n and the strain tensor ε_{n+1} at the end of the time interval are known. Within the context of the pure mechanical theory α_n and ε_{n+1} together must determine σ_{n+1} - the stress at the end of the time interval. The constitutive function for the stress tensor can be defined as $\sigma_{n+1} = \sigma(\alpha_n, \varepsilon_{n+1})$. The outcome of this function must lead to the exact solution of the actual problem with very small strain increments. Internal variables can be obtained as follows: $\alpha_{n+1} = \hat{\alpha}(\alpha_n, \varepsilon_{n+1})$. Further details regarding the integration algorithm can be found in Chapter 4.

Equation (2.12) can be rewritten in the following way for pseudo-time moment t_{n+1}:

$$\left[\int_\Omega (\mathbf{B}^g)^T \sigma(\alpha_n, \varepsilon_{n+1}(\mathbf{u}_{f\ n+1}))dV - \int_\Omega (\mathbf{N}^g)^T \mathbf{b}_{n+1} dV - \int_{S_t} (\mathbf{N}^g)^T \mathbf{w}_{n+1} dS\right] \eta_f = 0, \quad \forall \eta_f \in \Psi_f \tag{2.13}$$

where

$\boldsymbol{b}_{n+1}$ and $\boldsymbol{w}_{n+1}$ are the body and surface loads at the pseudo-time moment t_{n+1}.

Global internal and external force vectors are defined in the following way:

$$\begin{aligned} \mathbf{f}^{int}(\mathbf{u}_{f\ n+1}) &= \int_\Omega (\mathbf{B}^g)^T \sigma(\alpha_n, \mathbf{u}_{f\ n+1}) dV; \\ \mathbf{f}^{ext}_{n+1} &= \int_\Omega (\mathbf{N}^g)^T \mathbf{b}_{n+1} dV + \int_{S_t} (\mathbf{N}^g)^T \mathbf{w}_{n+1} dS. \end{aligned} \tag{2.14}$$

These vectors are assembled from the appropriate element vectors (the same integrals which are taken over one element only):

$$\mathbf{f}^{int}_{(e)}(\mathbf{u}_{f\ n+1}) = \int_{\Omega^{(e)}} (\mathbf{B}^e)^T \sigma(\alpha_n, \mathbf{u}_{f\ n+1}) dV;$$

$$\mathbf{f}^{ext}_{(e)\ n+1} = \int_{\Omega^{(e)}} (\mathbf{N}^e)^T \mathbf{b}_{n+1} dV + \int_{S_t^{(e)}} (\mathbf{N}^e)^T \mathbf{w}_{n+1} dS,$$

where

$$\mathbf{B}^{\mathbf{e}} = \begin{pmatrix} \frac{\partial N_1^e}{\partial x} & 0 & \frac{\partial N_2^e}{\partial x} & 0 & \cdots & \frac{\partial N_{n_{node}}^e}{\partial x} & 0 \\ 0 & \frac{\partial N_1^e}{\partial y} & 0 & \frac{\partial N_2^e}{\partial y} & \cdots & 0 & \frac{\partial N_{n_{node}}^e}{\partial y} \\ \frac{\partial N_1^e}{\partial y} & \frac{\partial N_1^e}{\partial x} & \frac{\partial N_2^e}{\partial y} & \frac{\partial N_2^e}{\partial x} & \cdots & \frac{\partial N_{n_{node}}^e}{\partial y} & \frac{\partial N_{n_{node}}^e}{\partial x} \end{pmatrix}$$ is the matrix of the element

strain displacement operator;

$\mathbf{N}^{\mathbf{e}}(x) = \left(diag\left[N_1^e(x)\right] \ldots\ldots diag\left[N_{n_{node}}^e(x)\right]\right)_{n_{dim} \times n_{dim} n_{node}}$ is the element interpolation matrix;

$$diag\left[N_i^e(x)\right] = \begin{pmatrix} N_i^e & 0 & \cdots & 0 \\ 0 & N_i^e & \cdots & 0 \\ & & \ddots & \\ 0 & 0 & \cdots & N_i^e \end{pmatrix}_{n_{\dim} \times n_{\dim}}$$ is the $n_{\dim} \times n_{\dim}$ diagonal matrix.

Hence, the finite element problem (2.13) can be reformulated as follows:

find the nodal displacement array $\mathbf{u}_{\mathbf{f}\ n+1}$, *such that*

$$\mathbf{r}\left(\mathbf{u}_{\mathbf{f}\ n+1}\right) = \mathbf{f}^{\mathbf{int}}\left(\mathbf{u}_{\mathbf{f}\ n+1}\right) - \mathbf{f}_{\mathbf{n+1}}^{\mathbf{ext}} = 0 \,. \tag{2.15}$$

As the material is path-dependant, equation (2.15) is nonlinear and has to be solved numerically. The full Newton-Raphson algorithm discussed in the next Section is suitable for this due to its quadratic rate of convergence.

The Newton-Raphson algorithm and a tangent stiffness matrix

The Newton-Raphson iteration scheme for integration of equation (2.15) is described below.

In order to get a solution of the k^{th} iteration, the correction $\delta\mathbf{u}_{\mathbf{f}}^{(\mathbf{k})}$ is added to the solution $\mathbf{u}_{\mathbf{f}\,\mathbf{n+1}}^{(\mathbf{k-1})}$ which was obtained during the $(k-1)^{th}$ iteration:

$$\mathbf{u}_{\mathbf{f}\,\mathbf{n+1}}^{(\mathbf{k})} = \mathbf{u}_{\mathbf{f}\,\mathbf{n+1}}^{(\mathbf{k-1})} + \delta\mathbf{u}_{\mathbf{f}}^{(\mathbf{k})}. \tag{2.16}$$

In order to obtain the correction $\delta\mathbf{u}_{\mathbf{f}}^{(\mathbf{k})}$ one must solve the following linear system:

$$\mathbf{K}_{\mathbf{T}}\delta\mathbf{u}_{\mathbf{f}}^{(\mathbf{k})} = -\mathbf{r}^{(\mathbf{k-1})} = -\left(\mathbf{f}^{\mathbf{int}}\left(\mathbf{u}_{\mathbf{f}\,\mathbf{n+1}}^{(\mathbf{k-1})}\right) - \mathbf{f}_{\mathbf{n+1}}^{\mathbf{ext}}\right) \tag{2.17}$$

where

$\mathbf{K}_{\mathbf{T}}$ is the global tangent stiffness matrix:

$$\mathbf{K}_T = \left.\frac{\partial \mathbf{r}}{\partial \mathbf{u}_{f\,n+1}}\right|_{\mathbf{u}_{f\,n+1}^{(k-1)}}. \tag{2.18}$$

This matrix (2.18) is the assembly of the element tangent stiffness matrices $\mathbf{K}_T^{(e)}$:

$$\mathbf{K}_T^{(e)} = \int_{\Omega^{(e)}} \left(\mathbf{B}^e\right)^T \hat{\mathbf{D}} \mathbf{B}^e dV, \tag{2.19}$$

where

$\hat{\mathbf{D}}$ is a consistent tangent matrix:

$$\hat{\mathbf{D}} = \left.\frac{\partial \sigma(\alpha_n, \varepsilon_{n+1})}{\partial \varepsilon_{n+1}}\right|_{\varepsilon_{n+1}^{(k-1)}}. \tag{2.20}$$

One should note that matrix (2.20) contains the derivative of a generally implicit function $\sigma(\alpha_n, \varepsilon_{n+1})$ which is defined by an integration algorithm for the constitutive equations of a material model. In the article by Simo and Taylor (1985) it was shown that in order to obtain the quadratic rate of convergence of the iterative solution for problems of rate-independent elastoplasticity it is necessary to ensure that the tangent operator and the integration algorithm are consistent. Please refer to Section 4.2 for detailed procedure to obtain the consistent tangent matrix (2.20).

Finally, the Newton-Raphson iteration scheme for obtaining the finite element solution at the $n+1$ load step (loads are $\boldsymbol{b}_{n+1}$ and $\boldsymbol{w}_{n+1}$) of problem (2.1)-(2.6) may be represented as the following algorithm:

1. $k = 0$. Set initial guess $\mathbf{u}_{f\,n+1}^{(0)} = \mathbf{u}_{f\,n}$; $\mathbf{r} = \mathbf{f}^{int}\left(\mathbf{u}_{f\,n}\right) - \mathbf{f}_{n+1}^{ext}$.

2. Calculate consistent tangent matrices $\hat{\mathbf{D}} = \dfrac{\partial \sigma}{\partial \varepsilon_{n+1}}$.

3. Assemble element tangent stiffness matrices $\mathbf{K}_T^{(e)} = \sum_{i=1}^{n_{gausp}} z_i \left(\mathbf{B}_i^{\,e}\right)^T \hat{\mathbf{D}}_i \mathbf{B}_i^{\,e}$ (where z_i is the Gaussian weight and n_{gausp} is the number of Gauss points).

4. $k = k+1$. Assemble the global stiffness and solve the system $\mathbf{K}_T \delta \mathbf{u}_f^{(k)} = -\mathbf{r}^{(k-1)}$.

5. Apply a Newton correction to the displacements $\mathbf{u}_{f\,n+1}^{(k)} = \mathbf{u}_{f\,n+1}^{(k-1)} + \delta \mathbf{u}_f^{(k)}$.

6. Update strains $\boldsymbol{\varepsilon}_{n+1}^{(k)} = \mathbf{B}^{g}\mathbf{u}_{f\,n+1}^{(k)}$.

7. Update stresses and internal variables $\boldsymbol{\sigma}_{n+1}^{(k)} = \boldsymbol{\sigma}\left(\boldsymbol{\alpha}_n, \boldsymbol{\varepsilon}_{n+1}^{(k)}\right)$, $\boldsymbol{\alpha}_{n+1}^{(k)} = \hat{\boldsymbol{\alpha}}\left(\boldsymbol{\alpha}_n, \boldsymbol{\epsilon}_{n+1}^{(k)}\right)$.

8. Compute element internal force vectors $\mathbf{f}_{(e)}^{int} = \sum_{i=1}^{n_{gausp}} z_i j_i \left(\mathbf{B}^{e}\right)^{T} \boldsymbol{\sigma}_{n+1}^{(k)}\Big|_i$ (where j_i is the determinant of the Jacobian).

9. Assemble global internal force vector $\mathbf{f}^{int}\left(\mathbf{u}_{f\,n+1}^{(k)}\right)$ and update residual $\mathbf{r} = \mathbf{f}^{int}\left(\mathbf{u}_{f\,n+1}^{(k)}\right) - \mathbf{f}_{n+1}^{ext}$.

10. Check for convergence. If $\dfrac{\|\mathbf{r}\|}{\|\mathbf{f}_{n+1}^{ext}\|} \leq \mathbf{tol}$ then goto 11 else goto 2.

11. Update solution $(\cdot)_{n+1} = (\cdot)_{n+1}^{(k)}$.

2.2. Overview of the HYPLAS program

In this section a brief description of the HYPLAS program is provided. Detailed description is provided in the text book by de Souza Neto *et al.* (2003).

HYPLAS is a finite element code for implicit small and large strain analysis of hyperelastic and elasto-plastic solids in plane stress, plane strain and axisymmetric states. In general, its structure includes (de Souza Neto *et al.* 2003):

1. A general displacement-based incremental finite element procedure;
2. Iterative schemes (for example, Newton-Raphson) for solution of nonlinear incremental finite element equations;
3. An arc-length scheme for problems involving structural instability.

To ensure material and element modularity HYPLAS was designed in such a way that element-specific and material-specific procedures are connected to relatively local parts of the program. That is why it is quite easy to incorporate a new material model into HYPLAS. The developer should write associated numerical procedures only and then ensure that these subroutines will be called at appropriate points.

The HYPLAS program can be divided into three basic parts (these parts are practically independent of the finite element types and material models adopted):

1. Data input and initialisation. This phase is carried out at the beginning of the program execution and includes reading from files all the necessary data and initialising all arrays.
2. The incremental finite element procedure. This procedure is the main part of the program and consists of a loop over load increments with a nested loop over equilibrium iterations.
3. Output of converged results to the result file and/or dumping an image of the database into a restart output file.

2.2.1. Data input and initialisation

Input data can be read either from an input file only or from an input restart file and an input data file. The input data file is an ASCII file containing all the information defining the problem to be analysed including the data related to the definition of the proportional load incrementation programme. The input restart file contains the image of the database where most arrays and program control parameters required in the solution process are stored. This database contains 2 types of data:

1. Problem-defining data which does not change during the solution process and consists of nodal coordinates and connectivity; material and element properties; boundary conditions such as kinematic constraints and external loads. It is worth noting that material properties can be divided into real (elastic constants, yield stresses and points of piece-wise linear approximation of the hardening curve) and integer (number of points of this linear approximation; material class and type numbers). This data is set once according to the input file.
2. Solution-related data that changes during the solution process. These data include nodal displacements, stresses and state variables at Gauss points, internal forces, etc.

Geometry of the problem, mesh topology and boundary conditions are also read during this stage.

2.2.2. The load incremental loop

This incremental loop is the central part of the finite element analysis code. This loop carries out the proportional loading programme. Within each step of the

loop an iterative procedure (typically the Newton-Raphson algorithm) is carried out to solve the non-linear equilibrium problem. The main concept of this loop was discussed in Section 2.1.

The structure of the programme code of the load increment loop under fixed increments option can be seen in Figure 2.1. Detailed explanation of the HYPLAS subroutines is provided in the text book by de Souza Neto *et al.* (2003). Under fixed increments option the incremental load factors are taken from the input data file.

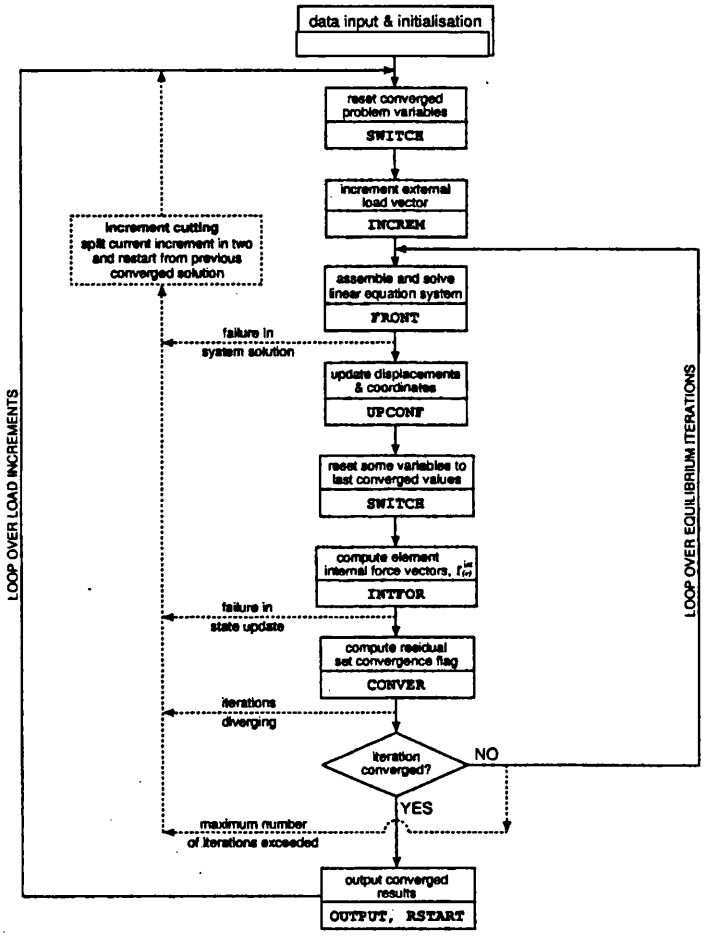

Figure 2.1. The load incrementation loop with fixed increments (de Souza Neto *et al.* 2003).

There is also an increment cutting option in HYPLAS. This procedure is activated when a converged equilibrium solution can not be attained in the equilibrium iterations. Whenever this happens the current step is restarted with a reduced increment size. There are the following causes for the absence of convergence:

1. Load increment is too large. The total load of the structure is beyond the limit load of the structure or the initial guess is out of the convergence radius of the iterative solution method.
2. The algorithm for numerical integration of the path-dependant constitutive equation (the state update procedure) fails to give a solution at a Gauss point. This may be caused by too large strain increments.
3. The system of linear equations can not be solved because of a zero pivot in the stiffness matrix (the tangent operator is singular).

So, the loop over load increments is ended either if the load programme is successfully finished or if the number of increment cuts (Figure 2.1) causes the sub-increment stack array to become full.

The equations of the linear system are assembled with the contribution of each element to the global system matrix and the load vector. This system is solved using the classical frontal method where the system is solved by Gauss elimination. Details of the technique can be seen in the book by Hinton and Owen (1977).

2.2.3. Material modularity

The basic idea of HYPLAS is isolating element and material-specific operations to special code areas to avoid interference with general procedures that are non-related to special elements or materials. This concept is illustrated on the Figure 2.2.

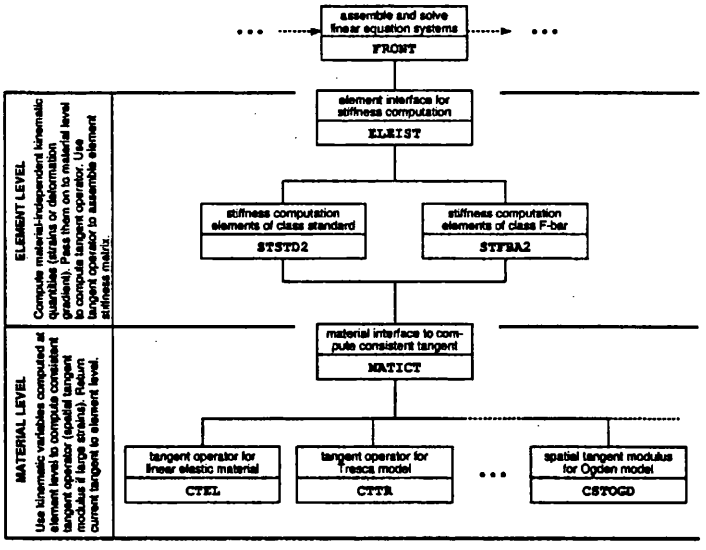

Figure 2.2. Consistent tangent computation.
Modular structure (de Souza Neto *et al.* 2003).

It is easy to see that the consistent tangent computation is split into two levels:

1. The element level on which all element related quantities (matrix B) are computed. From this level an appropriate subroutine is called for each Gauss point to obtain the tangent modulus. Finally, the element tangent matrix is assembled.
2. The material level that is the lowest layer of code. It receives the stress conditions and state variables from the element level, and computes the consistent tangent modulus for the Gauss point.

2.2.4. Implementation of a new material model

There is a material database in HYPLAS in which materials are identified by types and grouped into classes. Grouping materials into classes is not necessary for modularity but is valuable particularly in the finite strain regime where different models require the same transformation of the kinematic variables.

Within the HYPLAS modular structure the incorporation of a new material model requires coding of the following material-specific subroutines (their names were chosen to follow the HYPLAS style):

1. State update procedure SUHF. This subroutine calculates new stresses, algorithmic (such as the plastic multiplier) and state variables at the end of load increment for each Gauss point (Section 4.1).
2. Tangent computation procedure CTHF. It calculates the consistent tangent operator using converged values of stresses, algorithmic and state variables for each Gauss point (Section 4.2).
3. Switching / initialisation subroutine SWHF. It is used for the initialisation of variables as well as switching between current and converged values in material specific routines.
4. Data input procedure RDHF that reads all material model/algorithm-related data and stores them in the appropriate HYPLAS arrays.
5. Output subroutine ORHF writes the results to a result file.

Moreover, to incorporate a new material model into the HYPLAS code one should perform two additional steps:

1. Adding a new material type identification parameter to the material database

2. Adding calls to 5 material interface routines to the existing HYPLAS material interfaces.

Chapter 3. Elasto-plastic constitutive Hoffman material model

This chapter is dedicated to a description of the Hoffman yield criterion for orthotropic composite materials (Hoffman, 1967). A corresponding elasto-plastic constitutive model used in state update procedure (Section 4.1) is discussed as well.

3.1. The Hoffman yield criterion

It is well known that composite materials are highly anisotropic in terms of elastic moduli and yield strengths. They are weaker in the transverse direction than in the longitudinal one. A typical ply of a composite structure can be considered as orthotropic with three principal material directions. In the case of fibrous composites, the direction parallel to the fibres is normally referred to as the longitudinal direction (one in the plane of the ply and one normal to it). These three material directions are denoted as material axes x_1, x_2 and x_3 respectively (Koh *et al.* 1995).

Composite materials controlled by plastic flow are studied in this project. So, it is assumed that no fracture or debonding occurs. In this context it should be mentioned that many fibrous composites have significantly different tensile and compressive yield stresses, particularly in the transverse directions (Koh *et al.* 1995). That is why in these cases the commonly adopted Hill yield criterion (Hill, 1947) is inadequate and a more general Hoffman yield criterion should be used.

Originally the Hoffman yield criterion was designed as a fracture condition for brittle anisotropic materials of which fibre-reinforced plastics are the most important examples (Hoffman, 1967). It should be mentioned that there are some other fracture criteria for these materials such as Tsai–Hill and Tsai–Wu (Schellekens and de Borst, 1990; Gürdal, 1999).

The Hoffman yield criterion is a modification of the criterion proposed by Hill (Hill, 1947) through inclusion of terms which are linear in the stress. This can overcome the restriction of the Hill criterion, according to which the tensile and the compression yield strength should be equal (in other words, a Bauschinger effect is neglected).

Hoffman originally formulated his failure criterion by a quadratic function

$$C_1(\sigma_{22}-\sigma_{33})^2+C_2(\sigma_{33}-\sigma_{11})^2+C_3(\sigma_{11}-\sigma_{22})^2+$$
$$+C_4\sigma_{11}+C_5\sigma_{22}+C_6\sigma_{33}+C_7\sigma_{23}^2+C_8\sigma_{13}^2+C_9\sigma_{12}^2=1,$$

where the constants C_i, $i=1...9$ are nine independent material parameters which can be uniquely defined from three tensile tests, three compression tests and three shear tests. It is evident that this expression does not allow hardening to be taken into account as it was designed to predict failure, not to describe a plastic flow. The possibilities to take different types of hardening (both isotropic and anisotropic) into account will be discussed later.

The geometric form of the Hoffman failure surface is described by a quadratic function of nine independent variables C_i. When the criterion is represented graphically in the principal stress space it is an elliptic paraboloid (Schellekens and de Borst, 1990). The intersections of the limit surface with planes parallel to the deviatoric plane are ellipses, the shapes of which are determined by the quadratic part of the function (Figure 3.1).

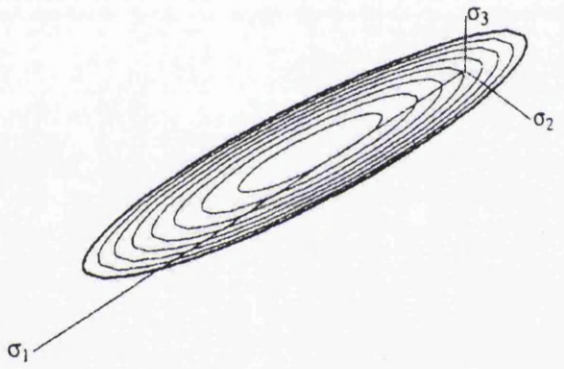

Figure 3.1. Cross section of an anisotropic Hoffman yield surface and the deviatoric plane (Schellekens and de Borst, 1990).

3.2. The Hoffman material model in tensor notation

Having discussed the Hoffman yield criterion, it is possible to write down the Hoffman plasticity model for orthotropic composite material with isotropic hardening (anisotropic hardening will be discussed later):

$$\boldsymbol{\varepsilon} = \boldsymbol{\varepsilon}^e + \boldsymbol{\varepsilon}^p, \tag{3.1}$$

$$\boldsymbol{\sigma} = \boldsymbol{C} : \boldsymbol{\varepsilon}^e, \tag{3.2}$$

$$F(\boldsymbol{\sigma},k) = \left(c_1 - \frac{c_3}{2}\right)(\sigma_{11}-\sigma_{33})^2 + \left(c_2 - \frac{c_3}{2}\right)(\sigma_{22}-\sigma_{33})^2 + \frac{c_3}{2}(\sigma_{11}-\sigma_{22})^2 + \\ + c_4\sigma_{12}^2 + c_5\sigma_{11} + c_6\sigma_{22} + c_7\sigma_{33} + c_8\sigma_{23}^2 + c_9\sigma_{13}^2 - \sigma_Y^2(k), \tag{3.3}$$

$$k = \int_o^t \sqrt{\frac{2}{3}\left(\dot{\boldsymbol{\varepsilon}}^p : \dot{\boldsymbol{\varepsilon}}^p\right)}dt = \sqrt{\frac{2}{3}}\int_o^t \sqrt{\dot{\varepsilon}_{ij}^p \dot{\varepsilon}_{ij}^p}\, dt = \sqrt{\frac{2}{3}}\int_o^t \left\|\dot{\boldsymbol{\varepsilon}}^p\right\| dt = \bar{\boldsymbol{\varepsilon}}^p \tag{3.4}$$

$$\dot{\boldsymbol{\varepsilon}}^p = \dot{\lambda}\,\frac{\partial F(\boldsymbol{\sigma},k)}{\partial \boldsymbol{\sigma}}\,, \tag{3.5}$$

$$F(\boldsymbol{\sigma},k) \le 0\,,\quad \dot{\lambda} \ge 0\,,\quad \dot{\lambda}\, F(\boldsymbol{\sigma},k) = 0\,, \tag{3.6}$$

where

$\boldsymbol{\varepsilon}$ is the Cauchy full strain tensor;

$\boldsymbol{\varepsilon}^e$ is the Cauchy elastic strain tensor;

$\boldsymbol{\varepsilon}^p$ is the Cauchy plastic strain tensor;

$\boldsymbol{\sigma}$ is the Cauchy stress tensor and σ_{ij} $(i,j = 1,2,3)$ are its components;

$\boldsymbol{C}$ is the elasticity tensor;

$F(\boldsymbol{\sigma},k)$ is the yield function;

σ_Y is the reference yield stress;

k is the hardening variable;

: denotes the double contraction operator, i.e. $\boldsymbol{A} : \boldsymbol{B} = A_{ij}B_{ij}$; $\boldsymbol{C} : \boldsymbol{B} = C_{ijkl}B_{kl}$;

$\dot{\boldsymbol{\varepsilon}}^p$ is the plastic strain rate tensor;

$\bar{\boldsymbol{\varepsilon}}^p$ is the accumulated plastic strain;

$c_1, \ldots c_9$ are nine independent material parameters (3.7);

$\dot{\lambda}$ is the plastic multiplier.

The expression (3.1) is an additive decomposition of the strain tensor, expression (3.2) is a linear elastic law, expression (3.3) is the Hoffman yield function for isotropic hardening, expression (3.4) defines the hardening parameter for strain hardening model, expression (3.5) is a standard associative flow rule, and expressions (3.6) show the loading/unloading criterion.

A model is said to be isotropic hardening if the evolution of the yield surface is such that, at any state of hardening, corresponds to an uniform (isotropic) expansion of the initial yield surface, without any translation. In other words, yield stresses (including the reference yield stress) have the same hardening rate. That is why for the isotropic hardening model $c_1, \ldots c_9$ are constants and appear as follows (Koh *et al.* 1995):

$$c_1 = \frac{\sigma_{Y_0}^2}{\sigma_{11T_0}\sigma_{11C_0}} \equiv \frac{\sigma_Y^2(k)}{\sigma_{11T}(k)\sigma_{11C}(k)} \quad \forall k \geq 0,$$

$$c_2 = \frac{\sigma_{Y_0}^2}{\sigma_{22T_0}\sigma_{22C_0}},$$

$$c_3 = c_1 + c_2 - \frac{\sigma_{Y_0}^2}{\sigma_{33T_0}\sigma_{33C_0}},$$

$$c_4 = \frac{\sigma_{Y_0}^2}{\sigma_{12S_0}^2},$$

$$c_5 = \sigma_{Y_0}^2 \frac{\sigma_{11C_0} - \sigma_{11T_0}}{\sigma_{11T_0}\sigma_{11C_0}}, \tag{3.7}$$

$$c_6 = \sigma_{Y_0}^2 \frac{\sigma_{22C_0} - \sigma_{22T_0}}{\sigma_{22T_0}\sigma_{22C_0}},$$

$$c_7 = \sigma_{Y_0}^2 \frac{\sigma_{33C_0} - \sigma_{33T_0}}{\sigma_{33T_0}\sigma_{33C_0}},$$

$$c_8 = \frac{\sigma_{Y_0}^2}{\sigma_{23S_0}^2},$$

$$c_9 = \frac{\sigma_{Y_0}^2}{\sigma_{31S_0}^2},$$

where subscripts "T","C" and "S" denote the yield stresses in tensile, compressive and shear tests respectively and subscript "0" means that the corresponding yield stresses are initial.

The anisotropic Hill material is recovered when the yield stresses are equal in the tensile and compressive directions leading to $c_5 = c_6 = c_7 = 0$. For isotropic von Mises material the constants are the following: $c_1 = c_2 = c_3 = 1$, $c_4 = c_8 = c_9 = 3$ and $c_5 = c_6 = c_7 = 0$.

In the case of anisotropic hardening all 9 stresses σ_T, σ_C and σ_S in all 3 directions depend on their own corresponding hardening variables k_i, $i = 1 \ldots 9$. So, the nine independent material parameters $c_1, \ldots c_9$ are not constants any more. At the

same time, σ_Y in the expression (3.3) does not change and is equal to the virgin yield strength of the material in the first material direction. This model of hardening is discussed in detail in the article by Hashagen and de Borst (2001).

For an orthotropic material components of the elasticity tensor C appear as follows:

$$\begin{aligned}
C_{1111} &= B_{11}, \\
C_{2222} &= B_{22}, \\
C_{3333} &= B_{33}, \\
C_{1133} &= C_{3311} = B_{13}, \\
C_{2233} &= C_{3322} = B_{23}, \\
C_{1122} &= C_{2211} = B_{12}, \\
C_{1212} &= C_{1221} = C_{2112} = C_{2121} = B_{44}/2, \\
C_{1313} &= C_{1331} = C_{3113} = C_{3131} = B_{55}/2, \\
C_{3232} &= C_{3223} = C_{2332} = C_{2323} = B_{66}/2,
\end{aligned} \tag{3.8}$$

where these 9 coefficients are uniquely determined by 9 elastic constants, i.e. Young's moduli E_1, E_2, E_3, shear moduli G_{12}, G_{23}, G_{31} and Poisson ratios $\nu_{12}, \nu_{23}, \nu_{31}$:

$$\begin{aligned}
B_{11} &= \frac{E_1(1-\nu_{23}\nu_{32})}{(1-\nu_{31}\nu_{13})(1-\nu_{23}\nu_{32})-(\nu_{12}+\nu_{13}\nu_{32})(\nu_{21}+\nu_{23}\nu_{31})}, \\
B_{22} &= \frac{E_2(1-\nu_{31}\nu_{13})}{(1-\nu_{12}\nu_{21})(1-\nu_{31}\nu_{13})-(\nu_{23}+\nu_{21}\nu_{13})(\nu_{32}+\nu_{31}\nu_{12})}, \\
B_{33} &= \frac{E_3(1-\nu_{12}\nu_{21})}{(1-\nu_{23}\nu_{32})(1-\nu_{12}\nu_{21})-(\nu_{31}+\nu_{32}\nu_{21})(\nu_{13}+\nu_{12}\nu_{23})}, \\
B_{12} &= \frac{(\nu_{21}+\nu_{23}\nu_{31})}{(1-\nu_{23}\nu_{32})}B_{11}, \\
B_{23} &= \frac{(\nu_{32}+\nu_{31}\nu_{12})}{(1-\nu_{31}\nu_{13})}B_{22}, \\
B_{13} &= \frac{(\nu_{13}+\nu_{12}\nu_{23})}{(1-\nu_{12}\nu_{21})}D_{33}, \\
B_{44} &= 2G_{12}, \\
B_{55} &= 2G_{31},
\end{aligned} \tag{3.9}$$

$$B_{66} = 2G_{23},$$

$$\nu_{21} = \nu_{12}\frac{E_2}{E_1},$$

$$\nu_{32} = \nu_{23}\frac{E_3}{E_2}, \tag{3.9}$$

$$\nu_{13} = \nu_{31}\frac{E_1}{E_3},$$

By definition,

$$\nu_{ij} = \frac{contraction\ \ in\ \ the\ \ j-th\ \ direction}{extension\ \ in\ \ the\ \ i-th\ \ direction}.$$

As the HYPLAS program (de Souza Neto *et al.* 2003) was designed for such two-dimensional problems as plane strain or axisymmetric cases ($\varepsilon^e_{13} = \varepsilon^e_{23} = \varepsilon^p_{13} = \varepsilon^p_{23} \equiv 0$ and $\sigma_{13} = \sigma_{23} \equiv 0$) and the aim of this project is to implement a Hoffman material model in HYPLAS (de Souza Neto *et al.* 2003), all further calculations will be restricted to these two cases.

The associative flow rule (3.5) consists of a tensor derivative. That is why the Hoffman yield function (3.3) should be used in a tensor form. To obtain this form the following calculations are necessary to perform:

$$F(\sigma) = \left(c_1 - \frac{c_3}{2}\right)(\sigma_{11} - \sigma_{33})^2 + \left(c_2 - \frac{c_3}{2}\right)(\sigma_{22} - \sigma_{33})^2 + \frac{c_3}{2}(\sigma_{11} - \sigma_{22})^2 +$$

$$+ c_4\sigma_{12}^2 + c_5\sigma_{11} + c_6\sigma_{22} + c_7\sigma_{33} =$$

$$= \left(c_1 - \frac{c_3}{2}\right)\left(\sigma_{11}{}^2 - 2\sigma_{11}\sigma_{33} + \sigma_{33}{}^2\right) + \left(c_2 - \frac{c_3}{2}\right)\left(\sigma_{22}{}^2 - 2\sigma_{22}\sigma_{33} + \sigma_{33}{}^2\right) +$$

$$+ \frac{c_3}{2}\left(\sigma_{11}{}^2 - 2\sigma_{11}\sigma_{22} + \sigma_{22}{}^2\right) + c_4\sigma_{12}^2 + c_5\sigma_{11} + c_6\sigma_{22} + c_7\sigma_{33} =$$

$$= \frac{1}{2}\left\{(2c_1 - c_3)\left(\sigma_{11}{}^2 - 2\sigma_{11}\sigma_{33} + \sigma_{33}{}^2\right) + (2c_2 - c_3)\left(\sigma_{22}{}^2 - 2\sigma_{22}\sigma_{33} + \sigma_{33}{}^2\right)\right\} +$$

$$= \frac{1}{2}\left\{c_3\left(\sigma_{11}{}^2 - 2\sigma_{11}\sigma_{22} + \sigma_{22}{}^2\right)\right\} + c_4\sigma_{12}^2 + c_5\sigma_{11} + c_6\sigma_{22} + c_7\sigma_{33} =$$

$$= \frac{1}{2}\left\{2c_1\sigma_{11}{}^2 + 2c_2\sigma_{22}{}^2 + (2c_1 + 2c_2 - 2c_3)\sigma_{33}{}^2 - 2(2c_1 - c_3)\sigma_{11}\sigma_{33}\right\} +$$

$$+ \frac{1}{2}\left\{-2(2c_2 - c_3)\sigma_{22}\sigma_{33} - 2c_3\sigma_{11}\sigma_{22} + 2c_4\sigma_{12}^2\right\} +$$

$$+ c_5\sigma_{11} + c_6\sigma_{22} + c_7\sigma_{33} = \frac{1}{2}\sigma_{ij}W_{ijkl}\sigma_{kl} + V_{ij}\sigma_{ij} =$$

$$= \frac{1}{2}\boldsymbol{\sigma} : \boldsymbol{W} : \boldsymbol{\sigma} + \boldsymbol{V} : \boldsymbol{\sigma}$$

where

$W_{1111} = 2c_1$,

$W_{2222} = 2c_2$,

$W_{3333} = 2c_1 + 2c_2 - 2c_3$,

$W_{1133} = W_{3311} = c_3 - 2c_1$,

$W_{2233} = W_{3322} = c_3 - 2c_2$,

$W_{1122} = W_{2211} = -c_3$,

$W_{1212} = W_{1221} = W_{2112} = W_{2121} = c_4/2$,

$$V = \begin{pmatrix} c_5 & 0 & 0 \\ 0 & c_6 & 0 \\ 0 & 0 & c_7 \end{pmatrix}.$$

In this case

$$\frac{\partial f(\boldsymbol{\sigma})}{\partial \boldsymbol{\sigma}} = \boldsymbol{W} : \boldsymbol{\sigma} + \boldsymbol{V}. \tag{3.10}$$

3.3. The Hoffman material model in matrix notation

As was shown in Chapter 2, the HYPLAS program (de Souza Neto *et al.* 2003) uses matrix and vector notations. So, the same data structure should be used in order to numerically implement the model (3.1)-(3.6) in HYPLAS.

For example, the three-dimensional elasticity relationship for orthotropic materials in matrix notation is:

$$\begin{pmatrix} \sigma_{11} \\ \sigma_{22} \\ \sigma_{33} \\ \sigma_{12} \\ \sigma_{13} \\ \sigma_{23} \end{pmatrix} = \begin{pmatrix} B_{11} & B_{12} & B_{13} & 0 & 0 & 0 \\ B_{12} & B_{22} & B_{23} & 0 & 0 & 0 \\ B_{13} & B_{23} & B_{33} & 0 & 0 & 0 \\ 0 & 0 & 0 & B_{44} & 0 & 0 \\ 0 & 0 & 0 & 0 & B_{55} & 0 \\ 0 & 0 & 0 & 0 & 0 & B_{66} \end{pmatrix} \begin{pmatrix} \varepsilon^e_{11} \\ \varepsilon^e_{22} \\ \varepsilon^e_{33} \\ \varepsilon^e_{12} \\ \varepsilon^e_{13} \\ \varepsilon^e_{23} \end{pmatrix}.$$

However, for the plane strain or axisymmetric cases this relation in matrix notation has to be amended:

$$\boldsymbol{\sigma} = \mathbf{D}\boldsymbol{\varepsilon}^{\mathbf{e}},$$

where

$$\boldsymbol{\sigma} = \begin{pmatrix} \sigma_{11} \\ \sigma_{22} \\ \sigma_{12} \\ \sigma_{33} \end{pmatrix},$$

$$\boldsymbol{\varepsilon}^{\mathbf{e}} = \begin{pmatrix} \varepsilon_{11}^{e} \\ \varepsilon_{22}^{e} \\ \varepsilon_{12}^{e} \\ \varepsilon_{33}^{e} \end{pmatrix},$$

$$\mathbf{D} = \begin{pmatrix} B_{11} & B_{12} & 0 & B_{13} \\ B_{12} & B_{22} & 0 & B_{23} \\ 0 & 0 & B_{44} & 0 \\ B_{13} & B_{23} & 0 & B_{33} \end{pmatrix}.$$

Furthermore, in matrix notation the Hoffman yield function (3.3) will appear as

$$F(\sigma,k) = \frac{1}{2}\boldsymbol{\sigma}^{\mathrm{T}}\mathbf{P}\boldsymbol{\sigma} + \mathbf{q}^{\mathrm{T}}\boldsymbol{\sigma} - \sigma_Y^2(k),$$

where

$$\mathbf{P} = \begin{pmatrix} 2c_1 & -c_3 & 0 & -2c_1 + c_3 \\ -c_3 & 2c_2 & 0 & -2c_2 + c_3 \\ 0 & 0 & 2c_4 & 0 \\ -2c_1 + c_3 & -2c_2 + c_3 & 0 & 2c_1 + 2c_2 - 2c_3 \end{pmatrix},$$

$$\mathbf{q} = \begin{pmatrix} c_5 \\ c_6 \\ 0 \\ c_7 \end{pmatrix}.$$

Finally, expression (3.10) for the tensor derivative should be put in matrix form in order to rewrite the associative flow rule (3.5) in matrix form. It is easy to see that

$$W:\sigma=\begin{pmatrix} 2c_1\sigma_{11}+(c_3-2c_1)\sigma_{33}-c_3\sigma_{22} & c_4\sigma_{12} & 0 \\ c_4\sigma_{12} & \begin{matrix}2c_2\sigma_{22}+\\ +(c_3-2c_2)\sigma_{33}-\\ -c_2\sigma_{11}\end{matrix} & 0 \\ 0 & 0 & \begin{matrix}(2c_1+2c_2-2c_3)\sigma_{33}+\\ +(c_3-2c_1)\sigma_{11}+\\ +(c_3-2c_2)\sigma_{22}\end{matrix} \end{pmatrix}.$$

In matrix notation the inner tensor product $W:\sigma$ corresponds to a matrix vector product $\mathbf{S}\sigma$, where

$$\mathbf{S}=\begin{pmatrix} 2c_1 & -c_3 & 0 & -2c_1+c_3 \\ -c_3 & 2c_2 & 0 & -2c_2+c_3 \\ 0 & 0 & c_4 & 0 \\ -2c_1+c_3 & -2c_2+c_3 & 0 & 2c_1+2c_2-2c_3 \end{pmatrix}.$$

It is evident that the vector $\mathbf{q}$ corresponds to a second order tensor V. That is why the right part of the derivative (3.10) may be rewritten in matrix notation as $S\sigma+q$.

Chapter 4. Computational implementation of the Hoffman material model

Due to the mathematical complexity of the flow theory the exact solution of boundary value problems of practical engineering interest can be obtained under very simple conditions only. The existing analytical solutions are normally restricted to perfectly plastic models and are used for the determination of limit loads and steady plastic flow of bodies with quite simple geometries (de Souza Neto *et al.* 2003). That is why the analysis of the elasto-plastic behaviour of structures under realistic conditions requires the creation of adequate numerical methods that produce solution within reasonable accuracy. In this project the finite element method is used in this context. This method is the most commonly adopted for the solution of elasto-plastic problems and is used by the majority of commercial software packages for elasto-plastic stress analysis.

This chapter is dedicated to a detailed description of 2 main numerical subroutines - state update SUHF and tangent computation CTHF. These procedures must be added to the existing HYPLAS code (de Souza Neto *et al.* 2003) in order to obtain the finite element solution of small strain plasticity problem for the Hoffman material model.

There are also 3 other material-related subroutines to be coded: data input RDHF; switching / initialisation SWHF and output ORHF.

All these 5 procedures were briefly described in Section 2.2.

4.1. State update procedure SUHF and the integration algorithm

As was mentioned in the second chapter, the state update procedure is a material level subroutine. It uses kinematic variables computed at the element level to update stress and other state variables at every Gauss point of the element and returns it to the element level to assemble an element internal force vector.

If the material model is path dependent then the stress tensor is no longer a function of the instantaneous value of the infinitesimal strain only. It is dependent on the whole history of strains to which the solid body has been subjected and the analytical solutions of the initial value problems are generally unknown for complex deformation paths.

For the general path-dependant case the state update procedure defines an incremental constitutive function within the typical (pseudo-) time increment $[t_n, t_{n+1}]$ (de Souza Neto *et al.* 2003):

$$\sigma_{n+1} = \hat{\sigma}(\alpha_n, \varepsilon_{n+1}), \tag{4.1}$$

where

n is the iteration number of the global Newton-Raphson structural iteration scheme for the fixed load incrementation step;

α_n is the set of internal variables of the converged state at t_n;

ε_{n+1} is the given strain at the end of the interval t_{n+1};

σ_{n+1} is the stress at the end of the interval t_{n+1}.

The outcome σ_{n+1} must tend to the exact solution of the actual evolution problem with vanishingly small strain increments.

The incremental constitutive function (4.1) may be also expressed in the equivalent form

$$\sigma_{n+1} = \hat{\sigma}(\alpha_n, \Delta\varepsilon), \tag{4.2}$$

where

$\Delta\varepsilon \equiv \varepsilon_{n+1} - \varepsilon_n$ is the incremental strain.

The numerical constitutive law (4.1) is non-linear and path-dependant within one argument. That is, within each increment σ_{n+1} is a function of ε_{n+1} alone (α_n is constant within $[t_n, t_{n+1}]$), analogous to a non-elastic law. The integration algorithm also defines a similar incremental constitutive function for the internal variables of the model:

$$\alpha_{n+1} = \hat{\alpha}(\alpha_n, \varepsilon_{n+1}). \tag{4.3}$$

The incremental constitutive functions (4.1), (4.3) are defined by the integration algorithm adopted and the stress delivered by (4.1) is used to assemble the element internal force vector.

The operator split method and elastic predictor / plastic corrector algorithm described below were used as the integration algorithm of the state update procedure SUHF for the Hoffman material model.

4.1.1. The general operator split method

The additive decomposition of the total strain into elastic and plastic contributions makes algorithms based on the so-called operator split methodology particularly suitable to integrate numerically the initial value problem of elastoplasticity. The basic idea underlying the operator split algorithm is illustrated by taking the initial value problem following an example provided in texts by de Souza Neto *et al.* (2003) and Simo and Hughes (1987).

Let $\boldsymbol{A}$ be a linear operator (tensor) in the space of vectors in $\Re^m$ and assume that $\boldsymbol{A}$ can be split additively as $\boldsymbol{A} = \boldsymbol{B} + \boldsymbol{C}$. The basic initial value problem is the following:

Problem A. Find the vector-valued function $\boldsymbol{x}(t)$ that satisfies the differential equation

$$\dot{\boldsymbol{x}}(t) = \boldsymbol{A}\boldsymbol{x}(t)$$

with the initial conditions

$$\boldsymbol{x}(t_0) = \boldsymbol{x}_0 .$$

The analytical solution to Problem A (Hirsh and Smale, 1974) is given by the expression

$$\boldsymbol{x}(t) = \exp[(t - t_0)\boldsymbol{A}]\boldsymbol{x}_0 ,$$

where $\exp[\cdot]$ denotes the tensor exponential of $[\cdot]$. Thus at the time $t_0 + \Delta t$ the exact value of $x(t)$ appears as follows:

$$\boldsymbol{x}(t_0 + \Delta t) = \exp[\Delta t \boldsymbol{A}]\boldsymbol{x}_0 = \exp[\Delta t(\boldsymbol{B} + \boldsymbol{C})]\boldsymbol{x}_0 . \tag{4.4}$$

The numerical approximation to the exact solution $\boldsymbol{x}(t_0 + \Delta t)$ at a point $t_0 + \Delta t$ can be derived by splitting Problem A into the following sequence of two problems B and C.

Problem B. Find the vector-valued function $\boldsymbol{y}(t)$ that satisfies the differential equation

$$\dot{\boldsymbol{y}}(t) = \boldsymbol{B}\boldsymbol{y}(t)$$

with the initial condition

$$\boldsymbol{y}(t_0) = \boldsymbol{x}_0 .$$

Problem B is solved first and its exact solution at the time $t_0 + \Delta t$ appears as follows:

$$y(t_0 + \Delta t) = \exp[\Delta t \boldsymbol{B}]\boldsymbol{x}_0 .$$

Problem C. Find the vector-valued function $x(t)$ that satisfies the differential equation

$$\dot{\boldsymbol{x}}(t) = \boldsymbol{C}\boldsymbol{x}(t)$$

with the initial condition

$$\boldsymbol{x}(t_0) = \boldsymbol{y}(t_0 + \Delta t).$$

The solution $\boldsymbol{y}(t_0 + \Delta t)$ to Problem B is taken as an initial condition in Problem C, whose exact solution is

$$\boldsymbol{x}(t_0 + \Delta t) = \exp[\Delta t \boldsymbol{C}]\exp[\Delta t \boldsymbol{B}]\boldsymbol{x}_0 . \tag{4.5}$$

Formula (4.5) provides a first order accurate approximation to the exact expression (4.4), i.e. the difference between the exact value of $\boldsymbol{x}(t_0 + \Delta t)$ and its operator split approximation vanishes faster than the interval Δt. However, expression (4.5) is exact if tensors $\boldsymbol{B}$ and $\boldsymbol{C}$ commute.

So, a first order accurate (in the sense of time discretisation) algorithm for the numerical solution of the Problem A, can be obtained by splitting the original problem into a sequence of the two subproblems B and C. The resulting operator split algorithm comprises the following steps:

1. Solve Problem B, whose initial condition is that of the original Problem A.
2. Solve problem C, taking the solution of Problem B as initial condition. The solution to Problem C is a numerical approximation to the solution of the problem A.

This operator split idea remains valid when the operator $\boldsymbol{A}$ is non-linear. There were exact solutions to subproblems B and C used in the considered algorithm. However, upon construction of a first order accurate operator split algorithm it is required that the adopted solutions to the associated subproblems be only first order accurate.

Application of the above operator split algorithm to a numerical solution of the elasto-plastic problem can be found below in Section 4.1.2.

4.1.2. Elastic predictor / plastic corrector algorithm

Following the operator split concept introduced in Section 4.1.1 an elastic predictor / plastic corrector algorithm for numerical integration of the elasto-plastic constitutive equations is derived below following the text book by de Souza

Neto *et al.* (2003). The name of this algorithm means that the original initial problem of elastoplasticity will be split in two: the elastic predictor and the plastic corrector.

It is worth reminding that the state update procedure updates stresses and hardening parameters at an element's Gauss point for the incremental strain $\Delta\varepsilon$ at this point.

The main assumption of the elastic predictor problem is that the given incremental strain $\Delta\varepsilon$ corresponding to a typical (pseudo-) time increment $[t_n, t_{n+1}]$ is purely elastic. Hence, no plastic flow or hardening occurs. The state variables $\{\varepsilon_n^e, \bar{\varepsilon}_n^p\}$ are also given at the time t_n,

The solution of this linear elastic predictor problem at time t_{n+1} is evident and is denoted with superscript "*trial*" and subscript "$n+1$". It is easy to see that the elastic trial strain, plastic trial strain and trial accumulated plastic strain appear as follows:

$$\varepsilon_{n+1}^{e\ trial} = \varepsilon_n^e + \Delta\varepsilon, \tag{4.6}$$

$$\varepsilon_{n+1}^{p\ trial} = \varepsilon_n^p, \tag{4.7}$$

$$\bar{\varepsilon}_{n+1}^{p\ trial} = \bar{\varepsilon}_n^p. \tag{4.8}$$

The corresponding trial stress is computed by the expression

$$\sigma_{n+1}^{trial} = \boldsymbol{C} : \varepsilon_{n+1}^{e\ trial}. \tag{4.9}$$

Having the elastic predictor problem solved, two alternatives can be faced: either the obtained solution is plastically admissible or not.

The solution is plastically admissible if σ_{n+1}^{trial} lies inside the trial yield surface, i.e. $F\left(\sigma_{n+1}^{trial}, k\left(\bar{\varepsilon}_n^p\right)\right) \leq 0$. This means that the state update procedure has already provided the required solution (4.6)-(4.9). Note that for the pure elastic state $\Delta\lambda = 0$.

If σ_{n+1}^{trial} lies outside the trial yield surface, i.e. $F\left(\sigma_{n+1}^{trial}, k\left(\bar{\varepsilon}_n^p\right)\right) > 0$, it can not be the problem's solution and the following plastic corrector algorithm (return mapping procedure) has to be applied.

As was mentioned above, the operator split methodology requires that each of the associated subproblems be solved by a first order accurate algorithm only. One of the choices of numerical integration procedures is a fully implicit backward Euler scheme to discretise the plastic corrector equations.

The following system was obtained after application of this discretisation scheme to the constitutive material model:

$$\begin{cases} \boldsymbol{\varepsilon}^{e}_{n+1} = \boldsymbol{\varepsilon}^{e\ trial}_{n+1} - \Delta\lambda_{n+1} \left.\dfrac{\partial F\left(\boldsymbol{\sigma}, \bar{\varepsilon}^{p}\right)}{\partial \boldsymbol{\sigma}}\right|_{n+1} \\ \Delta\boldsymbol{\varepsilon}^{p} = \Delta\lambda_{n+1} \left.\dfrac{\partial F\left(\boldsymbol{\sigma}, \bar{\varepsilon}^{p}\right)}{\partial \boldsymbol{\sigma}}\right|_{n+1} \\ \bar{\varepsilon}^{p}_{n+1} = \bar{\varepsilon}^{p}_{n} + \sqrt{2\Delta\varepsilon^{p}_{ij}\Delta\varepsilon^{p}_{ij}/3} \\ f\left(\boldsymbol{\sigma}_{n+1}\right) - \sigma^{2}_{Y}\left(\bar{\varepsilon}^{p}_{n+1}\right) = 0 \\ \boldsymbol{\sigma}_{n+1} = \boldsymbol{C} : \boldsymbol{\varepsilon}^{e}_{n+1} \end{cases} \tag{4.10}$$

which has to be solved for $\boldsymbol{\varepsilon}^{e}_{n+1}$, $\bar{\varepsilon}^{p}_{n+1}$, $\boldsymbol{\sigma}_{n+1}$ and $\Delta\lambda_{n+1}$; and where $\Delta\lambda_{n+1} = \lambda_{n+1} - \lambda_{n}$.

The above system (4.10) written in a matrix notation will appear as follows

$$\begin{cases} \boldsymbol{\varepsilon}^{e}_{n+1} = \boldsymbol{\varepsilon}^{e\ trial}_{n+1} - \Delta\lambda_{n+1}\left(\mathbf{S}\boldsymbol{\sigma}_{n+1} + \mathbf{q}\right) \\ \Delta\boldsymbol{\varepsilon}^{p}_{n+1} = \Delta\lambda_{n+1}\left(\mathbf{S}\boldsymbol{\sigma}_{n+1} + \mathbf{q}\right) \\ \bar{\boldsymbol{\varepsilon}}^{p}_{n+1} = \bar{\boldsymbol{\varepsilon}}^{p}_{n} + \sqrt{2\left(\Delta\boldsymbol{\varepsilon}^{p}\right)^{\mathrm{T}}\mathbf{Z}\left(\Delta\boldsymbol{\varepsilon}^{p}\right)/3}, \\ f\left(\boldsymbol{\sigma}_{n+1}\right) - \sigma^{2}_{Y}\left(\bar{\boldsymbol{\varepsilon}}^{p}_{n+1}\right) = 0 \\ \boldsymbol{\sigma}_{n+1} = \mathbf{D}\boldsymbol{\varepsilon}^{e}_{n+1} \end{cases} \tag{4.11}$$

where

$$\boldsymbol{\varepsilon}^{e\ trial} = \begin{pmatrix} \varepsilon^{e\ trial}_{11} \\ \varepsilon^{e\ trial}_{22} \\ \varepsilon^{e\ trial}_{12} \\ \varepsilon^{e\ trial}_{33} \end{pmatrix};$$

$$\Delta\boldsymbol{\varepsilon}^{p} = \begin{pmatrix} \Delta\varepsilon^{p}_{11} \\ \Delta\varepsilon^{p}_{22} \\ \Delta\varepsilon^{p}_{12} \\ \Delta\varepsilon^{p}_{33} \end{pmatrix};$$

$$\mathbf{Z} = \begin{pmatrix} 1 & 0 & 0 & 0 \\ 0 & 1 & 0 & 0 \\ 0 & 0 & 2 & 0 \\ 0 & 0 & 0 & 1 \end{pmatrix}.$$

In particular, the discrete analogue of expression (3.5) appears as follows:

$$\Delta\boldsymbol{\varepsilon}^{p}_{n+1} = \Delta\lambda_{n+1}\left(\mathbf{S}\boldsymbol{\sigma}_{n+1} + \mathbf{q}\right).$$

Having applied the Euler discretisation scheme to the definition (3.4) of the accumulated plastic strain for a plane strain / axisymmetric problem one gets:

$$\Delta\bar{\varepsilon}^p_{n+1} = \bar{\varepsilon}^p_{n+1} - \bar{\varepsilon}^p_n = \sqrt{\frac{2}{3}}\left\|\Delta\varepsilon^p\right\| = \sqrt{\frac{2\Delta\varepsilon^p_{ij}\Delta\varepsilon^p_{ij}}{3}} = \tag{4.12}$$
$$= \sqrt{\frac{2\left(\Delta\varepsilon^p_{11}\Delta\varepsilon^p_{11} + \Delta\varepsilon^p_{22}\Delta\varepsilon^p_{22} + 2\Delta\varepsilon^p_{12}\Delta\varepsilon^p_{12} + \Delta\varepsilon^p_{33}\Delta\varepsilon^p_{33}\right)}{3}}.$$

That is why the $\mathbf{Z}$ matrix has to be used to provide $2\Delta\varepsilon^p_{12}\Delta\varepsilon^p_{12}$ in the norm expression in the second equation of system (4.11).

The point is that each of systems (4.10) or (4.11) is very difficult to solve as they consist of four equations. It is possible, however, to reduce them to one nonlinear equation in terms of one scalar unknown $\Delta\lambda_{n+1}$. This will be shown in Section 4.1.3.

4.1.3. Reducing the discrete system to a single equation

In this section it will be proved that system (4.11) can be reduced to one nonlinear equation in terms of one scalar unknown $\Delta\lambda_{n+1}$. So, $\boldsymbol{\varepsilon}^e_{n+1}$, $\bar{\boldsymbol{\varepsilon}}^p_{n+1}$, $\boldsymbol{\sigma}_{n+1}$ has to be expressed via $\Delta\lambda_{n+1}$.

By definition,

$$\boldsymbol{\varepsilon}^e_{n+1} = \boldsymbol{\varepsilon}^e_n + \Delta\boldsymbol{\varepsilon}^e = \boldsymbol{\varepsilon}^e_n + \Delta\boldsymbol{\varepsilon} - \Delta\boldsymbol{\varepsilon}^p_{n+1} = \boldsymbol{\varepsilon}^{e\ trial}_{n+1} - \Delta\lambda_{n+1}\left(\mathbf{S}\boldsymbol{\sigma}_{n+1} + \mathbf{q}\right) \tag{4.13}$$

From expression (4.13) for elastic strain vector and from the linear elastic law it follows that

$$\boldsymbol{\sigma}_{n+1} = \mathbf{D}\boldsymbol{\varepsilon}^e_{n+1} = \mathbf{D}\left(\boldsymbol{\varepsilon}^{e\ trial}_{n+1} - \Delta\lambda_{n+1}\left(\mathbf{S}\boldsymbol{\sigma}_{n+1} + \mathbf{q}\right)\right) = \boldsymbol{\sigma}^{trial}_{n+1} - \Delta\lambda_{n+1}\mathbf{D}\left(\mathbf{S}\boldsymbol{\sigma}_{n+1} + \mathbf{q}\right).$$

So, an expression for $\boldsymbol{\sigma}^{trial}_{n+1}$ can be written as follows:

$$\boldsymbol{\sigma}^{trial}_{n+1} = \boldsymbol{\sigma}_{n+1} + \Delta\lambda_{n+1}\mathbf{D}\left(\mathbf{S}\boldsymbol{\sigma}_{n+1} + \mathbf{q}\right) = \boldsymbol{\sigma}_{n+1} + \Delta\lambda_{n+1}\mathbf{D}\mathbf{S}\boldsymbol{\sigma}_{n+1} + \Delta\lambda_{n+1}\mathbf{D}\mathbf{q} =$$
$$= \left(\mathbf{I}_{4\times4} + \Delta\lambda_{n+1}\mathbf{D}\mathbf{S}\right)\boldsymbol{\sigma}_{n+1} + \Delta\lambda_{n+1}\mathbf{D}\mathbf{q},$$

where

$$\mathbf{I} = \begin{pmatrix} 1 & 0 & 0 & 0 \\ 0 & 1 & 0 & 0 \\ 0 & 0 & 1 & 0 \\ 0 & 0 & 0 & 1 \end{pmatrix}.$$

Hence, an expression for $\boldsymbol{\sigma}_{n+1}$ via $\Delta\lambda_{n+1}$ appears as follows:

$$\boldsymbol{\sigma}_{n+1}(\Delta\lambda_{n+1}) = (\mathbf{I} + \Delta\lambda_{n+1}\mathbf{DS})^{-1}\left(\boldsymbol{\sigma}_{n+1}^{trial} - \Delta\lambda_{n+1}\boldsymbol{Dq}\right). \tag{4.14}$$

The following expression may be obtained after using expressions (4.12) and (4.13) together :

$$\Delta\bar{\varepsilon}_{n+1}^{p} = \Delta\lambda_{n+1}\sqrt{\frac{2(\mathbf{S}\boldsymbol{\sigma}_{n+1} + \mathbf{q})^{T}\mathbf{Z}(\mathbf{S}\boldsymbol{\sigma}_{n+1} + \mathbf{q})}{3}}. \tag{4.15}$$

It was proved in Chapter 3 that the last equation $f(\boldsymbol{\sigma}_{n+1}) - \sigma_Y^2(\bar{\varepsilon}_{n+1}^{p}) = 0$ of system (4.11) can be rewritten in matrix form in the following way

$$F(\boldsymbol{\sigma}, k) = \frac{1}{2}\boldsymbol{\sigma}^{T}\mathbf{P}\boldsymbol{\sigma} + \mathbf{q}^{T}\boldsymbol{\sigma} - \sigma_Y^2\left(\Delta\bar{\boldsymbol{\varepsilon}}_{n+1}^{p} + \bar{\boldsymbol{\varepsilon}}_{n}^{p}\right) = 0. \tag{4.16}$$

Finally, substituting expressions (4.14) and (4.15) into expression (4.16) one gets one nonlinear equation in terms of one scalar unknown $\Delta\lambda_{n+1}$:

$$\begin{aligned}\frac{1}{2}\left[(\mathbf{I} + \Delta\lambda_{n+1}\mathbf{DS})^{-1}\left(\boldsymbol{\sigma}_{n+1}^{trial} - \Delta\lambda_{n+1}\mathbf{Dq}\right)\right]^{T}\mathbf{P}(\mathbf{I} + \Delta\lambda_{n+1}\mathbf{DS})^{-1}\left(\boldsymbol{\sigma}_{n+1}^{trial} - \Delta\lambda_{n+1}\mathbf{Dq}\right) + \\ + \mathbf{q}^{T}(\mathbf{I} + \Delta\lambda_{n+1}\mathbf{DS})^{-1}\left(\boldsymbol{\sigma}_{n+1}^{trial} - \Delta\lambda_{n+1}\mathbf{Dq}\right) - \\ - \sigma_Y^2\left(\bar{\epsilon}_{n}^{p} + \sqrt{2/3}\cdot\Delta\lambda_{n+1}\sqrt{(\mathbf{S}\boldsymbol{\sigma}(\Delta\lambda_{n+1}) + \mathbf{q})^{T}\mathbf{Z}(\mathbf{S}\boldsymbol{\sigma}(\Delta\lambda_{n+1}) + \mathbf{q})}\right) = 0.\end{aligned} \tag{4.17}$$

For the sake of convenience equation (4.17) was denoted in the following way:

$$\Psi(\Delta\lambda_{n+1}) = f(\boldsymbol{\sigma}_{n+1}) - \sigma_Y^2(\bar{\boldsymbol{\varepsilon}}_{n+1}^{p}) = 0. \tag{4.18}$$

So, it was proved that the system (4.11) can be reduced to one single equation (4.18). As this equation is nonlinear, a numerical method has to be applied to its solution. This method will be described below.

4.1.4. A Newton-Raphson iteration scheme

To solve equation (4.18) the Newton-Raphson iteration scheme will be used. This choice was motivated by its quadratic rate of convergence, which results in a very computationally efficient return mapping procedure.

However, in case that the degree of non-linearity of the plasticity model is very high, the convergence radius of this method becomes relatively small which may lead to physically inappropriate solutions such as $\Delta\lambda_{n+1} < 0$. It means that the method depends critically on an initial guess of the root. To decrease this dependence, i.e. to increase the convergence radius, a line search procedure (Dutko *et al.* 1993) can be incorporated within the Newton method procedure. The designed line search algorithm is described in Section 4.1.5.

A general Newton-Raphson iteration scheme for solving equation (4.18) appears as follows:

$$\Delta\lambda_{n+1}^{(i+1)} = \Delta\lambda_{n+1}^{(i)} - \frac{\Psi\left(\Delta\lambda_{n+1}^{(i)}\right)}{\left[\frac{d\Psi\left(\Delta\lambda_{n+1}\right)}{d\left(\Delta\lambda_{n+1}\right)}\right]_i}, \tag{4.19}$$

where i denotes the iteration number.

To use the scheme (4.19) the corresponding derivative must be obtained. Having used the chain derivation rule one gets:

$$\left.\frac{d\Psi\left(\Delta\lambda_{n+1}\right)}{d\left(\Delta\lambda_{n+1}\right)}\right|_i = \left.\frac{df(\boldsymbol{\sigma})}{d\boldsymbol{\sigma}} \cdot \frac{\partial\boldsymbol{\sigma}}{\partial\left(\Delta\lambda_{n+1}\right)}\right|_i - \left.\frac{d\sigma_Y^2\left(\bar{\boldsymbol{\varepsilon}}^p\right)}{d\bar{\boldsymbol{\varepsilon}}^p}\frac{\partial\bar{\boldsymbol{\varepsilon}}^p}{\partial\Delta\lambda_{n+1}}\right|_i. \tag{4.20}$$

To calculate the derivative (4.20) the derivative $\left.\frac{\partial\boldsymbol{\sigma}}{\partial\left(\Delta\lambda_{n+1}\right)}\right|_i$ must be obtained.

From expression (4.14) it follows that

$$\left(\mathbf{I} + \Delta\lambda_{n+1}^{(i)}\mathbf{DS}\right)\boldsymbol{\sigma}_{n+1}^{(i)}\left(\Delta\lambda_{n+1}^{(i)}\right) = \boldsymbol{\sigma}_{n+1}^{trial} - \Delta\lambda_{n+1}^{(i)}\mathbf{Dq}. \tag{4.21}$$

Having differentiated equation (4.21) one gets:

$$\mathbf{DS}\boldsymbol{\sigma}_{n+1}^{(i)}\left(\Delta\lambda_{n+1}^{(i)}\right) + \left(\mathbf{I} + \Delta\lambda_{n+1}^{(i)}\mathbf{DS}\right)\left.\frac{\partial\boldsymbol{\sigma}}{\partial\left(\Delta\lambda_{n+1}\right)}\right|_i = -\mathbf{Dq}.$$

Finally,

$$\left.\frac{\partial\boldsymbol{\sigma}_{n+1}}{\partial\left(\Delta\lambda_{n+1}\right)}\right|_i = -\left(\mathbf{I} + \Delta\lambda_{n+1}^{(i)}\mathbf{DS}\right)^{-1}\mathbf{D}\left(\mathbf{S}\boldsymbol{\sigma}_{n+1}^{(i)} + \mathbf{q}\right). \tag{4.22}$$

The second product term of expression (4.20) can also be found by using the chain rule:

$$\left.\frac{d\sigma_Y^2\left(\bar{\boldsymbol{\varepsilon}}_{n+1}^p\right)}{d\bar{\boldsymbol{\varepsilon}}_{n+1}^p}\frac{\partial\bar{\boldsymbol{\varepsilon}}_{n+1}^p}{\partial\left(\Delta\lambda_{n+1}\right)}\right|_i = \left.\left[2\sigma_Y\left(\bar{\epsilon}_{n+1}^p\right)\frac{d\sigma_Y\left(\bar{\boldsymbol{\varepsilon}}_{n+1}^p\right)}{d\bar{\boldsymbol{\varepsilon}}_{n+1}^p}\frac{\partial\bar{\boldsymbol{\varepsilon}}_{n+1}^p}{\partial\left(\Delta\lambda_{n+1}\right)}\right]\right|_i. \tag{4.23}$$

It easy to see that

$$\left.\frac{\partial\bar{\boldsymbol{\varepsilon}}_{n+1}^p}{\partial\left(\Delta\lambda_{n+1}\right)}\right|_i = \frac{\partial\left(\bar{\boldsymbol{\varepsilon}}_n^p + \sqrt{2/3}\cdot\Delta\lambda_{n+1}^{(i)}\sqrt{\left(\mathbf{S}\boldsymbol{\sigma}_{n+1}^{(i)} + \mathbf{q}\right)^{\mathrm{T}}\mathbf{Z}\left(\mathbf{S}\boldsymbol{\sigma}_{n+1}^{(i)} + \mathbf{q}\right)}\right)}{\partial\left(\Delta\lambda_{n+1}\right)} = \sqrt{\frac{2}{3}}\frac{\partial\left(\Delta\lambda_{n+1}^{(i)}\sqrt{\left(\mathbf{S}\boldsymbol{\sigma}_{n+1}^{(i)} + \mathbf{q}\right)^{\mathrm{T}}\mathbf{Z}\left(\mathbf{S}\boldsymbol{\sigma}_{n+1}^{(i)} + \mathbf{q}\right)}\right)}{\partial\left(\Delta\lambda_{n+1}\right)} =$$

$$= \sqrt{\frac{2}{3}}\left(\sqrt{\left(\mathbf{S}\boldsymbol{\sigma}_{n+1}^{(i)} + \mathbf{q}\right)^{\mathrm{T}}\mathbf{Z}\left(\mathbf{S}\boldsymbol{\sigma}_{n+1}^{(i)} + \mathbf{q}\right)} + \Delta\lambda_{n+1}^{(i)}\frac{\partial\left(\sqrt{\left(\mathbf{S}\boldsymbol{\sigma}_{n+1}^{(i)} + \mathbf{q}\right)^{\mathrm{T}}\mathbf{Z}\left(\mathbf{S}\boldsymbol{\sigma}_{n+1}^{(i)} + \mathbf{q}\right)}\right)}{\partial\left(\Delta\lambda_{n+1}\right)}\right) =$$

$$=\sqrt{\frac{2}{3}}\left(\sqrt{\left(\mathbf{S}\boldsymbol{\sigma}_{n+1}^{(i)}+\mathbf{q}\right)^{\mathrm{T}}\mathbf{Z}\left(\mathbf{S}\boldsymbol{\sigma}_{n+1}^{(i)}+\mathbf{q}\right)}+\Delta\lambda_{n+1}^{(i)}\frac{1}{2\sqrt{\left(\mathbf{S}\boldsymbol{\sigma}_{n+1}^{(i)}+\mathbf{q}\right)^{\mathrm{T}}\mathbf{Z}\left(\mathbf{S}\boldsymbol{\sigma}_{n+1}^{(i)}+\mathbf{q}\right)}}\frac{\partial\left(\left(\mathbf{S}\boldsymbol{\sigma}_{n+1}^{(i)}+\mathbf{q}\right)^{\mathrm{T}}\mathbf{Z}\left(\mathbf{S}\boldsymbol{\sigma}_{n+1}^{(i)}+\mathbf{q}\right)\right)}{\partial\left(\Delta\lambda_{n+1}\right)}\right)$$

The derivative of the following expression was calculated separately:

$$\frac{\partial\left(\left(\mathbf{S}\boldsymbol{\sigma}_{n+1}^{(i)}+\mathbf{q}\right)^{\mathrm{T}}\mathbf{Z}\left(\mathbf{S}\boldsymbol{\sigma}_{n+1}^{(i)}+\mathbf{q}\right)\right)}{\partial\left(\Delta\lambda_{n+1}\right)}=\frac{\partial\left(\left(\mathbf{S}\boldsymbol{\sigma}_{n+1}^{(i)}+\mathbf{q}\right)^{\mathrm{T}}\mathbf{Z}\left(\mathbf{S}\boldsymbol{\sigma}_{n+1}^{(i)}+\mathbf{q}\right)\right)}{\partial\boldsymbol{\sigma}_{n+1}^{(i)}}\cdot\left.\frac{\partial\boldsymbol{\sigma}_{n+1}}{\partial\left(\Delta\lambda_{n+1}\right)}\right|_{\mathrm{i}}.$$

To do this, the following derivative must be obtained:

$$\frac{\partial\left(\left(\mathbf{S}\boldsymbol{\sigma}_{n+1}^{(i)}+\mathbf{q}\right)^{\mathrm{T}}\mathbf{Z}\left(\mathbf{S}\boldsymbol{\sigma}_{n+1}^{(i)}+\mathbf{q}\right)\right)}{\partial\boldsymbol{\sigma}_{n+1}^{(i)}}=\frac{\partial\left(\boldsymbol{\sigma}_{n+1}^{(i)\,\mathrm{T}}\mathbf{S}^{\mathrm{T}}\mathbf{Z}\mathbf{S}\boldsymbol{\sigma}_{n+1}^{(i)}+\boldsymbol{\sigma}_{n+1}^{(i)\,\mathrm{T}}\mathbf{S}^{\mathrm{T}}\mathbf{Z}\mathbf{q}+\mathbf{q}^{\mathrm{T}}\mathbf{Z}\mathbf{S}\boldsymbol{\sigma}_{n+1}^{(i)}+\mathbf{q}^{\mathrm{T}}\mathbf{Z}\mathbf{q}\right)}{\partial\boldsymbol{\sigma}_{n+1}^{(i)}}=$$

$$=\frac{\partial\left(\boldsymbol{\sigma}_{n+1}^{(i)\,\mathrm{T}}\mathbf{S}^{\mathrm{T}}\mathbf{Z}\mathbf{S}\boldsymbol{\sigma}_{n+1}^{(i)}+\boldsymbol{\sigma}_{n+1}^{(i)\,\mathrm{T}}\mathbf{S}^{\mathrm{T}}\mathbf{Z}\mathbf{q}+\mathbf{q}^{\mathrm{T}}\mathbf{Z}\mathbf{S}\boldsymbol{\sigma}_{n+1}^{(i)}\right)}{\partial\boldsymbol{\sigma}_{n+1}^{(i)}}=2\mathbf{S}^{\mathrm{T}}\mathbf{Z}\mathbf{S}\boldsymbol{\sigma}_{n+1}^{(i)}+2\mathbf{Z}\mathbf{S}\mathbf{q}.$$

It should be mentioned that $\boldsymbol{\sigma}_{n+1}^{(i)\,\mathrm{T}}\mathbf{S}^{\mathrm{T}}\mathbf{Z}\mathbf{q}=\mathbf{q}^{\mathrm{T}}\mathbf{Z}\mathbf{S}\boldsymbol{\sigma}_{n+1}^{(i)}$ as $\mathbf{S}=\mathbf{S}^{\mathrm{T}},\mathbf{Z}=\mathbf{Z}^{\mathrm{T}}$, and $\mathbf{Z}$ is a diagonal matrix. That is why $\mathbf{SZ}=\mathbf{ZS}$.

Finally, expression (4.23) appears as follows:

$$\left.\frac{d\sigma_Y^2\left(\bar{\varepsilon}_{n+1}^p\right)}{d\bar{\varepsilon}_{n+1}^p}\frac{\partial\bar{\varepsilon}_{n+1}^p}{\partial\left(\Delta\lambda_{n+1}\right)}\right|_{\mathrm{i}}=2\sqrt{\frac{2}{3}}\sigma_Y\left(\bar{\varepsilon}_{n+1}^p\right)\left.\frac{d\sigma_Y\left(\bar{\varepsilon}_{n+1}^p\right)}{d\bar{\varepsilon}_{n+1}^p}\right|_{\mathrm{i}}\times$$

$$\times\left(\sqrt{\left(\mathbf{S}\boldsymbol{\sigma}_{n+1}^{(i)}+\mathbf{q}\right)^{\mathrm{T}}\mathbf{Z}\left(\mathbf{S}\boldsymbol{\sigma}_{n+1}^{(i)}+\mathbf{q}\right)}+\Delta\lambda_{n+1}^{(i)}\frac{\mathbf{S}^{\mathrm{T}}\mathbf{Z}\mathbf{S}\boldsymbol{\sigma}_{n+1}^{(i)}+\mathbf{Z}\mathbf{S}\mathbf{q}}{\sqrt{\left(\mathbf{S}\boldsymbol{\sigma}_{n+1}^{(i)}+\mathbf{q}\right)^{\mathrm{T}}\mathbf{Z}\left(\mathbf{S}\boldsymbol{\sigma}_{n+1}^{(i)}+\mathbf{q}\right)}}\left.\frac{\partial\boldsymbol{\sigma}_{n+1}^{(i)}}{\partial\left(\Delta\lambda_{n+1}\right)}\right|_{\mathrm{i}}\right). \tag{4.24}$$

It should be also mentioned that the derivative of function $f\left(\boldsymbol{\sigma}_{n+1}\right)=\frac{1}{2}\boldsymbol{\sigma}_{n+1\,\mathbf{n}+1}^{\mathrm{T}}\mathbf{P}\boldsymbol{\sigma}_{n+1}+\mathbf{q}^{\mathrm{T}}\boldsymbol{\sigma}_{n+1}$ is

$$\frac{df(\boldsymbol{\sigma})}{d\boldsymbol{\sigma}}=\mathbf{P}\boldsymbol{\sigma}+\mathbf{q}. \tag{4.25}$$

Having substituted expressions (4.22), (4.24) and (4.25) into equation (4.20), one obtains the derivative of function $\Psi\left(\Delta\lambda_{n+1}\right)$:

$$\left.\frac{d\Psi\left(\Delta\lambda_{n+1}\right)}{d\left(\Delta\lambda_{n+1}\right)}\right|_{i}=-\left(\mathbf{P}\boldsymbol{\sigma}_{n+1}^{(i)}+\mathbf{q}\right)\cdot\left(\mathbf{I}+\Delta\lambda_{n+1}^{(i)}\mathbf{D}\mathbf{S}\right)^{-1}\mathbf{D}\left(\mathbf{S}\boldsymbol{\sigma}_{n+1}^{(i)}+\mathbf{q}\right)-$$

$$-2\sqrt{\frac{2}{3}}\sigma_{\mathrm{Y}}\left(\bar{\varepsilon}_{n+1}^p\right)\left.\frac{d\sigma_Y\left(\bar{\varepsilon}_{n+1}^p\right)}{d\bar{\varepsilon}_{n+1}^p}\right|_{\mathrm{i}}\left(\sqrt{\left(\mathbf{S}\boldsymbol{\sigma}_{n+1}^{(i)}+\mathbf{q}\right)^{\mathrm{T}}\mathbf{Z}\left(\mathbf{S}\boldsymbol{\sigma}_{n+1}^{(i)}+\mathbf{q}\right)}\right)+$$

$$+2\sqrt{\frac{2}{3}}\sigma_{\mathrm{Y}}\left(\bar{\varepsilon}_{n+1}^p\right)\left.\frac{d\sigma_Y\left(\bar{\varepsilon}_{n+1}^p\right)}{d\bar{\varepsilon}_{n+1}^p}\right|_{\mathrm{i}}\times \tag{4.26}$$

$$\times\left(\Delta\lambda_{n+1}^{(i)}\frac{\mathbf{S}^{\mathrm{T}}\mathbf{Z}\mathbf{S}\boldsymbol{\sigma}_{n+1}^{(i)}+\mathbf{Z}\mathbf{S}\mathbf{q}}{\sqrt{\left(\mathbf{S}\boldsymbol{\sigma}_{n+1}^{(i)}+\mathbf{q}\right)^{\mathrm{T}}\mathbf{Z}\left(\mathbf{S}\boldsymbol{\sigma}_{n+1}^{(i)}+\mathbf{q}\right)}}\left(\mathbf{I}+\Delta\lambda_{n+1}^{(i)}\mathbf{D}\mathbf{S}\right)^{-1}\mathbf{D}\left(\mathbf{S}\boldsymbol{\sigma}_{n+1}^{(i)}+\mathbf{q}\right)\right)$$

Finally, the Newton-Raphson iteration scheme (4.19) may be represented as the following algorithm:

1. Set initial guess $\Delta\lambda_{n+1}^{(0)}=0$.
2. Calculate $\Psi\left(\lambda_{n+1}^{(0)}\right)=f\left(\boldsymbol{\sigma}_{n}\right)-\sigma_{Y}^{2}\left(\bar{\boldsymbol{\varepsilon}}_{n}^{p}\right)$
3. For $i=0$ to MXITER (MXITER - maximum number of iterations – HYPLAS variable)
   i. Calculate $\left[\frac{d\Psi\left(\Delta\lambda_{n+1}\right)}{d\left(\Delta\lambda_{n+1}\right)}\right]_{i}$
   ii. Calculate $\Delta\lambda_{n+1}^{(i+1)}=\Delta\lambda_{n+1}^{(i)}-\frac{\Psi\left(\Delta\lambda_{n+1}^{(i)}\right)}{\left[\frac{d\Psi\left(\Delta\lambda_{n+1}\right)}{d\left(\Delta\lambda_{n+1}\right)}\right]_{i}}$,
   iii. In order to calculate $\Psi\left(\Delta\lambda_{n+1}^{(i+1)}\right)=f\left(\boldsymbol{\sigma}_{n+1}^{(i+1)}\right)-\sigma_{Y}^{2}\left(\bar{\boldsymbol{\varepsilon}}_{n+1}^{p}\right)\Big|_{i+1}$
      1. update $\boldsymbol{\sigma}_{n+1}^{(i+1)}\left(\Delta\lambda_{n+1}^{(i+1)}\right)=\left(\mathbf{I}+\Delta\lambda_{n+1}^{(i+1)}\mathbf{D}\mathbf{S}\right)^{-1}\left(\boldsymbol{\sigma}_{n+1}^{trial}-\Delta\lambda_{n+1}^{(i+1)}\mathbf{D}\mathbf{q}\right)$
      2. update $\bar{\boldsymbol{\varepsilon}}_{n+1}^{p}\Big|_{i+1}=\bar{\boldsymbol{\varepsilon}}_{n}^{p}+\Delta\lambda_{n+1}^{(i+1)}\sqrt{\frac{2}{3}\left(\mathbf{S}\boldsymbol{\sigma}_{n+1}^{(i)}+\mathbf{q}\right)^{\mathrm{T}}\mathbf{Z}\left(\mathbf{S}\boldsymbol{\sigma}_{n+1}^{(i)}+\mathbf{q}\right)}$
   iv. Check for convergence. IF $\left|\Psi\left(\Delta\lambda_{n+1}^{(i+1)}\right)\Big/\sigma_{Y}^{2}\left(\bar{\boldsymbol{\varepsilon}}_{n+1}^{p}\right)\Big|_{i+1}\right|\le tol$ ($tol=10^{-6}$ – HYPLAS variable) THEN GOTO 4 ELSE GOTO 3
4. update solution (n is the iteration number of the global Newton-Raphson structural iteration scheme for the fixed load incrementation step)

b. $\Delta\lambda_{n+1}=\Delta\lambda_{n+1}^{(i+1)}$,

c. $\boldsymbol{\sigma}_{n+1}\left(\Delta\lambda_{n+1}\right)=\boldsymbol{\sigma}_{n+1}^{(i+1)}\left(\Delta\lambda_{n+1}^{(i+1)}\right)$,

d. $\bar{\varepsilon}^{p}_{n+1} = \bar{\varepsilon}^{p}_{n+1}\big|_{i+1}$,

e. $\boldsymbol{\varepsilon}^{e}_{n+1} = \boldsymbol{\varepsilon}^{e\ trial}_{n+1} - \Delta\lambda_{n+1}\left(\mathbf{S}\boldsymbol{\sigma}_{n+1} + \mathbf{q}\right)$.

4.1.5. A line search algorithm

There were some tests performed which have showed that the convergence radius of the Newton method depends on the degree of elastic anisotropy of the material.

If the degree of elastic anisotropy is relatively low, the typical graph of the yield function (4.18) appears as in Figure 4.1. It is evident that in this case the initial guess $\Delta\lambda^{(0)}_{n+1} = 0$ lies within the convergence radius of the Newton method and that allows to obtain a physically reasonable solution $\Delta\lambda_{n+1} \geq 0$.

On the other hand, if the degree of elastic anisotropy is relatively high (a good example of it can be found in the article by Koh *et al.* (1995)) the initial guess $\Delta\lambda^{(0)}_{n+1} = 0$ does not lie within the convergence radius of the Newton method and that results in physically wrong solutions $\Delta\lambda_{n+1} < 0$. A typical 'bad' yield function can be seen in Figures 4.2-4.4 (elastic constants are close to those used in the article by Koh *et al.* (1995) and are the following: $E_1 = 25000000 kN/m^2$, $E_2 = E_3 = 1700000 kN/m^2$, $\nu_{12} = \nu_{23} = \nu_{31} = 0.25$, $G_{12} = 500000 kN/m^2$).

A line search algorithm was designed to obtain physically reasonable solutions in such cases when the yield function is 'bad'. Moreover, this algorithm is always used in the state update procedure not only to ensure physically reasonable solutions but also to increase the convergence rate of the Newton method by providing a better initial guess.

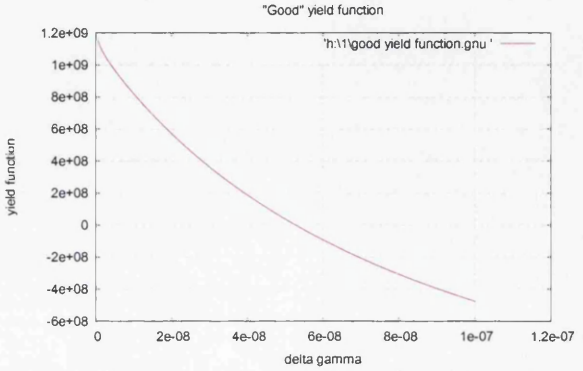

Figure 4.1. The graph of the 'good' yield function when the degree of elastic anisotropy is relatively low.

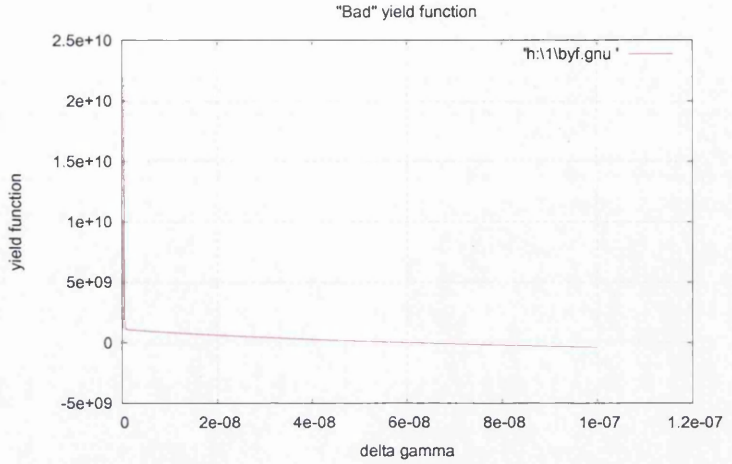

Figure 4.2. The graph of the 'bad' yield function when the degree of elastic anisotropy is relatively high

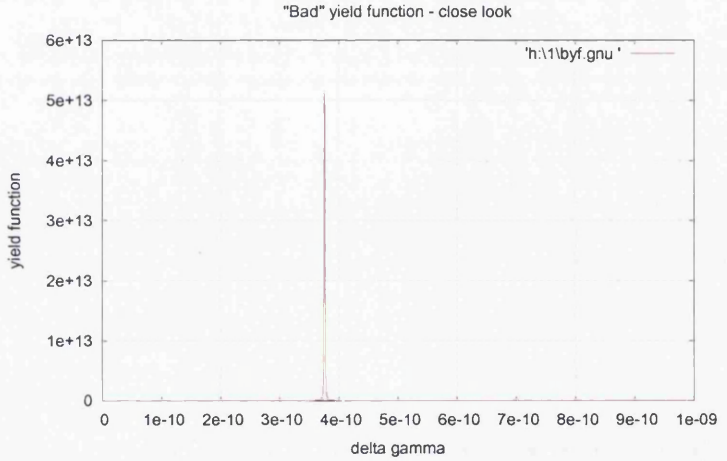

Figure 4.3. The graph of the 'bad' yield function when the degree of elastic anisotropy is relatively high (zoom in of Figure 4.2).

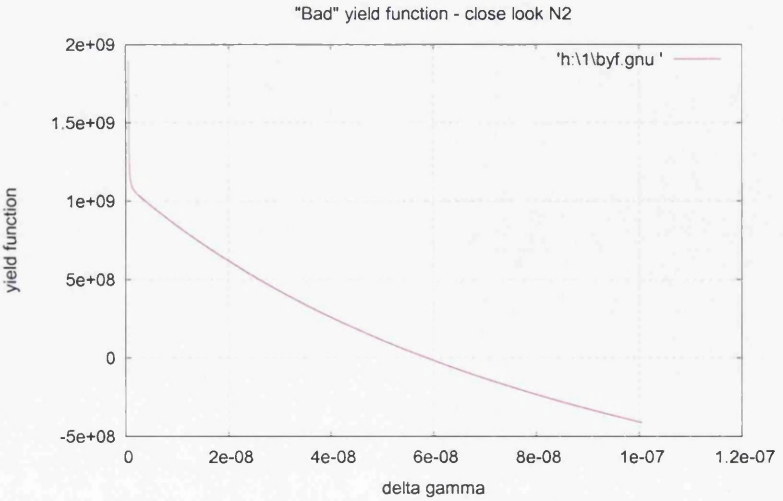

Figure 4.4. The graph of the 'bad' yield function when the degree of elastic anisotropy is relatively high (zoom in of Figure 4.2).

This algorithm consists of two parts.

First of all, a value $\Delta\lambda^*$ such that $\Psi(\Delta\lambda^*)\leq 0$ should be found. In order to do this a *step* value should be chosen and values of the yield function (4.18) at the following points: $\Delta\lambda^* = step$, $\Delta\lambda^* = 2*step$, $\Delta\lambda^* = 3*step$ and so on should be calculated until such $\Delta\lambda^*$ is found for which $\Psi(\Delta\lambda^*)\leq 0$. From expression $\Delta\boldsymbol{\varepsilon}^p_{n+1} = \Delta\lambda_{n+1}(\mathbf{S}\boldsymbol{\sigma}_{n+1} + \mathbf{q})$ it is evident that $\Delta\lambda^*$ has the order of $\frac{strain}{stress}$. That is why it was chosen

$$step = \left.\frac{\left|\varepsilon_{11}^{trial}\right| + \left|\varepsilon_{22}^{trial}\right| + \left|\varepsilon_{33}^{trial}\right| + \left|\varepsilon_{12}^{trial}\right|}{\left|\sigma_{11}^{trial}\right| + \left|\sigma_{22}^{trial}\right| + \left|\sigma_{33}^{trial}\right| + \left|\sigma_{12}^{trial}\right|}\right|_{n+1}. \tag{4.27}$$

During the second step of this line search algorithm an improved initial guess is searched using the bisection method with initial segment $[0, \Delta\lambda*]$. The dichotomy search is continued until the current segment's length becomes less than $step/15$ (a number 15 had been chosen experimentally to increase the convergence rate of the entire algorithm). The initial guess is finally equal to

$$\Delta\lambda_{n+1}^{(0)} = \frac{a+b}{2}, \tag{4.28}$$

where

a, b are the ends of the final segment.

Since two phases of this line search algorithm are completed, the Newton-Raphson iteration scheme (Section 4.1.4) with the improved initial guess (4.28) can be started.

4.1.6. Verifying accuracy of the state update procedure

Following the text book by de Souza Neto *et al.* (2003), by the term accuracy it is understood the so-called finite step accuracy. It is measured by means of numerical experiments in which the state update procedure is used to integrate the elasto-plastic equations under a wide range of initial conditions and strain increment sizes and directions. Finite step accuracy measurements can give important information on the practical limitations of integration algorithms, especially with regard to the permissible size of strain increments for which the error remains within reasonable bounds.

There were 3 different methods used to check the accuracy of the state update procedure for the Hoffman material model: comparing with HYPLAS (de Souza Neto *et al.* 2003) results for elastically isotropic von Mises material; comparing with self-created test examples and iso-error maps. All these methods are described below.

Comparing with HYPLAS results for elastically isotropic von Mises material

As was mentioned before in Chapter 3, if $c_1 = c_2 = c_3 = 1$, $c_4 = 3$ and $c_5 = c_6 = c_7 = 0$ the Hoffman material corresponds to an isotropic von Mises one.

On the other hand, the von Mises model featuring the standard associative law and linear isotropic elastic behaviour with non-linear isotropic strain hardening was developed within HYPLAS (de Souza Neto *et al.* 2003).

Therefore, the HYPLAS von Mises routine was used to check results of the state update procedure for the Hoffman material. The tests were made for different materials, different stress conditions (pure shear, longitudinal strains and both) and different elastic trial strain increments. All the results were identical.

In Figure 4.5 one can see results for isotropic material in plane strain conditions with linear hardening. Please note that for the von Mises model described in text book by de Souza Neto *et al.* (2003) $\Delta\lambda \equiv \bar{\varepsilon}^p$ and that is why results for $\Delta\lambda$ are different. However, the results obtained for stresses, accumulated plastic strain and elastic strains are identical.

The material used for the test was steel with the following parameters:

$$E = 200GPa, \quad \nu = 0.3,$$
$$\sigma_Y = 1000MPa, \quad H = 40GPa \text{ - hardening modulus.} \tag{4.29}$$

The elastic trial strain was the following:

$$\boldsymbol{\varepsilon}^{e\ trial} = \begin{pmatrix} 0.01 \\ 0.007 \\ 0.002 \\ 0.002 \end{pmatrix}.$$

```
Results of the State Update Procedure for Hoffman
stresses
          1          3650115305.23
          2          3254566514.53
          3          263699230.529
          4          2595318417.48

DGAMa          3.614659701854E-13

Accumulated plastic strain        7.444596867903E-04

Engineering elastic strain (eng)
          1       9.475749168722E-03
          2       6.904681890457E-03
          3       3.428090421317E-03
          4       2.619569028365E-03


Results of the State Update Procedure for von Mises
stresses
          1          3650115359.55
          2          3254566573.01
          3          263699242.190
          4          2595318482.89

DGAMa          7.444598554481E-04

Accumulated plastic strain        7.444598554481E-04

Engineering elastic strain
          1       9.475749059298E-03
          2       6.904681870562E-03
          3       3.428090250119E-03
          4       2.619569157684E-03
```

Figure 4.5. Results provided by designed state update procedure for the Hoffman material and the state update procedure for von Mises from HYPLAS (de Souza Neto *et al.* 2003).

Comparing with self-created test examples

Another way to check the State update procedure is to create test examples assuming that the answer is known. For instance, for material with linear isotropic hardening:

1. It is assumed that the elastic strain $\boldsymbol{\varepsilon}^{e}_{n+1}$ is known.
2. Hence, $\boldsymbol{\sigma}_{n+1} = \mathbf{D}\boldsymbol{\varepsilon}^{e}_{n+1}$ is known.
3. Hence, $f(\boldsymbol{\sigma}_{n+1})$ is known.
4. Hence, the reference yield stress $\sigma_{Y\,n+1}$ corresponding to this stress state is known.
5. Hence, $\Delta\bar{\varepsilon}^{p}_{n+1} = \dfrac{\sigma_{Y\,n+1} - \sigma_{Y\,n}}{H}$ corresponding to $\sigma_{Y\,n+1}$ is known.
6. Hence, having used the expression (4.15) $\Delta\lambda_{n+1}$ is known.
7. From expression $\Delta\boldsymbol{\varepsilon}^{p}_{n+1} = \Delta\lambda_{n+1}(\mathbf{S}\boldsymbol{\sigma}_{n+1} + \mathbf{q})$ it is possible to obtain $\Delta\boldsymbol{\varepsilon}^{p}_{n+1}$.

8. Finally, the elastic trial strain $\boldsymbol{\varepsilon}_{n+1}^{e\ trial} = \boldsymbol{\varepsilon}_{n+1}^{e} + \Delta\boldsymbol{\varepsilon}_{n+1}^{p}$ is known.

These tests were used to check results of the state update procedure for the Hoffman material. The tests were performed for different materials (both elastically isotropic and anisotropic) with different yield surfaces (von Mises, Hill, and Hoffman), different stress conditions (pure shear, only longitudinal strains and both) and different elastic trial strain increments. R results obtained by state update procedure and identical to test examples.

The iso-error maps

Within the context of the state update procedure it is desirable for this procedure to be sufficiently accurate at the Gauss point level for sufficiently large strain increments to ensure that that the global finite element solution also remains within reasonable bounds of accuracy. That is why studying the finite step accuracy of such algorithms is very important.

A survey of the relevant literature is given in the text book by de Souza Neto *et al.* (2003). Such finite step accuracy analysis of elasto-plastic algorithms was firstly performed by Krieg and Krieg (1977) who investigated the behaviour of procedures for integration of the von Mises plastic model.

In the text book by de Souza Neto *et al.* (2003) it is remarked that iso-error maps have proved very effective and are currently accepted as the most reliable (if not the only) tool for the assessment of the finite step accuracy of integration algorithms for elasto-plasticity.

To generate an iso-error map an arbitrary stress state at a point P on the von Mises (just for example) yield surface in the deviatoric plane is considered as shown in Figure 4.6. From this point a sequence of strain increments which corresponds to specified normalised elastic trial stress increments is applied (de Souza Neto *et al.* 2003):

$$\Delta\boldsymbol{\sigma}^{trial} = \frac{\Delta\sigma_T}{s}\boldsymbol{t} + \frac{\Delta\sigma_N}{s}\boldsymbol{n}, \tag{4.30}$$

where

$\Delta\sigma^{trial}$ is the elastic trial stress increment;

$\boldsymbol{n}$ and $\boldsymbol{t}$ are respectively the unit (in Euclidian norm) normal and tangent vectors to the yield surface;

s is the von Mises equivalent stress;

$\Delta\sigma_T$ and $\Delta\sigma_N$ are appropriate factors.

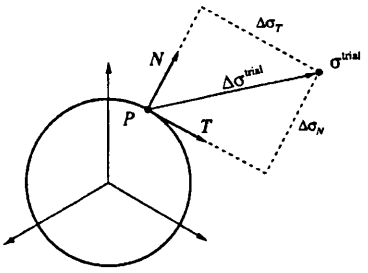

Figure 4.6. Iso-error map. Typical increment directions in the deviatoric plane (de Souza Neto *et al.* 2003).

State update procedure computes an approximated stress $\boldsymbol{\sigma}^{num}$ for elastic trial stress $\boldsymbol{\sigma}^{trial}$. It is assumed that the exact solution $\boldsymbol{\sigma}^{exact}$ is known. In this case the error in % associated with each increment $\Delta\boldsymbol{\sigma}^{trial}$ can be defined as follows:

$$\text{ERROR} = \frac{\sqrt{\left(\boldsymbol{\sigma}^{\text{exact}} - \boldsymbol{\sigma}^{\text{trial}}\right) : \left(\boldsymbol{\sigma}^{\text{exact}} - \boldsymbol{\sigma}^{\text{trial}}\right)}}{\sqrt{\boldsymbol{\sigma}^{\text{exact}} : \boldsymbol{\sigma}^{\text{exact}}}} \times 100\% . \tag{4.31}$$

A contour plot for an error field (the iso-error map) can be obtained by varying the increment sizes $\Delta\sigma_T$ and $\Delta\sigma_N$.

In fact, analytical solution $\boldsymbol{\sigma}^{\text{exact}}$ is generally not available. That is why $\boldsymbol{\sigma}^{\text{exact}}$ is obtained by dividing each stress increment $\Delta\boldsymbol{\sigma}^{\text{trial}}$ into a sufficiently large number of subincrements (in this project this number is equal to 1000).

It is also important to say that for von Mises model the starting point P is immaterial due to the material isotropy. However, for the Hoffman material (Figure 3.1) this point is important due to material anisotropy.

To compare obtained results with the results provided in the article by Schellekens and de Borst (1990) the stress increments and appropriate factors have been chosen according to the mentioned article. For the radial and tangential stress increments in the deviatoric plane, the unit stress magnitude is defined to be equal to a stress increment which, starting from a stress-free state, induces initial yielding in the corresponding direction. The radial and tangential trial stresses ranges up to 5 times the unit magnitude (the factors from 0 to 5 are shown on the borders of an iso-error map).

There were tests performed and iso-error maps obtained for the following materials:

1. Steel with material properties (4.29). It was assumed that no hardening occurs. Results obtained by SUHF can be seen on the Figure 4.7. Results obtained by von Mises state update procedure SUVM from HYPLAS can be seen in Figure 4.8. An iso-error map for the von Mises yield function (unknown material properties) from the article by Schellekens and de Borst (1990) is represented in Figure 4.9 for reference only.
2. Four materials with anisotropic yield surface from the article by Schellekens and de Borst (1990) whose material properties are represented in Table 4.1. It is worth saying that in this article the elastic properties of these materials are isotropic but not specified. That is why they were chosen by the author (4.32). It was assumed that no hardening occurs. Iso-error maps for different starting points (points of smallest and strongest curvature of the Hoffman yield surface as well as normal and tangent vectors will be obtained later) and their comparison with the results obtained in the article by Schellekens and de Borst (1990) are represented in Figures 4.10-4.20.

Results of these tests will be analysed later in a separate section.

	σ_{11C_0} kN/m^2	σ_{11T_0} kN/m^2	σ_{22C_0} kN/m^2	σ_{22T_0} kN/m^2	σ_{33C_0} kN/m^2	σ_{33T_0} kN/m^2
Material 1	10000	1000	10000	1000	10000	1000
Material 2	5000	1000	1000	1000	1000	1000
Material 3	10000	1000	1000	1000	1000	1000
Material 4	20000	1000	1000	1000	1000	1000

Table 4.1. Material sets for iso-error maps.

$$\begin{aligned} E &= 25000000 kN/m^2, \\ \nu &= 0.25, \\ \sigma_{Y_0} &= 1000 kN/m^2. \end{aligned} \tag{4.32}$$

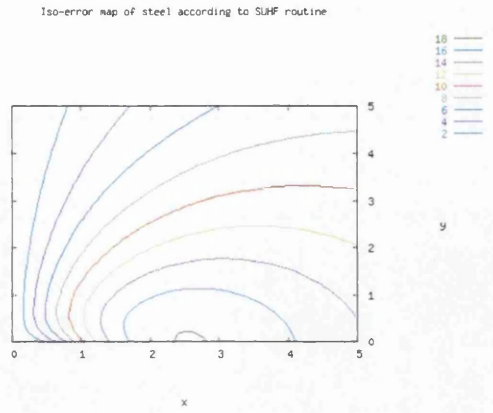

Figure 4.7. Iso-error (error shown in %) map obtained with SUHF for steel (4.29). Factors for tangential and radial trial stresses are shown on axis X and Y respectively

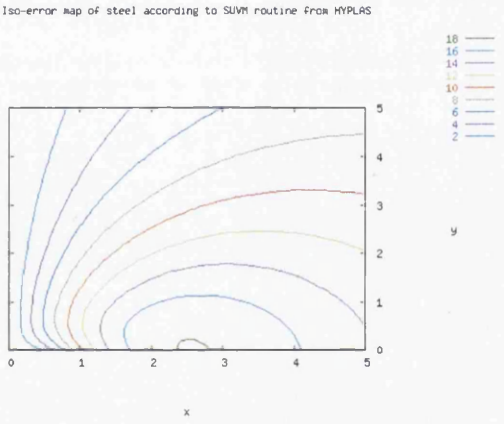

Figure 4.8. Iso-error (error shown in %) map obtained with von Mises State update procedure from HYPLAS for steel (4.29). Factors for tangential and radial trial stresses are shown on axis X and Y respectively

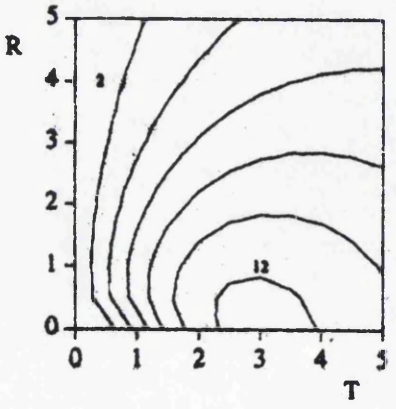

Figure 4.9. Iso-error (error shown in %) map for the von Mises yield function (unknown material properties) from the article by Schellekens and de Borst (1990). Factors for tangential and radial trial stresses are shown on axis X and Y respectively

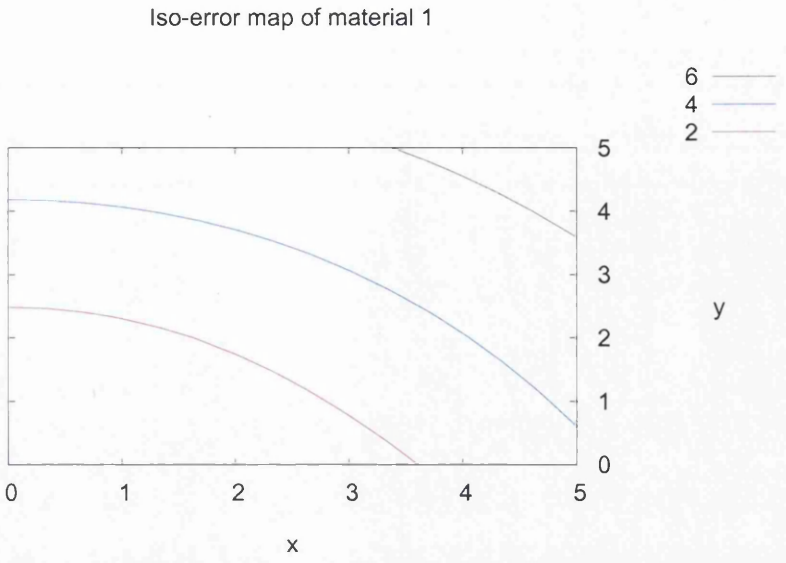

Figure 4.10. Iso-error (error shown in %) map of material 1 with properties (4.32) obtained with SUHF. Factors for tangential and radial trial stresses are shown on axis X and Y respectively

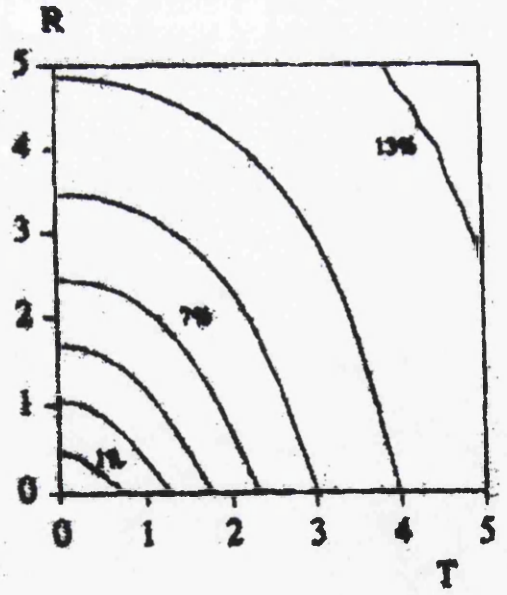

Figure 4.11. Iso-error (error shown in %) map of material 1 obtained by Schellekens and de Borst (1990). Factors for tangential and radial trial stresses are shown on axis X and Y respectively

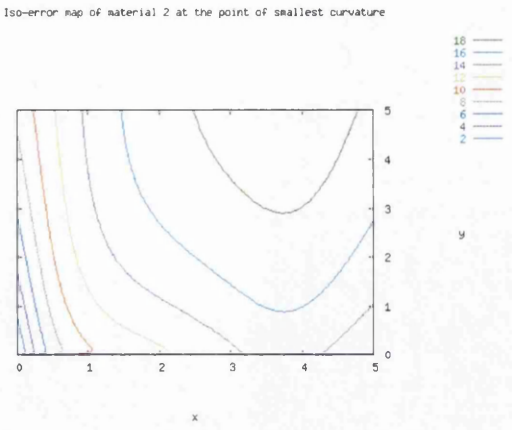

Figure 4.12. Iso-error (error shown in %) map of material 2 with properties (4.32) obtained with SUHF at point of smallest curvature. Factors for tangential and radial trial stresses are shown on axis X and Y respectively

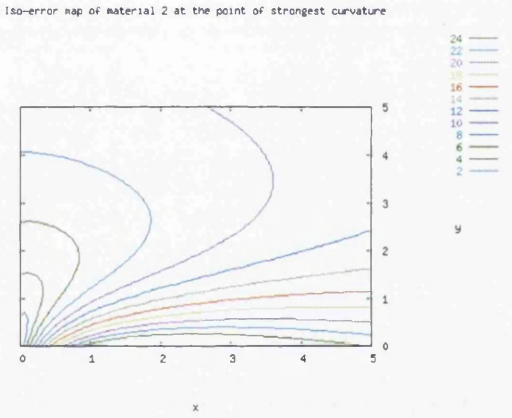

Figure 4.13. Iso-error (error shown in %) map of material 2 with properties (4.32) obtained with SUHF at the point of strongest curvature. Factors for tangential and radial trial stresses are shown on axis X and Y respectively

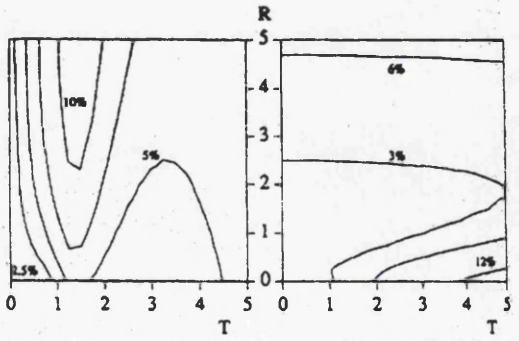

Figure 4.14. Iso-error (error shown in %) map of material 2 obtained by Schellekens and de Borst (1990). Left - point of smallest curvature; right - point of strongest curvature. Factors for tangential and radial trial stresses are shown on axis X and Y respectively

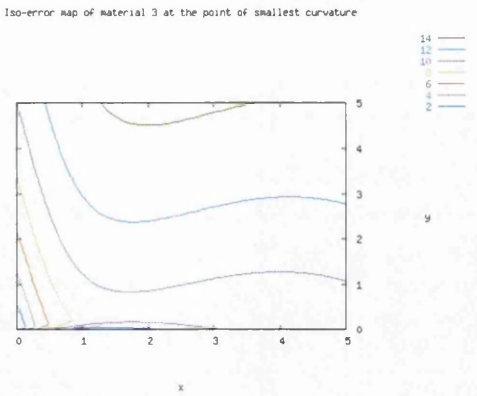

Figure 4.15. Iso-error (error shown in %) map of material 3 with properties (4.32) obtained with SUHF at point of smallest curvature. Factors for tangential and radial trial stresses are shown on axis X and Y respectively

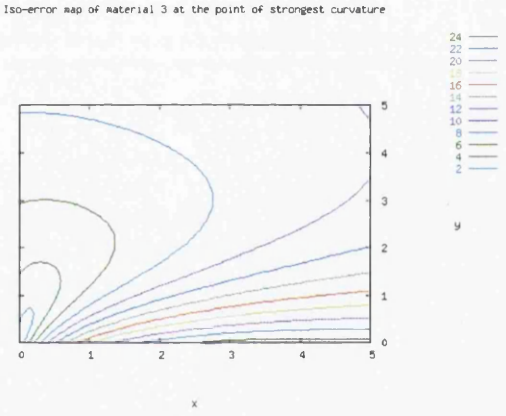

Figure 4.16. Iso-error (error shown in %) map of material 3 with properties (4.32) obtained with SUHF at the point of strongest curvature. Factors for tangential and radial trial stresses are shown on axis X and Y respectively

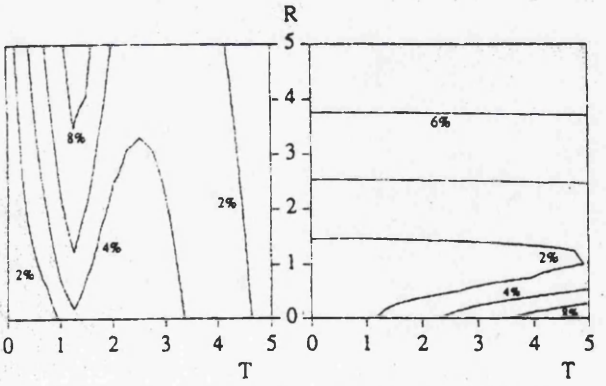

Figure 4.17. Iso-error (error shown in %) map of material 3 obtained by Schellekens and de Borst (1990). Left - point of smallest curvature; right - point of strongest curvature. Factors for tangential and radial trial stresses are shown on axis X and Y respectively

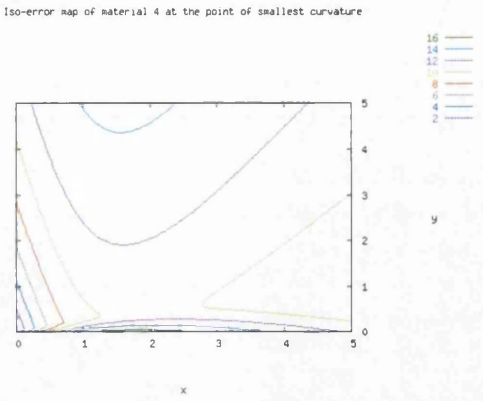

Figure 4.18. Iso-error (error shown in %) map of material 4 with properties (4.32) obtained with SUHF at point of smallest curvature. Factors for tangential and radial trial stresses are shown on axis X and Y respectively

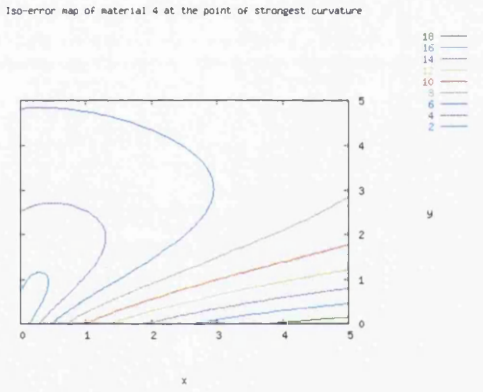

Figure 4.19. Iso-error (error shown in %) map of material 4 with properties (4.32) obtained with SUHF at the point of strongest curvature. Factors for tangential and radial trial stresses are shown on axis X and Y respectively

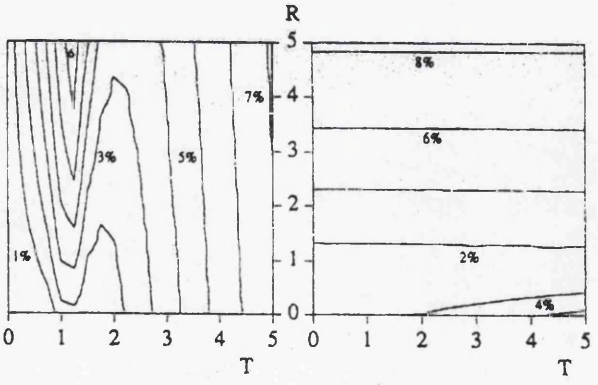

Figure 4.20. Iso-error (error shown in %) map of material 4 obtained by Schellekens and de Borst (1990). Left - point of smallest curvature; right - point of strongest curvature. Factors for tangential and radial trial stresses are shown on axis X and Y respectively

Obtaining points of extreme curvature of the intersection of the Hoffman yield with the deviatoric plane surface for materials N 2-4

First of all, the intersection of the Hoffman yield surface and the deviatoric plane for materials N2-4 should be obtained (for material N1 such point will be obtained in the next section).

For the deviatoric plane $\sigma_{11}+\sigma_{22}+\sigma_{33}=0$. Since $\sigma_{33}=-\sigma_{11}-\sigma_{22}$, stress component σ_{33} can be excluded from the expression of the yield function:

$$f(\sigma)=\left(c_1-\frac{c_3}{2}\right)(\sigma_{11}-\sigma_{33})^2+\left(c_2-\frac{c_3}{2}\right)(\sigma_{22}-\sigma_{33})^2+$$

$$+\frac{c_3}{2}(\sigma_{11}-\sigma_{22})^2+c_4\sigma_{12}^2+c_5\sigma_{11}+c_6\sigma_{22}+c_7\sigma_{33}=$$

$$=\left(c_1-\frac{c_3}{2}\right)(2\sigma_{11}+\sigma_{22})^2+\left(c_2-\frac{c_3}{2}\right)(2\sigma_{22}+\sigma_{11})^2+\frac{c_3}{2}(\sigma_{11}-\sigma_{22})^2+$$

$$+c_4\sigma_{12}^2+c_5\sigma_{11}+c_6\sigma_{22}-c_7(\sigma_{11}+\sigma_{22})=$$

$$=\left(c_1-\frac{c_3}{2}\right)(4\sigma^2{}_{11}+\sigma^2{}_{22}+4\sigma_{11}\sigma_{22})+\left(c_2-\frac{c_3}{2}\right)(\sigma^2{}_{11}+4\sigma^2{}_{22}+4\sigma_{11}\sigma_{22})+$$

$$+\frac{c_3}{2}(\sigma^2{}_{11}+\sigma^2{}_{22}-2\sigma_{11}\sigma_{22})+$$

$$+c_4\sigma_{12}^2+c_5\sigma_{11}+c_6\sigma_{22}-c_7(\sigma_{11}+\sigma_{22})=$$

$$=\sigma^2{}_{11}(4c_1-2c_3+c_2)+\sigma^2{}_{22}(4c_2-2c_3+c_1)+\sigma_{11}\sigma_{22}(4c_1-2c_3+4c_2-2c_3-c_3)+$$
$$+c_4\sigma_{12}^2+(c_5-c_7)\sigma_{11}+(c_6-c_7)\sigma_{22}.$$

Finally, the following expression was obtained:

$$f(\sigma)=\sigma^2{}_{11}(4c_1-2c_3+c_2)+\sigma^2{}_{22}(4c_2-2c_3+c_1)+ \qquad (4.33)$$
$$\sigma_{11}\sigma_{22}(4c_1+4c_2-5c_3)+c_4\sigma_{12}^2+(c_5-c_7)\sigma_{11}+(c_6-c_7)\sigma_{22}.$$

For tests using iso-error it was assumed that $\sigma_{12}=0$. In this case expression (4.33) will appear as follows:

$$f(\sigma)=\sigma^2{}_{11}(4c_1-2c_3+c_2)+\sigma^2{}_{22}(4c_2-2c_3+c_1)+ \qquad (4.34)$$
$$+\sigma_{11}\sigma_{22}(4c_1+4c_2-5c_3)+(c_5-c_7)\sigma_{11}+(c_6-c_7)\sigma_{22}.$$

Expression (4.34) can be rewritten in matrix notation:

$$f(\sigma)=\begin{pmatrix}\sigma_{11} & \sigma_{22}\end{pmatrix}\begin{pmatrix}4c_1-2c_3+c_2 & 2c_1+2c_2-2.5c_3\\ 2c_1+2c_2-2.5c_3 & 4c_2-2c_3+c_1\end{pmatrix}\begin{pmatrix}\sigma_{11}\\ \sigma_{22}\end{pmatrix}+$$
$$+\begin{pmatrix}(c_5-c_7) & (c_6-c_7)\end{pmatrix}\begin{pmatrix}\sigma_{11}\\ \sigma_{22}\end{pmatrix}. \qquad (4.35)$$

It was denoted that:

$$\mathbf{L}=\begin{pmatrix} 4c_1-2c_3+c_2 & 2c_1+2c_2-2.5c_3 \\ 2c_1+2c_2-2.5c_3 & 4c_2-2c_3+c_1 \end{pmatrix}=\begin{pmatrix} A & C \\ C & B \end{pmatrix},$$

$$\begin{aligned} A&=4c_1-2c_3+c_2, \\ B&=4c_2-2c_3+c_1, \\ C&=2c_1+2c_2-2.5c_3. \end{aligned} \tag{4.36}$$

Expression (4.35) contains a quadratic form from an equation of an ellipse. To find its points of smallest and strongest curvatures it must be rotated to the main axis of the ellipse (i.e. matrix $\mathbf{L}$ should be diagonalysed). So, the eigenvalues and eigenvectors of the matrix $\mathbf{L}$ should be found.

The characteristic equation of the matrix L appears as follows

$$\det\begin{pmatrix} A-\lambda & C \\ C & B-\lambda \end{pmatrix}=(A-\lambda)(B-\lambda)-C^2=\lambda^2-(A+B)\lambda+AB-C^2=0,$$

and its roots (eigenvalues of the matrix $\mathbf{L}$) are:

$$\lambda_{1,2}=\frac{A+B\pm\sqrt{(A+B)^2+4C^2-4AB}}{2}. \tag{4.37}$$

In order to find the first eigenvector of this matrix the following matrix equation should be solved:

$$\begin{pmatrix} A-\lambda_1 & C \\ C & B-\lambda_1 \end{pmatrix}\begin{pmatrix} x_1 \\ x_2 \end{pmatrix}=\begin{pmatrix} 0 \\ 0 \end{pmatrix}.$$

Let $x_1=1$. In this case $x_2=\frac{\lambda_1-A}{C}$.

The second eigenvector can be obtained after solving another matrix equation:

$$\begin{pmatrix} A-\lambda_2 & C \\ C & B-\lambda_2 \end{pmatrix}\begin{pmatrix} y_1 \\ y_2 \end{pmatrix}=\begin{pmatrix} 0 \\ 0 \end{pmatrix}$$

Let $y_1=1$. In this case $y_2=\frac{\lambda_2-A}{C}$.

It is well known that if a symmetric matrix $\mathbf{L}$ has real entries then it has real eigenvalues and its eigenvectors corresponding to different eigenvalues are orthogonal (Perry, 1988). In the basis of its eigenvectors such a matrix will be diagonal.

A matrix $\mathbf{U}$ (4.38) such that the eigenvectors of matrix $\mathbf{L}$ are its columns is considered below. In this case a matrix $\Lambda = \mathbf{U}^{-1}\mathbf{L}\mathbf{U}$ is diagonal as $\mathbf{U}$ is an orthogonal matrix ($\mathbf{U}^{\mathrm{T}} = \mathbf{U}^{-1}$). Hence, $\mathbf{U}\Lambda\mathbf{U}^{\mathrm{T}} = \mathbf{L}$.

$$\mathbf{U} = \begin{pmatrix} x_1 & y_1 \\ x_2 & y_2 \end{pmatrix}. \tag{4.38}$$

After all, the quadratic form of expression (4.35) can be rewritten as

$$(\sigma_{11} \quad \sigma_{22})\mathbf{L}\begin{pmatrix} \sigma_{11} \\ \sigma_{22} \end{pmatrix} = (\sigma_{11} \quad \sigma_{22})\mathbf{U}\Lambda\mathbf{U}^{\mathrm{T}}\begin{pmatrix} \sigma_{11} \\ \sigma_{22} \end{pmatrix} = (\sigma'_{11} \quad \sigma'_{22})\Lambda\begin{pmatrix} \sigma'_{11} \\ \sigma'_{22} \end{pmatrix}, \tag{4.39}$$

where new variables appear as follows:

$$\begin{pmatrix} \sigma'_{11} \\ \sigma'_{22} \end{pmatrix} = \mathbf{U}^{\mathrm{T}}\begin{pmatrix} \sigma_{11} \\ \sigma_{22} \end{pmatrix} = \begin{pmatrix} x_1 & x_2 \\ y_1 & y_2 \end{pmatrix}\begin{pmatrix} \sigma_{11} \\ \sigma_{22} \end{pmatrix},$$

$$\Lambda = \begin{pmatrix} \lambda_1 & 0 \\ 0 & \lambda_2 \end{pmatrix}, \tag{4.40}$$

$$\mathbf{U}\begin{pmatrix} \sigma'_{11} \\ \sigma'_{22} \end{pmatrix} = \begin{pmatrix} \sigma_{11} \\ \sigma_{22} \end{pmatrix}.$$

Finally, expression (4.35) may be rewritten in the following way:

$$f(\boldsymbol{\sigma}) = (\sigma'_{11} \quad \sigma'_{22})\Lambda\begin{pmatrix} \sigma'_{11} \\ \sigma'_{22} \end{pmatrix} + ((c_5 - c_7) \quad (c_6 - c_7))\begin{pmatrix} x_1 & y_1 \\ x_2 & y_2 \end{pmatrix}\begin{pmatrix} \sigma'_{11} \\ \sigma'_{22} \end{pmatrix} = \lambda_1(\sigma'_{11})^2 + \lambda_2(\sigma'_{22})^2 +$$
$$+ (c_5 - c_7)(x_1\sigma'_{11} + y_1\sigma'_{22}) + (c_6 - c_7)(x_2\sigma'_{11} + y_2\sigma'_{22}) =$$
$$= \lambda_1(\sigma'_{11})^2 + \lambda_2(\sigma'_{22})^2 + \sigma'_{11}((c_5 - c_7)x_1 + (c_6 - c_7)x_2) + \sigma'_{22}((c_5 - c_7)y_1 + (c_6 - c_7)y_2) =$$
$$= \lambda_1\left((\sigma'_{11})^2 + 2\frac{(c_5 - c_7)x_1 + (c_6 - c_7)x_2}{2\lambda_1}\sigma'_{11} + \left(\frac{(c_5 - c_7)x_1 + (c_6 - c_7)x_2}{2\lambda_1}\right)^2\right) -$$
$$- \lambda_1\left(\frac{(c_5 - c_7)x_1 + (c_6 - c_7)x_2}{2\lambda_1}\right)^2 +$$
$$+ \lambda_2\left((\sigma'_{22})^2 + 2\frac{(c_5 - c_7)y_1 + (c_6 - c_7)y_2}{2\lambda_2}\sigma'_{22} + \left(\frac{(c_5 - c_7)y_1 + (c_6 - c_7)y_2}{2\lambda_2}\right)^2\right) -$$
$$- \lambda_2\left(\frac{(c_5 - c_7)y_1 + (c_6 - c_7)y_2}{2\lambda_2}\right)^2 =$$
$$= \lambda_1\left(\sigma'_{11} + \frac{(c_5 - c_7)x_1 + (c_6 - c_7)x_2}{2\lambda_1}\right)^2 + \lambda_2\left(\sigma'_{22} + \frac{(c_5 - c_7)y_1 + (c_6 - c_7)y_2}{2\lambda_2}\right)^2 -$$

$$-\lambda_1\left(\frac{(c_5-c_7)x_1+(c_6-c_7)x_2}{2\lambda_1}\right)^2-\lambda_2\left(\frac{(c_5-c_7)y_1+(c_6-c_7)y_2}{2\lambda_2}\right)^2$$

Finally, expression (4.35) is equal to

$$f(\sigma)=\lambda_1\left(\sigma'_{11}+\frac{(c_5-c_7)x_1+(c_6-c_7)x_2}{2\lambda_1}\right)^2+\lambda_2\left(\sigma'_{22}+\frac{(c_5-c_7)y_1+(c_6-c_7)y_2}{2\lambda_2}\right) \tag{4.41}$$
$$-\lambda_1\left(\frac{(c_5-c_7)x_1+(c_6-c_7)x_2}{2\lambda_1}\right)^2-\lambda_2\left(\frac{(c_5-c_7)y_1+(c_6-c_7)y_2}{2\lambda_2}\right)^2$$

For the initial state the yield function is equal to $F(\sigma,0)=f(\sigma)-\sigma_{Y_0}^2=0$. Substituting expression (4.41) into this equation one gets:

$$\lambda_1\left(\sigma'_{11}+\frac{(c_5-c_7)x_1+(c_6-c_7)x_2}{2\lambda_1}\right)^2+\lambda_2\left(\sigma'_{22}+\frac{(c_5-c_7)y_1+(c_6-c_7)y_2}{2\lambda_2}\right)^2-$$
$$-\lambda_1\left(\frac{(c_5-c_7)x_1+(c_6-c_7)x_2}{2\lambda_1}\right)^2-\lambda_2\left(\frac{(c_5-c_7)y_1+(c_6-c_7)y_2}{2\lambda_2}\right)^2-\sigma_{Y_0}^2=0. \tag{4.42}$$

Evidently, expression (4.42) is an equation of an ellipse. It was denoted:

$$E=\lambda_1\left(\frac{(c_5-c_7)x_1+(c_6-c_7)x_2}{2\lambda_1}\right)^2+\lambda_2\left(\frac{(c_5-c_7)y_1+(c_6-c_7)y_2}{2\lambda_2}\right)^2+\sigma_{Y_0}^2.$$

Then expression (4.41) appears as follows:

$$\lambda_1\left(\sigma'_{11}+\frac{(c_5-c_7)x_1+(c_6-c_7)x_2}{2\lambda_1}\right)^2+\lambda_2\left(\sigma'_{22}+\frac{(c_5-c_7)y_1+(c_6-c_7)y_2}{2\lambda_2}\right)^2=E,$$

or, equivalently

$$\frac{\left(\sigma'_{11}+\frac{(c_5-c_7)x_1+(c_6-c_7)x_2}{2\lambda_1}\right)^2}{\left(\sqrt{E/\lambda_1}\right)^2}+\frac{\left(\sigma'_{22}+\frac{(c_5-c_7)y_1+(c_6-c_7)y_2}{2\lambda_2}\right)^2}{\left(\sqrt{E/\lambda_2}\right)^2}=1. \tag{4.43}$$

Expression (4.43) is an equation of an ellipse with the centre point

$$\left(-\frac{(c_5-c_7)x_1+(c_6-c_7)x_2}{2\lambda_1},-\frac{(c_5-c_7)y_1+(c_6-c_7)y_2}{2\lambda_2}\right)$$

and semi-axes $\sqrt{E/\lambda_1}$ and $\sqrt{E/\lambda_2}$.

The point of strongest curvature corresponds to the greater semi-axis and the point of smallest curvature corresponds to the small semi-axis.

These 4 points of extreme curvature are listed below:

$$(\sigma'_{11} \quad \sigma'_{22}) = \left(\pm\sqrt{E/\lambda_1} - \frac{(c_5 - c_7)x_1 + (c_6 - c_7)x_2}{2\lambda_1}, -\frac{(c_5 - c_7)y_1 + (c_6 - c_7)y_2}{2\lambda_2} \right),$$

$$(\sigma'_{11} \quad \sigma'_{22}) = \left(-\frac{(c_5 - c_7)x_1 + (c_6 - c_7)x_2}{2\lambda_1}, \pm\sqrt{E/\lambda_2} - \frac{(c_5 - c_7)y_1 + (c_6 - c_7)y_2}{2\lambda_2} \right). \quad (4.44)$$

In order to obtain points (4.44) in old coordinate system $(\sigma_{11} \quad \sigma_{22})$ one should use expression (4.40).

Obtaining points of the intersection of the Hoffman yield with the deviatoric plane for material N 1

Results of the previous section will be used to obtain a point at the intersection of the Hoffman yield surface for material N1 and the deviatoric plane. It should be mentioned that as the material 1 has an isotropic yield function, any point at this intersection curve can be chosen.

In case $\sigma_{11} \equiv \sigma_{22}$ the yield function $F(\sigma, 0) = f(\sigma) - \sigma_{Y_0}^2$ appears as follows:

$$\sigma^2{}_{11}(4c_1 - 2c_3 + c_2 + 4c_2 - 2c_3 + c_1 + 4c_1 + 4c_2 - 5c_3) + (c_5 - c_7 + c_6 - c_7)\sigma_{11} - \sigma_{Y_0}^2 = \quad (4.45)$$
$$= \sigma^2{}_{11}(9c_1 + 9c_2 - 9c_3) + (c_5 + c_6 - 2c_7)\sigma_{11} - \sigma_{Y_0}^2 = 0.$$

The quadratic equation (4.45) has the following roots:

$$\sigma_{111,2} = \frac{-(c_5 + c_6 - 2c_7) \pm \sqrt{(c_5 + c_6 - 2c_7)^2 + 4(9c_1 + 9c_2 - 9c_3)\sigma_{Y_0}^2}}{2(9c_1 + 9c_2 - 9c_3)} \quad (4.46)$$

Obtaining normal and tangent vectors to the Hoffman yield surface

To obtain an iso-error map one should know not only a point on a yield surface, but also the normal and tangent vectors to this yield surface. Evidently, these vectors should belong to the deviatoric plane.

It is well known that a gradient of a yield function is a normal vector to the yield surface. That is why a projection of this gradient to the deviatoric plane will belong to the deviatoric plane and be also a normal vector to a curve which is an intersection of the yield surface and the deviatoric plane. In general,

$$gradf(\sigma)=\begin{pmatrix}\dfrac{\partial f(\sigma)}{\partial\sigma_{11}}\\ \dfrac{\partial f(\sigma)}{\partial\sigma_{22}}\\ \dfrac{\partial f(\sigma)}{\partial\sigma_{12}}\\ \dfrac{\partial f(\sigma)}{\partial\sigma_{33}}\end{pmatrix}=\begin{pmatrix}2c_1\sigma_{11}-(2c_1-c_3)\sigma_{33}-c_3\sigma_{22}+c_5\\ 2c_2\sigma_{22}-(2c_2-c_3)\sigma_{33}-c_3\sigma_{11}+c_6\\ 2c_4\sigma_{12}\\ (2c_1+2c_2-2c_3)\sigma_{33}-(2c_1-c_3)\sigma_{11}-(2c_2-c_3)\sigma_{22}+c_7\end{pmatrix} \tag{4.47}$$

If $\sigma_{12}\equiv 0$ than the gradient (4.47) may be reduced as follows as the yield function does not depend on a shear stress:

$$\boldsymbol{a}=gradf(\sigma)=\begin{pmatrix}\dfrac{\partial f(\sigma)}{\partial\sigma_{11}}\\ \dfrac{\partial f(\sigma)}{\partial\sigma_{22}}\\ \dfrac{\partial f(\sigma)}{\partial\sigma_{33}}\end{pmatrix}=\begin{pmatrix}2c_1\sigma_{11}-(2c_1-c_3)\sigma_{33}-c_3\sigma_{22}+c_5\\ 2c_2\sigma_{22}-(2c_2-c_3)\sigma_{33}-c_3\sigma_{11}+c_6\\ (2c_1+2c_2-2c_3)\sigma_{33}-(2c_1-c_3)\sigma_{11}-(2c_2-c_3)\sigma_{22}+c_7\end{pmatrix} \tag{4.48}$$

A projection $\boldsymbol{b}$ of the gradient $\boldsymbol{a}$ (4.48) onto the deviatoric plane, having the normal vector $\boldsymbol{l}=\left(1/\sqrt{3}\quad 1/\sqrt{3}\quad 1/\sqrt{3}\right)$, may be found according to the following expression:

$$\boldsymbol{b}=\boldsymbol{a}-\boldsymbol{l}(\boldsymbol{a}\cdot\boldsymbol{l}). \tag{4.49}$$

Finally, the required normal $\boldsymbol{n}$ and tangent $\boldsymbol{t}$ vectors to the Hoffman yield surface appear as follows:

$$\boldsymbol{n}=\frac{\boldsymbol{b}}{\sqrt{(\boldsymbol{b}\cdot\boldsymbol{b})}},\qquad \boldsymbol{t}=\boldsymbol{n}\times\boldsymbol{l}. \tag{4.50}$$

Iso-error maps comparison analysis

On the basis of Figures 4.7-4.20 with different iso-error maps the following remarks can be made:

1. Results for steel with material properties (4.29) obtained by SUHF and by von Mises state update procedure SUVM from HYPLAS are identical. Moreover, it is very similar in shape to the iso-error map for the von Mises material (Figure 4.9) from the article by Schellekens and de Borst (1990).

2. Before analysing results obtained for materials with properties represented in the Table 4.1 which was taken from an article Schellekens and de Borst (1990) it should be reminded that in this article neither elastic properties nor the reference yield stress were specified. Normal and tangent vectors to the Hoffman yield surface were not represented either. That is why it was impossible to perform exactly the same tests that were performed in this article.
3. However, the similarities in shape and error distribution between the iso-error maps obtained by SUHF and the iso-error maps found by Schellekens and de Borst (1990) are evident.
4. Moreover, the same tendencies were found both for iso-error maps obtained by SUHF and iso-error maps found by Schellekens and de Borst (1990):
    a. When the anisotropy of the yield surface becomes more pronounced, the errors in numerical results decrease. The observed tendency of decreasing error at points with a strong curvature may be explained by the fact that implicit integration at corners of the yield surface leads to exact results (de Borst, 1987).
    b. The calculated errors are comparable to the errors obtained for the von Mises criterion
    c. When an initial stress point is located at the strongly curved part of the yield surface, it is evident that for large $\Delta\sigma_N/\Delta\sigma_T$ ratios the errors become less dependant on the tangential stress increments when a material becomes more anisotropic.

Finally, a conclusion can be drawn that the accuracy analysis of the state update procedure SUHF for the Hoffman material model gave good results. So, correctness of the designed algorithm has been proved.

4.1.7. Influence of the degree of elastic anisotropy at the iso-error maps

Since correctness of the state update algorithm was proved in the previous Section, it may be used to present iso-error maps for material that is both plastically and elastically anisotropic. Tests for materials with elastic moduli listed in Table 4.2 and other properties (4.51) have been performed. It should be mentioned that plastic properties of all these materials are the same as those of material 1 (Table 4.1). It is

shown that the accuracy decreases as the degree of elastic anisotropy increases (Figures 4.10, 4.21-4.27)

	$E_1,\ kN/m^2$	$E_2 = E_3,\ kN/m^2$
Material 5	25000000	20000000
Material 6	25000000	15000000
Material 7	25000000	10000000
Material 8	25000000	5000000
Material 9	25000000	2000000
Material 10	25000000	1500000
Material 11	25000000	1000000

Table 4.2. Elastic moduli of anisotropic material sets for iso-error maps

$$\begin{aligned} \nu_{12} &= \nu_{23} = \nu_{31} = 0.25, \\ G_{12} &= 500000 kN/m^2, \\ \sigma_{11C_0} &= \sigma_{22C_0} = \sigma_{33C_0} = 10000 kN/m^2, \\ \sigma_{11T_0} &= \sigma_{22T_0} = \sigma_{33T_0} = 1000 kN/m^2, \\ \sigma_{Y_0} &= 1000 kN/m^2. \end{aligned} \tag{4.51}$$

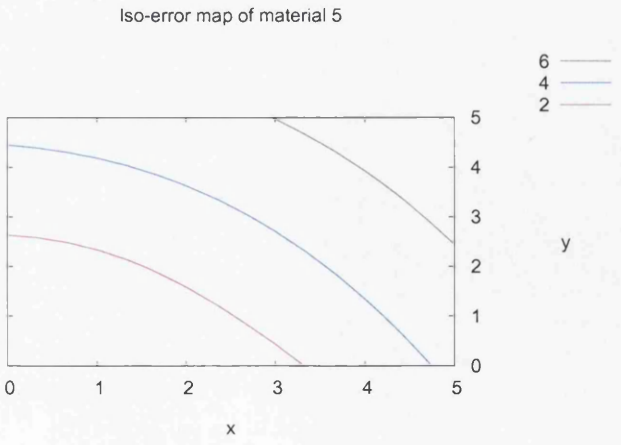

Figure 4.21. Iso-error (error shown in %) map of material 5. Factors for tangential and radial trial stresses are shown on axis X and Y respectively

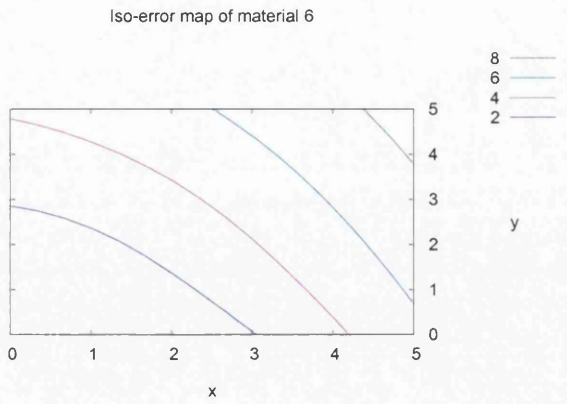

Figure 4.22. Iso-error (error shown in %) map of material 6. Factors for tangential and radial trial stresses are shown on axis X and Y respectively

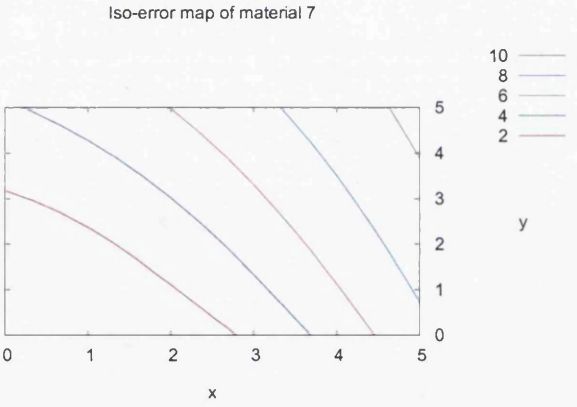

Figure 4.23. Iso-error (error shown in %) map of material 7. Factors for tangential and radial trial stresses are shown on axis X and Y respectively

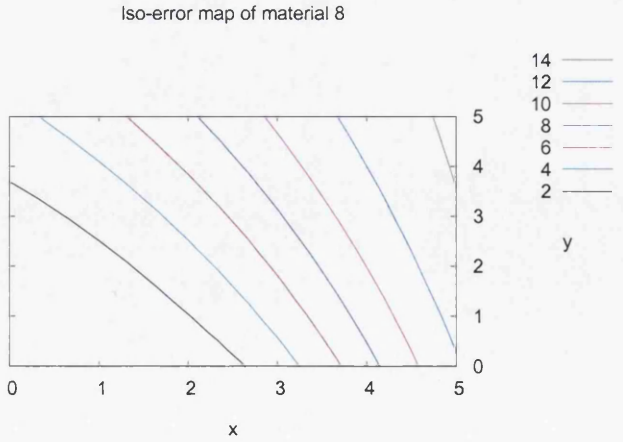

Figure 4.24. Iso-error (error shown in %) map of material 8 Factors for tangential and radial trial stresses are shown on axis X and Y respectively

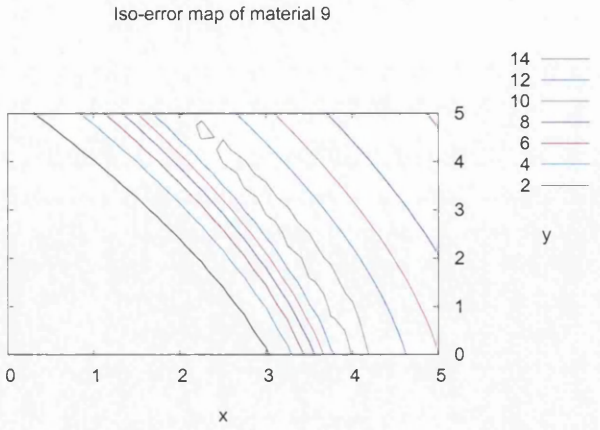

Figure 4.25. Iso-error (error shown in %) map of material 9 Factors for tangential and radial trial stresses are shown on axis X and Y respectively

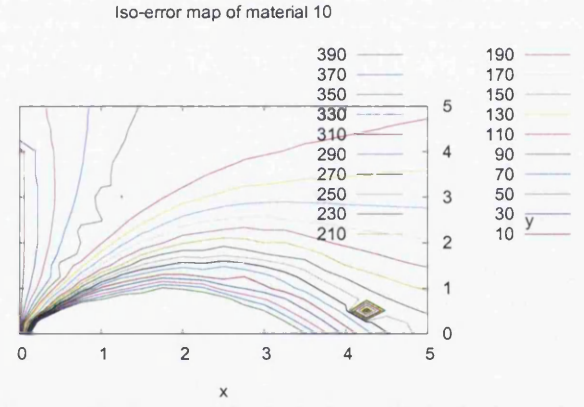

Figure 4.26. Iso-error (error shown in %) map of material 10 Factors for tangential and radial trial stresses are shown on axis X and Y respectively

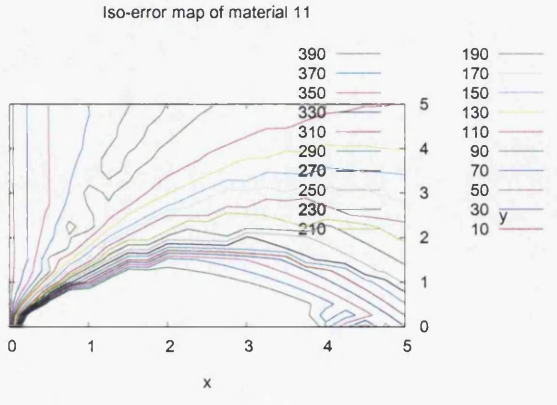

Figure 4.27. Iso-error (error shown in %) map of material 11 Factors for tangential and radial trial stresses are shown on axis X and Y respectively

Most probably, such large errors for materials 10 and 11 were caused by the fact that components (3.9) of the elasticity tensor become negative (for other material they are positive).

So, to decrease an error, the stress increments should be relatively small when the degree of anisotropy is very high. This means that load steps in this case should be much smaller.

4.2. The consistent tangent modulus

The computation of the consistent tangent modulus is a material specific subroutine and is required to assemble element tangent stiffness matrices in order to obtain the global tangent stiffness matrix.

To derive an element tangent stiffness matrix one requires the consistent tangent matrix – the matrix form of the fourth order consistent tangent operator:

$$\boldsymbol{D} \equiv \frac{\partial \boldsymbol{\sigma}_{n+1}}{\partial \boldsymbol{\varepsilon}_{n+1}}. \tag{4.52}$$

In the article by Simo and Taylor (1985) it was shown that for problems of rate-independent elastoplasticity the notion of consistency between the tangent operator and the integration algorithm employed in the solution of the incremental problem plays a crucial role in preserving the quadratic rate of asymptotic convergence of iterative solution schemes based upon Newton's method. That is why system (4.10) has to be used in order to obtain the tangent modulus.

In the case of a purely linear elastic material the stress is an explicit function of the strain tensor and the consistent tangent modulus is the standard elasticity tensor $\boldsymbol{C}$.

For path-dependant elasto-plastic material stress tensor is defined implicitly via an algorithmic constitutive function (4.1), defined by a state update procedure (Section 4.1). As only the total strain $\boldsymbol{\varepsilon}_{n+1}$ changes during the global Newton-Raphson iteration, the stress $\boldsymbol{\sigma}_{n+1}$ is a function of the total strain only. The function (4.1) with fixed $\boldsymbol{\alpha}_n$ defines a stress/strain relation equivalent to a non-linear elastic law. The consistent tangent modulus is the derivative of this non-linear elastic law (de Souza Neto *et al.*, 2003) appears as follows:

$$\boldsymbol{D} \equiv \frac{d\boldsymbol{\sigma}_{n+1}}{d\boldsymbol{\varepsilon}_{n+1}} = \left.\frac{\partial \hat{\boldsymbol{\sigma}}}{\partial \boldsymbol{\varepsilon}_{n+1}}\right|_{\boldsymbol{\alpha}_n}.$$

It is worth remarking that the actual input to the SUHF procedure is the elastic trial strain $\varepsilon_{n+1}^{trial}$, not the total strain ε_{n+1}. So, one can write

$$\sigma_{n+1} = \hat{\sigma}\left(\alpha_n, \varepsilon_{n+1}^{trial}\left(\varepsilon_{n+1}\right)\right).$$

Due to the definition of the total and elastic trial strains one can write

$$\Delta\varepsilon = d\varepsilon_{n+1} = d\varepsilon_{n+1}^{trial}.$$

So, expression (4.52) after straightforward differentiation will appear as follows:

$$\boldsymbol{D} \equiv \frac{\partial\hat{\sigma}}{\partial\varepsilon_{n+1}^{trial}}. \tag{4.53}$$

This expression is the derivative of the implicit function defined by the return mapping equations and is derived by standard procedure for differentiation of implicit functions.

4.2.1. The consistent tangent modulus for elasto-plastic material in tensor notation

Using the definition of the elastic trial strain and the associative flow rule one can write the following expression:

$$\boldsymbol{\varepsilon}_{n+1}^{e} = \boldsymbol{\varepsilon}_{n}^{e} + \Delta\boldsymbol{\varepsilon}^{e} = \boldsymbol{\varepsilon}_{n}^{e} + \Delta\boldsymbol{\varepsilon} - \Delta\boldsymbol{\varepsilon}^{p} = \boldsymbol{\varepsilon}_{n+1}^{e\ trial} - \Delta\lambda_{n+1}\left(\boldsymbol{W} : \boldsymbol{\sigma}_{n+1} + \boldsymbol{V}\right). \tag{4.54}$$

Having applied Hook's linear elastic law to expression (4.54) one obtains

$$\boldsymbol{\sigma}_{n+1} = \boldsymbol{C} : \boldsymbol{\varepsilon}_{n+1}^{e} = \boldsymbol{C} : \left(\boldsymbol{\varepsilon}_{n+1}^{e\ trial} - \Delta\lambda_{n+1}\left(\boldsymbol{W} : \boldsymbol{\sigma}_{n+1} + \boldsymbol{V}\right)\right) = \boldsymbol{\sigma}_{n+1}^{trial} - \Delta\lambda_{n+1}\boldsymbol{C} : \left(\boldsymbol{W} : \boldsymbol{\sigma}_{n+1} + \boldsymbol{V}\right). \tag{4.55}$$

From expression (4.55) it follows that

$$\boldsymbol{\sigma}_{n+1}^{trial} = \boldsymbol{\sigma}_{n+1} + \Delta\lambda_{n+1}\boldsymbol{C} : \left(\boldsymbol{W} : \boldsymbol{\sigma}_{n+1} + \boldsymbol{V}\right) = \boldsymbol{\sigma}_{n+1} + \Delta\lambda_{n+1}\boldsymbol{C} : \left(\boldsymbol{W} : \boldsymbol{\sigma}_{n+1}\right) + \Delta\lambda_{n+1}\boldsymbol{C} : \boldsymbol{V}. \tag{4.56}$$

It is necessary to prove that

$$\boldsymbol{C} : \left(\boldsymbol{W} : \boldsymbol{\sigma}\right) = \left(\boldsymbol{C} : \boldsymbol{W}\right) : \boldsymbol{\sigma} = \boldsymbol{T} : \boldsymbol{\sigma},$$

where $\boldsymbol{T} = \boldsymbol{C} : \boldsymbol{W}$ is a fourth order tensor.

One component of the tensor $\boldsymbol{H} = \boldsymbol{C} : \left(\boldsymbol{W} : \boldsymbol{\sigma}\right)$ looks as follows:

$$H_{ij} = C_{ijkl}\left(W_{klab}\sigma_{ab}\right) = \sum_{k,l} C_{ijkl}\left(\sum_{a,b} W_{klab}\sigma_{ab}\right) = \sum_{k,l} C_{ijkl}\left(W_{kl11}\sigma_{11} + W_{kl12}\sigma_{12} + \ldots + W_{kl33}\sigma_{33}\right) =$$

$$= \sum_{k,l} C_{ijkl}W_{kl11}\sigma_{11} + \sum_{k,l} C_{ijkl}W_{kl12}\sigma_{21} + \ldots + \sum_{k,l} C_{ijkl}W_{kl33}\sigma_{33} = \sum_{a,b}\left(\sum_{k,l} C_{ijkl}W_{klab}\right)\sigma_{ab} = T_{ijab}\sigma_{ab}$$

Finally, expression (4.56) will appear as follows

$$\boldsymbol{\sigma}_{n+1}^{trial} - \Delta\lambda_{n+1}\boldsymbol{C}:\boldsymbol{V} = \left(\mathrm{I} + \Delta\lambda_{n+1}\boldsymbol{T}\right):\boldsymbol{\sigma}_{n+1}, \tag{4.57}$$

where $\boldsymbol{I}$ is identity fourth order tensor whose Cartesian components are $\mathrm{I}_{ijkl} = \frac{1}{2}\left(\delta_{ik}\delta_{jl} + \delta_{il}\delta_{jk}\right)$.

Finally one gets:

$$\boldsymbol{\sigma}_{n+1} = \left(\boldsymbol{I} + \Delta\lambda_{n+1}\boldsymbol{T}\right)^{-1}:\left(\boldsymbol{\sigma}_{n+1}^{trial} - \Delta\lambda_{n+1}\boldsymbol{C}:\boldsymbol{V}\right), \tag{4.58}$$

Equation (4.57) was differentiated to find a differential of $\boldsymbol{\sigma}_{n+1}$:

$$d\Delta\lambda_{n+1}\boldsymbol{T}:\boldsymbol{\sigma}_{n+1} + \left(\boldsymbol{I} + \Delta\lambda_{n+1}\boldsymbol{T}\right):d\boldsymbol{\sigma}_{n+1} = \boldsymbol{C}:d\boldsymbol{\varepsilon}_{n+1}^{trial} - d\Delta\lambda_{n+1}\boldsymbol{C}:\boldsymbol{V}.$$

Finally,

$$\left(\boldsymbol{I} + \Delta\lambda_{n+1}\boldsymbol{T}\right):d\boldsymbol{\sigma}_{n+1} = \boldsymbol{C}:d\boldsymbol{\varepsilon}_{n+1}^{trial} - d\Delta\lambda_{n+1}\left(\boldsymbol{C}:\boldsymbol{V} + \boldsymbol{T}:\boldsymbol{\sigma}_{n+1}\right),$$

or

$$d\boldsymbol{\sigma}_{n+1} = \left(\boldsymbol{I} + \Delta\lambda_{n+1}\boldsymbol{T}\right)^{-1}:\left(\boldsymbol{C}:d\boldsymbol{\varepsilon}_{n+1}^{trial} - d\Delta\lambda_{n+1}\left(\boldsymbol{C}:\boldsymbol{V} + \boldsymbol{T}:\boldsymbol{\sigma}_{n+1}\right)\right). \tag{4.59}$$

A differential $d\Delta\lambda_{n+1}$ must be obtained in order to use expression (4.59). The yield condition $f\left(\boldsymbol{\sigma}_{n+1}\right) - \sigma_Y^2\left(\bar{\boldsymbol{\varepsilon}}_{n+1}^{p}\right) = 0$ may be rewritten in the following way:

$$\frac{1}{2}\boldsymbol{\sigma}_{n+1}:\boldsymbol{W}:\boldsymbol{\sigma}_{n+1} + \boldsymbol{V}:\boldsymbol{\sigma}_{n+1} - \sigma_Y^2\left(\bar{\boldsymbol{\varepsilon}}_{n}^{p} + \Delta\bar{\boldsymbol{\varepsilon}}_{n+1}^{p}\right) = 0. \tag{4.60}$$

Expression (4.60) was differentiated as follows:

$$\boldsymbol{W}:\boldsymbol{\sigma}_{n+1}:d\boldsymbol{\sigma}_{n+1} + \boldsymbol{V}:d\boldsymbol{\sigma}_{n+1} - 2\sigma_Y\frac{d\sigma_Y}{d\bar{\boldsymbol{\varepsilon}}_{n+1}^{p}}d\Delta\bar{\boldsymbol{\varepsilon}}_{n+1}^{p} = 0. \tag{4.61}$$

In order to find $d\Delta\bar{\boldsymbol{\varepsilon}}_{n+1}^{p}$ it is necessary to differentiate expression (4.12) for the effective plastic strain $\Delta\bar{\boldsymbol{\varepsilon}}_{n+1}^{p} = \sqrt{2/3}\left\|\Delta\boldsymbol{\varepsilon}^{p}\right\| = \sqrt{2/3}\cdot\sqrt{\Delta\boldsymbol{\varepsilon}^{p}:\Delta\boldsymbol{\varepsilon}^{p}}$:

$$d\Delta\bar{\boldsymbol{\varepsilon}}_{n+1}^{p} = \sqrt{2/3}\cdot\frac{\Delta\boldsymbol{\varepsilon}^{p}}{\sqrt{\Delta\boldsymbol{\varepsilon}^{p}:\Delta\boldsymbol{\varepsilon}^{p}}}:d\Delta\boldsymbol{\varepsilon}^{p} =$$

$$= \sqrt{2/3}\cdot\frac{\left(\boldsymbol{W}:\boldsymbol{\sigma}_{n+1} + \boldsymbol{V}\right)}{\sqrt{\left(\boldsymbol{W}:\boldsymbol{\sigma}_{n+1} + \boldsymbol{V}\right):\left(\boldsymbol{W}:\boldsymbol{\sigma}_{n+1} + \boldsymbol{V}\right)}}:d\left(\Delta\lambda_{n+1}\left(\boldsymbol{W}:\boldsymbol{\sigma}_{n+1} + \boldsymbol{V}\right)\right),$$

where

$$d\left(\Delta\lambda_{n+1}\left(\boldsymbol{W}:\boldsymbol{\sigma}_{n+1}+\boldsymbol{V}\right)\right)=d\Delta\lambda_{n+1}\left(\boldsymbol{W}:\boldsymbol{\sigma}_{n+1}+\boldsymbol{V}\right)+\Delta\lambda_{n+1}\boldsymbol{W}:\boldsymbol{d\sigma}_{n+1}.$$

Finally,

$$d\Delta\bar{\varepsilon}^{p}_{n+1}=\sqrt{2/3}\frac{\left(\boldsymbol{W}:\boldsymbol{\sigma}_{n+1}+\boldsymbol{V}\right):\left(d\Delta\lambda_{n+1}\left(\boldsymbol{W}:\boldsymbol{\sigma}_{n+1}+\boldsymbol{V}\right)+\Delta\lambda_{n+1}\boldsymbol{W}:d\boldsymbol{\sigma}_{n+1}\right)}{\sqrt{\left(\boldsymbol{W}:\boldsymbol{\sigma}_{n+1}+\boldsymbol{V}\right):\left(\boldsymbol{W}:\boldsymbol{\sigma}_{n+1}+\boldsymbol{V}\right)}}. \tag{4.62}$$

Hence, equation (4.61) may be rewritten as follows:

$$\begin{aligned}&\boldsymbol{W}:\boldsymbol{\sigma}_{n+1}:d\boldsymbol{\sigma}_{n+1}+\boldsymbol{V}:d\boldsymbol{\sigma}_{n+1}-\\&-2\sqrt{\frac{2}{3}}\sigma_{Y}\frac{d\sigma_{Y}}{d\bar{\epsilon}^{p}_{n+1}}\frac{\left(\boldsymbol{W}:\boldsymbol{\sigma}_{n+1}+\boldsymbol{V}\right):\left(d\Delta\lambda_{n+1}\left(\boldsymbol{W}:\boldsymbol{\sigma}_{n+1}+\boldsymbol{V}\right)+\Delta\lambda_{n+1}\boldsymbol{W}:d\boldsymbol{\sigma}_{n+1}\right)}{\sqrt{\left(\boldsymbol{W}:\boldsymbol{\sigma}_{n+1}+\boldsymbol{V}\right):\left(\boldsymbol{W}:\boldsymbol{\sigma}_{n+1}+\boldsymbol{V}\right)}}=0.\end{aligned} \tag{4.63}$$

Items with $d\boldsymbol{\sigma}_{n+1}$ were grouped on one side of the equation (4.63) and items with $d\Delta\lambda_{n+1}$ on the other.

$$\begin{aligned}&\left(\boldsymbol{W}:\boldsymbol{\sigma}_{n+1}+\boldsymbol{V}-\Delta\lambda_{n+1}2\sqrt{\frac{2}{3}}\sigma_{Y}\frac{d\sigma_{Y}}{d\bar{\varepsilon}^{p}_{n+1}}\frac{\left(\boldsymbol{W}:\boldsymbol{\sigma}_{n+1}+\boldsymbol{V}\right):\boldsymbol{W}}{\sqrt{\left(\boldsymbol{W}:\boldsymbol{\sigma}_{n+1}+\boldsymbol{V}\right):\left(\boldsymbol{W}:\boldsymbol{\sigma}_{n+1}+\boldsymbol{V}\right)}}\right):d\boldsymbol{\sigma}_{n+1}=\\&=d\Delta\boldsymbol{\lambda}_{n+1}\cdot 2\sqrt{\frac{2}{3}}\sigma_{Y}\frac{d\sigma_{Y}}{d\bar{\varepsilon}^{p}_{n+1}}\frac{\left(\boldsymbol{W}:\boldsymbol{\sigma}_{n+1}+\boldsymbol{V}\right):\left(\boldsymbol{W}:\boldsymbol{\sigma}_{n+1}+\boldsymbol{V}\right)}{\sqrt{\left(\boldsymbol{W}:\boldsymbol{\sigma}_{n+1}+\boldsymbol{V}\right):\left(\boldsymbol{W}:\boldsymbol{\sigma}_{n+1}+\boldsymbol{V}\right)}}\end{aligned}$$

Having substituted (4.59) into the above equation one obtains:

$$\begin{aligned}&\left(\boldsymbol{W}:\boldsymbol{\sigma}_{n+1}+\boldsymbol{V}-\Delta\lambda_{n+1}2\sqrt{\frac{2}{3}}\sigma_{Y}\frac{d\sigma_{Y}}{d\bar{\varepsilon}^{p}_{n+1}}\frac{\left(\boldsymbol{W}:\boldsymbol{\sigma}_{n+1}+\boldsymbol{V}\right):\boldsymbol{W}}{\sqrt{\left(\boldsymbol{W}:\boldsymbol{\sigma}_{n+1}+\boldsymbol{V}\right):\left(\boldsymbol{W}:\boldsymbol{\sigma}_{n+1}+\boldsymbol{V}\right)}}\right):\\&:\left[\left(\boldsymbol{I}+\Delta\lambda_{n+1}\boldsymbol{T}\right)^{-1}:\left(\boldsymbol{C}:d\boldsymbol{\varepsilon}^{\boldsymbol{trial}}_{n+1}-d\Delta\lambda_{n+1}\left(\boldsymbol{C}:\boldsymbol{V}+\boldsymbol{T}:\boldsymbol{\sigma}_{n+1}\right)\right)\right]=\\&=d\Delta\boldsymbol{\lambda}_{n+1}\cdot 2\sqrt{\frac{2}{3}}\sigma_{Y}\frac{d\sigma_{Y}}{d\bar{\varepsilon}^{p}_{n+1}}\frac{\left(\boldsymbol{W}:\boldsymbol{\sigma}_{n+1}+\boldsymbol{V}\right):\left(\boldsymbol{W}:\boldsymbol{\sigma}_{n+1}+\boldsymbol{V}\right)}{\sqrt{\left(\boldsymbol{W}:\boldsymbol{\sigma}_{n+1}+\boldsymbol{V}\right):\left(\boldsymbol{W}:\boldsymbol{\sigma}_{n+1}+\boldsymbol{V}\right)}}\end{aligned} \tag{4.64}$$

Items with $d\boldsymbol{\varepsilon}^{\boldsymbol{trial}}_{n+1}$ were grouped on one side of the equation (4.64) and items with $d\Delta\lambda_{n+1}$ on the other.

$$\begin{aligned}&\left(\boldsymbol{W}:\boldsymbol{\sigma}_{n+1}+\boldsymbol{V}-\Delta\lambda_{n+1}2\sqrt{\frac{2}{3}}\sigma_{Y}\frac{d\sigma_{Y}}{d\bar{\varepsilon}^{p}_{n+1}}\frac{\left(\boldsymbol{W}:\boldsymbol{\sigma}_{n+1}+\boldsymbol{V}\right):\boldsymbol{W}}{\sqrt{\left(\boldsymbol{W}:\boldsymbol{\sigma}_{n+1}+\boldsymbol{V}\right):\left(\boldsymbol{W}:\boldsymbol{\sigma}_{n+1}+\boldsymbol{V}\right)}}\right):\\&:\left(\boldsymbol{I}+\Delta\lambda_{n+1}\boldsymbol{T}\right)^{-1}:\boldsymbol{C}:d\boldsymbol{\varepsilon}^{\boldsymbol{trial}}_{n+1}=\\&=d\Delta\lambda_{n+1}\cdot 2\sqrt{\frac{2}{3}}\sigma_{Y}\frac{d\sigma_{Y}}{d\bar{\varepsilon}^{p}_{n+1}}\frac{\left(\boldsymbol{W}:\boldsymbol{\sigma}_{n+1}+\boldsymbol{V}\right):\left(\boldsymbol{W}:\boldsymbol{\sigma}_{n+1}+\boldsymbol{V}\right)}{\sqrt{\left(\boldsymbol{W}:\boldsymbol{\sigma}_{n+1}+\boldsymbol{V}\right):\left(\boldsymbol{W}:\boldsymbol{\sigma}_{n+1}+\boldsymbol{V}\right)}}+\\&+d\Delta\lambda_{n+1}\left(\boldsymbol{W}:\boldsymbol{\sigma}_{n+1}+\boldsymbol{V}-\Delta\boldsymbol{\lambda}_{n+1}2\sqrt{\frac{2}{3}}\sigma_{Y}\frac{d\sigma_{Y}}{d\bar{\varepsilon}^{p}_{n+1}}\frac{\left(\boldsymbol{W}:\boldsymbol{\sigma}_{n+1}+\boldsymbol{V}\right):\boldsymbol{W}}{\sqrt{\left(\boldsymbol{W}:\boldsymbol{\sigma}_{n+1}+\boldsymbol{V}\right):\left(\boldsymbol{W}:\boldsymbol{\sigma}_{n+1}+\boldsymbol{V}\right)}}\right):\\&:\left[\left(\boldsymbol{I}+\Delta\lambda_{n+1}\boldsymbol{T}\right)^{-1}:\left(\boldsymbol{C}:\boldsymbol{V}+\boldsymbol{T}:\boldsymbol{\sigma}_{n+1}\right)\right]\end{aligned} \tag{4.65}$$

Notations (4.66) were introduced to make equation (4.65) more readable:

$$A=\left(W:\sigma_{n+1}+V-\Delta\lambda_{n+1}2\sqrt{\frac{2}{3}}\sigma_Y\frac{d\sigma_Y}{d\bar{\varepsilon}^p_{n+1}}\frac{(W:\sigma_{n+1}+V):W}{\sqrt{(W:\sigma_{n+1}+V):(W:\sigma_{n+1}+V)}}\right):$$

$$:\left[(I+\Delta\lambda_{n+1}T)^{-1}:C\right],$$

$$B=2\sqrt{\frac{2}{3}}\sigma_Y\frac{d\sigma_Y}{d\bar{\varepsilon}^p_{n+1}}\frac{(W:\sigma_{n+1}+V):(W:\sigma_{n+1}+V)}{\sqrt{(W:\sigma_{n+1}+V):(W:\sigma_{n+1}+V)}}+ \tag{4.66}$$

$$+\left(W:\sigma_{n+1}+V-\Delta\lambda_{n+1}2\sqrt{\frac{2}{3}}\sigma_Y\frac{d\sigma_Y}{d\bar{\varepsilon}^p_{n+1}}\frac{(W:\sigma_{n+1}+V):W}{\sqrt{(W:\sigma_{n+1}+V):(W:\sigma_{n+1}+V)}}\right):$$

$$:\left[(I+\Delta\lambda_{n+1}T)^{-1}:(C:V+T:\sigma_{n+1})\right].$$

In this case expression (4.65) may be re written as

$$d\Delta\lambda_{n+1}=\frac{A:d\varepsilon^{trial}_{n+1}}{B}. \tag{4.67}$$

With the substitution of equation (4.67) in expression (4.59) for $d\sigma_{n+1}$ one finally obtains the tangent relation consistent with the implicit return mapping algorithm for the Hoffman material model:

$$\begin{aligned}d\sigma_{n+1}&=(I+\Delta\lambda_{n+1}T)^{-1}:C:d\varepsilon^{trial}_{n+1}-\\&-(I+\Delta\lambda_{n+1}T)^{-1}:\left(\frac{(C:V+T:\sigma_{n+1})\otimes A}{B}\right):d\varepsilon^{trial}_{n+1}=\\&=\left[(I+\Delta\lambda_{n+1}T)^{-1}:\left(C-\frac{R}{B}\right)\right]:d\varepsilon^{trial}_{n+1}=D^{ep}:d\varepsilon^{trial}_{n+1},\end{aligned} \tag{4.68}$$

where $R=(C:V+T:\sigma_{n+1})\otimes A$ is the 4th order tensor.

4.2.2. The consistent tangent modulus for elasto-plastic material in matrix notation

In order to use expression (4.68) for coding the appropriate subroutine for HYPLAS it must be put in a vector and matrix form.

Matrix form of a tensor of 4th order is defined as follows using a general tensor equation

$$E=F:G, \tag{4.69}$$

where $\boldsymbol{E},\boldsymbol{G}$ are symmetric tensors of the 2nd order (it was assumed that $E_{13}=E_{23}=G_{13}=G_{23}\equiv 0$) and $\boldsymbol{F}$ is a symmetric ($F_{ijkl}=F_{klij}$) tensor of 4th order and the F tensor's form is similar to that of the elasticity tensor (i.e. that only the following components are NOT equal to zero F_{1111}, F_{2222}, F_{3333}, $F_{1133}=F_{3311}$, $F_{2233}=F_{3322}$, $F_{1122}=F_{2211}$, $F_{1212}=F_{1221}=F_{2112}=F_{2121}$). Evidently, $\boldsymbol{E}$ and $\boldsymbol{G}$ tensors have the same form as the stress and strain tensors.

In vector-matrix notation equation (4.69) can be written as follows:

$$\mathbf{E}=\mathbf{F}\mathbf{G}, \tag{4.70}$$

where

$$\mathbf{E}=\begin{pmatrix} E_{11} \\ E_{22} \\ E_{12} \\ E_{33} \end{pmatrix};$$

$$\mathbf{G}=\begin{pmatrix} G_{11} \\ G_{22} \\ G_{12} \\ G_{33} \end{pmatrix};$$

$$\mathbf{F}=\begin{pmatrix} F_{1111} & F_{1122} & 0 & F_{1133} \\ F_{2211} & F_{2222} & 0 & F_{2233} \\ 0 & 0 & 2F_{1212} & 0 \\ F_{3311} & F_{3322} & 0 & F_{3333} \end{pmatrix}.$$

The third column of matrix $\mathbf{F}$ is multiplied by 2 to take into account shear components of tensors $\boldsymbol{E},\boldsymbol{G}$ because of the following expression:

$$E_{ij}=F_{ijkl}G_{kl}=F_{ij11}G_{11}+F_{ij22}G_{22}+F_{ij12}G_{12}+F_{ij21}G_{21}+F_{ij33}G_{33}=$$
$$=F_{ij11}G_{11}+F_{ij22}G_{22}+2F_{ij12}G_{12}+F_{ij33}G_{33}.$$

Matrix $\mathbf{F}$ is called *the tensor matrix of the tensor* $\boldsymbol{F}$ and $\mathbf{E}$, $\mathbf{G}$ are called *the tensor vectors of the tensors* $\boldsymbol{E},\boldsymbol{G}$ respectively.

It is easy to see that the tensor matrix of the tensor $\boldsymbol{T}=\boldsymbol{C}\cdot\cdot\boldsymbol{W}$ appears as follows:

$$\mathbf{T}=\begin{pmatrix} T_{1111} & T_{1122} & 0 & T_{1133} \\ T_{2211} & T_{2222} & 0 & T_{2233} \\ 0 & 0 & 2T_{1212} & 0 \\ T_{3311} & T_{3322} & 0 & T_{3333} \end{pmatrix}=$$

$$=\begin{pmatrix} C_{1111} & C_{1122} & 0 & C_{1133} \\ C_{2211} & C_{2222} & 0 & C_{2233} \\ 0 & 0 & 2C_{1212} & 0 \\ C_{3311} & C_{3322} & 0 & C_{3333} \end{pmatrix}\cdot\begin{pmatrix} W_{1111} & W_{1122} & 0 & W_{1133} \\ W_{2211} & W_{2222} & 0 & W_{2233} \\ 0 & 0 & 2W_{1212} & 0 \\ W_{3311} & W_{3322} & 0 & W_{3333} \end{pmatrix}.$$

For example,

$$2T_{1212}=2\sum_{k,l}C_{12kl}W_{kl12}=4C_{1212}W_{1212}.$$

As it was proved already that $\mathbf{D}$ and $\mathbf{S}$ are the tensor matrixes of the tensors C and W respectively, it is evident that $\mathbf{T}=\mathbf{DS}$.

The tensor vector of the 2nd order tensor A (4.66) appears as follows:

$$\mathbf{A}=\left(\mathbf{S}\sigma_{n+1}+\mathbf{q}-\Delta\lambda_{n+1}2\sqrt{\frac{2}{3}}\sigma_Y\frac{d\sigma_Y}{d\bar{\varepsilon}^{\mathrm{p}}_{\mathrm{n+1}}}\frac{\mathbf{S}(\mathbf{S}\sigma_{n+1}+\mathbf{q})}{\sqrt{(\mathbf{S}\sigma_{n+1}+\mathbf{q})\mathbf{Z}(\mathbf{S}\sigma_{n+1}+\mathbf{q})}}\right)\left[(\mathbf{I}+\Delta\lambda_{n+1}\mathbf{DS})^{-1}\mathbf{D}\right]. \tag{4.71}$$

where

$$\mathbf{Z}=\begin{pmatrix} 1 & 0 & 0 & 0 \\ 0 & 1 & 0 & 0 \\ 0 & 0 & 2 & 0 \\ 0 & 0 & 0 & 1 \end{pmatrix}.$$

On the other hand, expression (4.66) for B in matrix notation appears as follows:

$$B=2\sqrt{\frac{2}{3}}\sigma_Y\frac{d\sigma_Y}{d\bar{\varepsilon}^{\mathrm{p}}_{\mathrm{n+1}}}\frac{(\mathbf{S}\sigma_{n+1}+\mathbf{q})\mathbf{Z}(\mathbf{S}\sigma_{n+1}+\mathbf{q})}{\sqrt{(\mathbf{S}\sigma_{n+1}+\mathbf{q})\mathbf{Z}(\mathbf{S}\sigma_{n+1}+\mathbf{q})}}+$$

$$+\left(\mathbf{S}\sigma_{n+1}+\mathbf{q}-\Delta\lambda_{n+1}2\sqrt{\frac{2}{3}}\sigma_Y\frac{d\sigma_Y}{d\bar{\varepsilon}^{\mathrm{p}}_{\mathrm{n+1}}}\frac{\mathbf{S}(\mathbf{S}\sigma_{n+1}+\mathbf{q})}{\sqrt{(\mathbf{S}\sigma_{n+1}+\mathbf{q})\mathbf{Z}(\mathbf{S}\sigma_{n+1}+\mathbf{q})}}\right)\cdot \tag{4.72}$$

$$\cdot\mathbf{Z}\left[(\mathbf{I}+\Delta\lambda_{n+1}\mathbf{DS})^{-1}(\mathbf{Dq}+\mathbf{DS}\sigma_{n+1})\right].$$

A tensor product in expression (4.68) has to be expressed in matrix notation as well. It is evident that the 2nd order tensor $L=(C:V+T:\sigma_{n+1})$ (expression (4.68)) has the corresponding vector notation $\mathbf{L}=(\mathbf{Dq}+\mathbf{DS}\sigma_{n+1})$.

Now the tensor matrix of the 4th order tensor $\boldsymbol{R} = \boldsymbol{L} \otimes \boldsymbol{A}$ has to be obtained. By definition of a tensor product, $R_{ijkl} = L_{ij} A_{kl}$. That is why the tensor matrix of the tensor $\boldsymbol{R}$ should appear as follows (the third column of matrix R_M is multiplied by 2 to take into account shear components of tensor $d\varepsilon_{n+1}^{trial}$):

$$\mathbf{R} = \begin{pmatrix} L_{11}A_{11} & L_{11}A_{22} & 2L_{11}A_{12} & L_{11}A_{33} \\ L_{22}A_{11} & L_{22}A_{22} & 2L_{22}A_{12} & L_{22}A_{33} \\ L_{12}A_{11} & L_{12}A_{22} & 2L_{12}A_{12} & L_{12}A_{33} \\ L_{33}A_{11} & L_{33}A_{22} & 2L_{33}A_{12} & L_{33}A_{33} \end{pmatrix},$$

or

$$\mathbf{R} = \begin{pmatrix} L_1A_1 & L_1A_2 & 2L_1A_3 & L_1A_4 \\ L_2A_1 & L_2A_2 & 2L_2A_3 & L_2A_4 \\ L_3A_1 & L_3A_2 & 2L_3A_3 & L_3A_4 \\ L_4A_1 & L_4A_2 & 2L_4A_3 & L_4A_4 \end{pmatrix}.$$

Finally, expression (4.68) in matrix notation appears as follows:

$$d\boldsymbol{\sigma}_{n+1} = \left[\left(\mathbf{I} + \Delta\lambda_{n+1} \mathbf{D}\mathbf{S} \right)^{-1} \left(\mathbf{D} - \frac{\mathbf{R}}{B} \right) \right] d\boldsymbol{\varepsilon}_{n+1}^{trial}. \tag{4.73}$$

It should be mentioned that $\boldsymbol{\varepsilon}_{n+1}^{trial}$ is a Cauchy trial strain vector. However, according to the structure of the HYPLAS (de Souza Neto *et al.*, 2003) software, a matrix form of the consistent tangent modulus should be obtained for a trial strain vector where the shear component is multiplied by 2 (engineering shear strain)

$$\mathbf{e}_{n+1}^{trial} = \mathbf{Z}\boldsymbol{\varepsilon}_{n+1}^{trial}, \tag{4.74}$$

From expression (4.74) it follows that $d\boldsymbol{\varepsilon}_{n+1}^{trial} = \mathbf{Z}^{-1} d\mathbf{e}_{n+1}^{trial}$, and the tensor matrix (4.73) of the consistent tangent modulus should be changed as follows

$$\mathbf{D}^{ep} = \left[\left(\mathbf{I} + \Delta\lambda_{n+1} \mathbf{D}\mathbf{S} \right)^{-1} \left(\mathbf{D} - \frac{\mathbf{R}}{B} \right) \right] \mathbf{Z}^{-1}, \tag{4.75}$$

to ensure that the expression $d\boldsymbol{\sigma}_{n+1} = \mathbf{D}^{ep} d\mathbf{e}_{n+1}^{trial}$ is correct.

4.2.3. Verifying accuracy of the consistent tangent modulus

There were 2 different methods used to check the accuracy of the consistent tangent modulus for the Hoffman material model: comparing with HYPLAS (de Souza Neto *et al.*, 2003) results for isotropic von Mises material and comparing with numerical derivatives. These methods are described below.

Comparing with HYPLAS results for elastically isotropic von Mises material

The HYPLAS routine for calculation of the consistent tangent modulus for von Mises material was used to check the consistent tangent modulus for the Hoffman material. The tests were made for different materials and different stress conditions (pure shear, only longitudinal strains and both). All the results were virtually identical.

In Figure 4.28 one can compare results for steel with parameters (4.29). The elastic trial strain was the following:

$$\boldsymbol{\varepsilon}^{e\ trial} = \begin{pmatrix} 0.002 \\ 0.003 \\ 0.005 \\ 0.001 \end{pmatrix},$$

and the corresponding stress vector (obtained as a result of SUHF computations) was equal to:

$$\boldsymbol{\sigma} = \begin{pmatrix} 1000000058MPa \\ 1119228226MPa \\ 596140884MPa \\ 880771875MPa \end{pmatrix}.$$

Comparing with numerical derivatives

Having looked at expression (4.75) of the consistent tangent modulus one can easily see that

$$\mathbf{D}_{ij}^{ep} = \left.\frac{\partial \boldsymbol{\sigma}_i}{\partial \mathbf{e}_j^{trial}}\right|_{n+1}. \tag{4.76}$$

That is why it was natural to calculate numerical derivatives to estimate expression (4.76) in order to check its accuracy. However, as numerical derivation is complex itself, its errors will be discussed before its application.

Consistent tangent modulus for Hoffman

i	j	D(i,j)
1	1	246152121808.
1	2	126923945337.
1	3	-360.070010671
1	4	126923945481.
2	1	126923945337.
2	2	244296335162.
2	3	-9278933220.62
2	4	128779732128.
3	1	-360.070032975
3	2	-9278933736.53
3	3	13219421177.2
3	4	9278934096.60
4	1	126923945481.
4	2	128779732128.
4	3	9278933580.69
4	4	244296335018.

Consistent tangent modulus for von Mises

i	j	D(i,j)
1	1	246152125938.
1	2	126923946740.
1	3	-360.070009195
1	4	126923946884.
2	1	126923946740.
2	2	244296339393.
2	3	-9278933044.95
2	4	128779733429.
3	1	-360.070009195
3	2	-9278933044.95
3	3	13219422732.3
3	4	9278933405.02
4	1	126923946884.
4	2	128779733429.
4	3	9278933405.02
4	4	244296339249.

Figure 4.28. Results obtained by the designed consistent tangent modulus procedure for the Hoffman material (CTHF) and the analogous procedure for von Mises from HYPLAS (de Souza Neto *et al.*, 2003).

Accuracy of numerical derivation

There were 3 formulas of numerical derivation used in this project: right derivative (first order of accuracy)

$$f'(x)=\frac{f(x+h)-f(x)}{h}; \tag{4.77}$$

left derivative (first order of accuracy)

$$f'(x)=\frac{f(x)-f(x-h)}{h}; \tag{4.78}$$

central derivative (second order of accuracy)

$$f'(x)=\frac{f(x+h)-f(x-h)}{2h}. \tag{4.79}$$

Applied uncritically, formulas (4.77)-(4.79) are almost guaranteed to produce inaccurate results. There are two sources of errors: truncation error and roundoff error. The truncation error comes from higher terms in the Taylor series, which are not taken into account in expressions (4.77)-(4.79). The roundoff error has various contributions: a round off error in h and in expressions (4.77)-(4.79) themselves (Press *et al.,* 1992). It is very important to remind that the exact value of the function $f(x)=\sigma_i$ is unknown. This happens because only an approximate solution of equation (4.17), which corresponds to system (4.11), is obtained by the state update procedure. This fact causes additional error to expressions (4.77)-(4.79).

In the books by Press *et al.* (1992) and Bahvalov *et al.* (2000) it was clearly shown that the total error of expressions (4.77)-(4.79) depends on h significantly. For example, the total error of expression (4.77) is represented in Figure 4.29 (Bahvalov *et al.,* 2000).

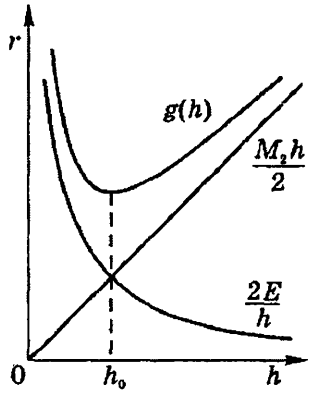

Figure 4.29. Total error of expression (4.77) (Bahvalov *et al.,* 2000).

In Figure 4.29 the following notations were used: $f''(\varsigma)\le M_2$, where ς is a point in the vicinity of the point x; $|\varepsilon(\varsigma)|\le E$, where $\varepsilon(\varsigma)$ is the error with which function $f(x)$ is calculated. So, $g(x)=\frac{M_2h}{2}+\frac{2E}{h}$, where $M_2h/2$ estimates influence of the truncation error and $2E/h$ estimates the influence of the fact that the exact value of function $f(x)$ is unknown.

Practical experience shows, however, that to find h_0 is very difficult.

In the book (Press *et al.,* 1992) it was shown that expressions (4.77) and (4.78) give at best only the square root $\sqrt{\varepsilon_m}$ of machine accuracy ε_m and expression (4.79) gives only $\varepsilon_m^{2/3}$. In the same reference book the conclusion is made that no one of expressions (4.77)-(4.79) give an accuracy comparable to the machine accuracy ε_m or even the lower accuracy to which $f(x)$ is evaluated.

In the book by Bahvalov *et al.* (2000) there is an even stronger statement: no h exists such that the error $g(h)$ will have the same order as $\sqrt{E}$.

Results of comparing CTHF results with numerical derivatives

Since the error of expressions (4.77)-(4.79) depends on h significantly, a special program was created to find numerical derivatives (4.77)-(4.79) for different values of h lying within an interval $(10^{-11}\ldots10^{-5})$ in order to find the value of h_0.

The results obtained by the CTHF routine for calculation of the consistent tangent modulus for the Hoffman material were compared with numerical derivatives for different materials and different stress conditions (pure shear, only longitudinal strains and mixed). The following materials were used for tests:

1. Steel (isotropic elasticity with von Mises yield surface),
2. Anisotropically elastic material with von Mises yield surface,
3. Anisotropically elastic material with the Hill yield surface,
4. Anisotropically elastic material with the Hoffman yield surface.

For all 4 material types mentioned before the results obtained by the CTHF routine and numerical derivation were identical, i.e. first 5-7 digits of the consistent tangent modulus and corresponding numerical derivatives were the same.

It should be also mentioned that the inequality

$$\left\|\boldsymbol{\sigma}\left(\mathbf{e}^{trial}+\mathbf{h}\right)-\boldsymbol{\sigma}\left(\mathbf{e}^{trial}\right)\right\| \geq \left\|\boldsymbol{\sigma}\left(\mathbf{e}^{trial}+\mathbf{h}\right)-\left\langle\boldsymbol{\sigma}\left(\mathbf{e}^{trial}\right)+\mathbf{D}^{ep}\mathbf{h}\right\rangle\right\|$$

was always correct for all calculations ($\mathbf{D}^{ep}$ were obtained by the CTHF routine). This fact once more proves that the CTHF subroutine delivers accurate results.

Finally, a conclusion can be drawn that the accuracy analysis performed for the consistent tangent modulus procedure CTHF for the Hoffman material model gave good results. So, correctness of the designed algorithm has been proved.

Chapter 5. Numerical examples

In this Chapter numerical examples are provided in order to illustrate the numerical algorithms discussed in Chapter 4 for the Hoffman material model (Chapter 3). Despite the fact that the correctness and reliability of these algorithms was successfully proved in Chapter 4, these examples are necessary to show that all 5 subroutines (Section 2.2.4) were correct and were able to work together with the main body of the HYPLAS program (de Souza Neto *et al.* 2003).

5.1. Model construction

A long pipe (Figure 5.1) with fixed ends loaded by internal pressure only is considered as a model construction. This pipe is therefore in a plane strain state (Section 5.2). However, this problem can be also treated as an axisymmetric one (Section 5.3). The loading is quasi-static (i.e. inertia effects are ignored), thermal effects are ignored, and strains are infinitesimal.

All calculations will be run for a pipe with inner r and outer R radii of 100mm and 200mm respectively.

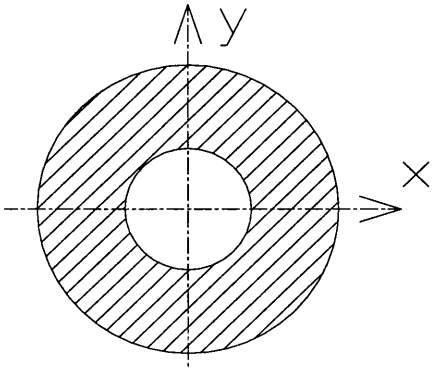

Figure 5.1. The cross-section of the pipe.

5.2. A plane strain model problem for von Mises material

As was shown in Chapter 3, for the specific values ($c_1 = c_2 = c_3 = 1$, $c_4 = 3$, $c_5 = c_6 = c_7 = 0$) of material constants (3.7), the Hoffman material model is equal to the isotropic von Mises case. That is why it was decided to solve the same problem for the pipe (Section 5.1) made of isotropic steel using both von Mises subroutines developed in the HYPLAS program (de Souza Neto *et al.,* 2003) and designed subroutines (Chapter 4). The results obtained were then compared.

5.2.1. Problem statement

The problem statement for the steel pipe is as follows:

Given the initial value $k(t_0)=0$ of the internal variable k and the history of internal pressure $P(t)$ for pseudo-time interval $t\in[t_0,\bar{t}]$ for each point M of the pipe find the functions $\sigma(M,t)$, $k(M,t)$, $\boldsymbol{u}(M,t)$ and $\varepsilon(M,t)$ which satisfy the following equations at each point M (all equations are written in the Cartesian coordinate system and x_1 corresponds to X, x_2 corresponds to Y, and x_3 corresponds to Z):

$$\frac{\partial\sigma(M,t)_{11}}{\partial x_1}+\frac{\partial\sigma(M,t)_{12}}{\partial x_2}=0,$$
$$\frac{\partial\sigma(M,t)_{21}}{\partial x_1}+\frac{\partial\sigma(M,t)_{22}}{\partial x_2}=0, \tag{5.1}$$

$$\varepsilon(M,t)_{11}=\frac{\partial u(M,t)_1}{\partial x_1},$$
$$\varepsilon(M,t)_{22}=\frac{\partial u(M,t)_2}{\partial x_2},$$
$$2\varepsilon(M,t)_{12}=\frac{\partial u(M,t)_1}{\partial x_2}+\frac{\partial u(M,t)_2}{\partial x_1}, \tag{5.2}$$

$$\varepsilon(M,t)_{33}=\varepsilon(M,t)^e_{13}=\varepsilon(M,t)^p_{13}=\varepsilon(M,t)^e_{23}=\varepsilon(M,t)^p_{23}\equiv 0,$$

$$\varepsilon(M,t)_{ij}=\varepsilon^e(M,t)_{ij}+\varepsilon^p(M,t)_{ij},\quad i,j=1,2,3, \tag{5.3}$$

$$\sigma(M,t)_{ij}=C_{ijkl}\varepsilon^e(M,t)_{kl},\quad i,j,k,l=1,2,3, \tag{5.4}$$

$$F(\sigma(M,t),k(M,t))=\left(c_1-\frac{c_3}{2}\right)(\sigma_{11}(M,t)-\sigma_{33}(M,t))^2+$$

$$+\left(c_2-\frac{c_3}{2}\right)(\sigma_{22}(M,t)-\sigma_{33}(M,t))^2+\frac{c_3}{2}(\sigma_{11}(M,t)-\sigma_{22}(M,t))^2+c_4\sigma_{12}^2(M,t)+ \tag{5.5}$$

$$+c_5\sigma_{11}(M,t)+c_6\sigma_{22}(M,t)+c_7\sigma_{33}(M,t)-\sigma_Y^2(k(M,t))$$

$$k(M,t)=\int_o^t\sqrt{\frac{2}{3}\left(\dot{\epsilon}^p(M,t)_{ij}\,\dot{\epsilon}^p(M,t)_{ij}\right)}d\tau=\sqrt{\frac{2}{3}}\int_o^t\left\|\dot{\boldsymbol{\varepsilon}}^p(M,t)\right\|d\tau=\bar{\boldsymbol{\varepsilon}}^p(M,t), \tag{5.6}$$

$$i,j=1,2,3,$$

$$\dot{\varepsilon}^p(M,t) = \dot{\lambda}(M,t)\frac{\partial F(\sigma(M,t),k(M,t))}{\partial \sigma}, \tag{5.7}$$

$$F(\sigma(M,t),k(M,t)) \le 0,$$

$$\dot{\lambda}(M,t) \ge 0, \tag{5.8}$$

$$\dot{\lambda}(M,t)F(\sigma(M,t),k(M,t)) = 0,$$

and boundary conditions

$$\begin{aligned}
&\sigma_{11}(H,t)n_1(H) + \sigma_{12}(H,t)n_2(H) = -P(t) \text{ on the internal pipe surface,}\\
&\sigma_{21}(H,t)n_1(H) + \sigma_{22}(H,t)n_2(H) = 0 \text{ on the internal pipe surface,}\\
&\sigma_{11}(H,t)n_1(H) + \sigma_{12}(H,t)n_2(H) = 0 \text{ on the external pipe surface,}\\
&\sigma_{21}(H,t)n_1(H) + \sigma_{22}(H,t)n_2(H) = 0 \text{ on the external pipe surface.}
\end{aligned} \tag{5.9}$$

Expressions (5.1) are equilibrium equations, expressions (5.2) are a definition of Cauchy strains, expression (5.3) is an additive decomposition of the strain tensor, expression (5.4) is a linear elastic law, expression (5.5) is the Hoffman yield function for isotropic hardening, expression (5.6) defines the hardening parameter for the strain hardening model, expression (5.7) is a standard associative flow rule, and expressions (5.8) show the loading/unloading criterion.

As for material constants, they should correspond to a fully isotropic von Mises material as the pipe is made of steel.

So, the elastic constants appear as follows:

$$\begin{aligned}
&C_{1111} = C_{2222} = C_{3333} = \frac{E(1-\nu)}{(1-2\nu)(1+\nu)},\\
&C_{1133} = C_{3311} = C_{2233} = C_{3322} = C_{1122} = C_{2211} = \frac{E\nu}{(1-2\nu)(1+\nu)},\\
&C_{1212} = C_{1221} = C_{2112} = C_{2121} = C_{1313} = C_{1331} = C_{3113} = C_{3131} =\\
&= C_{3232} = C_{3223} = C_{2332} = C_{2323} = \frac{E}{2(1+\nu)},
\end{aligned} \tag{5.10}$$

where

E is the Young's modulus;

ν is the Poisson ratio.

At the same time, plastic constants appear as follows

$$c_1 = c_2 = c_3 = 1,$$
$$c_4 = 3, \tag{5.11}$$
$$c_5 = c_6 = c_7 = 0.$$

As the problem (5.1)-(5.9) is also an axisymmetric one, only part of the pipe's cross-section (Figure 5.2) is taken into account. Hence, the boundary conditions on the radii HG and EF should be the following (in polar coordinate system):

$$\sigma_{r\varphi} = 0, \tag{5.12}$$
$$u_\varphi = 0.$$

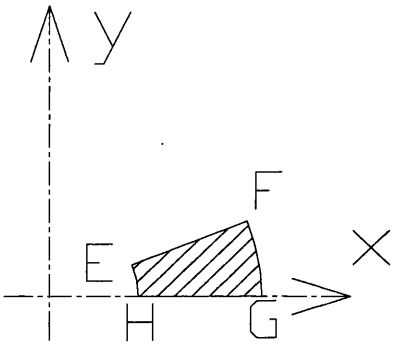

Figure 5.2. Domain for problem (5.1)-(5.9), (5.12).

5.2.2. Parameters of the numerical example

The steel had the following material parameters:

$$E = 200GPa,\ \nu = 0.3,\ \sigma_{Y_0} = 1000MPa. \tag{5.13}$$

The hardening curve is multi-linear and is presented in Figure 5.3. Its parameters can be seen in Table 5.1.

Accumulated plastic strain	Yield stress, MPa
0	1000
0.0005	1020
0.001	1039
0.0015	1057
1.000	4000

Table 5.1. Hardening curve's parameters for steel (5.13).

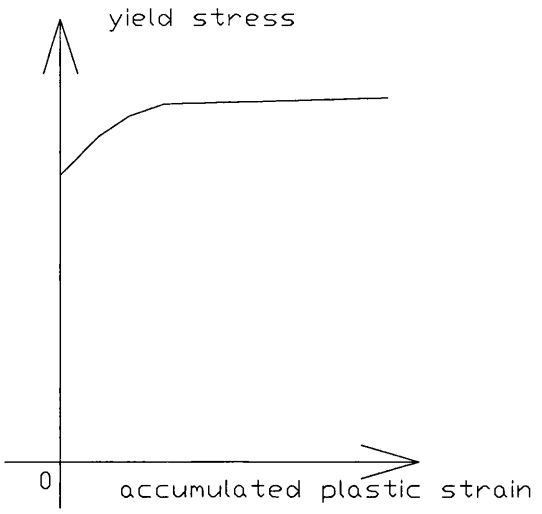

Figure 5.3. Hardening curve for steel (5.13).

Internal pressure for the problem (5.1)-(5.9), (5.12) was equal to:

$$P(\bar{t}) = 900MPa\,. \tag{5.14}$$

5.2.3. Finite element solution for hardening material

As was mentioned in Chapter 2, the HYPLAS program (de Souza Neto *et al.,* 2003) uses proportional loading. So, there were 6 load steps according to Table 5.2.

Number of load step	Percentage from the final load (5.13)
1	20
2	40
3	60
4	80
5	90
6	100

Table 5.2. Initial load steps for hardening material.

A mesh of four 8-noded isoparametric quadrilateral elements was used for this test example. Both von Mises and Hoffman calculations were performed using the same mesh. It should be mentioned that in HYPLAS (de Souza Neto *et al.*, 2003) the boundary of a domain is represented by a quadratic function. That is why a sufficiently thin slice of the pipe has to be used to ensure better solution accuracy as a circle is not congruent to a parabola.

It is easy to see from Table 5.3 that the nodal displacements obtained by the numerical algorithm developed for the Hoffman material model are virtually identical to the node displacements obtained by the von Mises numerical subroutines developed in HYPLAS (de Souza Neto *et al.*, 2003). The same correspondence was proved for stresses and accumulated plastic strains as well.

Node	Von Mises		Hoffman	
	u_x	u_y	u_x	u_y
1	0.480714E-02	0.000000E+00	0.480714E-02	0.000000E+00
2	0.480712E-02	0.125850E-04	0.480712E-02	0.125850E-04
3	0.480707E-02	0.251700E-04	0.480707E-02	0.251700E-04
4	0.444380E-02	0.000000E+00	0.444380E-02	0.000000E+00
5	0.444374E-02	0.232676E-04	0.444374E-02	0.232676E-04
6	0.413414E-02	0.000000E+00	0.413414E-02	0.000000E+00
7	0.413413E-02	0.108232E-04	0.413413E-02	0.108232E-04
8	0.413409E-02	0.216462E-04	0.413409E-02	0.216462E-04
9	0.380734E-02	0.000000E+00	0.380734E-02	0.000000E+00
10	0.380729E-02	0.199351E-04	0.380729E-02	0.199351E-04
11	0.353408E-02	0.000000E+00	0.353408E-02	0.000000E+00
12	0.353407E-02	0.925219E-05	0.353407E-02	0.925219E-05
13	0.353403E-02	0.185043E-04	0.353403E-02	0.185043E-04
14	0.322163E-02	0.000000E+00	0.322163E-02	0.000000E+00
15	0.322158E-02	0.168683E-04	0.322158E-02	0.168683E-04
16	0.297259E-02	0.000000E+00	0.297259E-02	0.000000E+00
17	0.297258E-02	0.778222E-05	0.297258E-02	0.778222E-05
18	0.297255E-02	0.155644E-04	0.297255E-02	0.155644E-04
19	0.272277E-02	0.000000E+00	0.272277E-02	0.000000E+00
20	0.272274E-02	0.142563E-04	0.272274E-02	0.142563E-04
21	0.253314E-02	0.000000E+00	0.253314E-02	0.000000E+00
22	0.253313E-02	0.663174E-05	0.253313E-02	0.663174E-05
23	0.253310E-02	0.132634E-04	0.253310E-02	0.132634E-04

Table 5.3. Nodal displacement of the pipe (plane strain problem) from initial configuration in case of hardening.

5.2.4. Finite element solution for perfectly plastic material

If the pipe's material is perfectly plastic, i.e. no hardening appears, the pipe has a limit load. For example, the limit internal pressure is equal to (Kachanov, 1969)

$$P^* = 2\tau_Y \ln\frac{R}{r}, \tag{5.15}$$

where

$\tau_Y = 1000/\sqrt{3} MPa$ is the shear yield stress.

For the steel (5.13) pipe the limit internal pressure is $P^* = 800.37742 MPa$.

There were 11 load steps during the finite element computation taken according to Table 5.4.

Number of load step	Percentage from the limit load (5.15)
1	20
2	40
3	60
4	80
5	90
6	95
7	97
8	98
9	99
10	99.8
11	99.975

Table 5.4. Initial load steps for perfectly plastic material.

All calculations were made with the same mesh used in Section 5.2.3.

The following results were achieved:

1. Both the von Mises and Hoffman algorithms converged for all loads less then 99.975% of the limit pressure (5.15).
2. Displacements obtained by the developed algorithm for Hoffman material were identical to displacements obtained by the von Mises subroutines developed in HYPLAS (de Souza Neto *et al.*, 2003).
3. As the load reached 99.3% of the limit pressure (5.15) the effective stress in all Gauss points reached the yield stress according to both algorithms.

5.2.5. Concluding remarks

By comparing the results obtained by the developed algorithm for the Hoffman material and by the von Mises subroutines developed in HYPLAS one can make the conclusion that for a plane strain problem for an isotropic material all 5 developed subroutines (Section 2.2.4) were correct and were able to work properly together with the main body of the HYPLAS program (de Souza Neto *et al.*, 2003).

5.3. An axisymmetric model problem for von Mises material

Analogously to the procedure described in Section 5.2, it was chosen to solve the same axisymmetric model problem for the pipe (Section 5.1) made of isotropic steel using both the von Mises subroutines realised in the HYPLAS program (de Souza Neto *et al.*, 2003) and subroutines designed in Chapter 4.

However, to perform an axisymmetric problem test, another domain was used: a different pipe's cross-section (Figure 5.4). Problem statement (5.1)-(5.9), (5.12) had to be amended as well.

The results obtained were then compared.

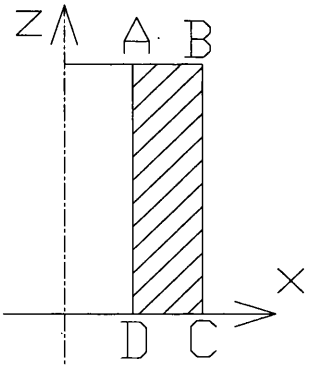

Figure 5.4. Domain for an axisymmetric model problem.

5.3.1. Problem statement

In order to take into account the differences between a plane strain and an axisymmetric problem the problem statement (5.1)-(5.9), (5.12) has to be amended.

First of all, all equations (5.1), (5.3)-(5.8) will remain the same. As for expressions (5.2) defining the Cauchy strains, they should be amended to take into account that $\varepsilon(M,t)_{33} \neq 0$ any more (all equations are written in the cylindrical coordinate system and x_1 corresponds to R, x_2 corresponds to Z, and x_3 corresponds to φ):

$$\varepsilon(M,t)_{11} = \frac{\partial u(M,t)_1}{\partial x_1},$$

$$\varepsilon(M,t)_{22} = \frac{\partial u(M,t)_2}{\partial x_2},$$

$$\varepsilon(M,t)_{33} = \frac{u(M,t)_1}{x_1}, \tag{5.16}$$

$$2\varepsilon(M,t)_{12} = \frac{\partial u(M,t)_1}{\partial x_2} + \frac{\partial u(M,t)_2}{\partial x_1},$$

$$\varepsilon(M,t)^e_{13} = \varepsilon(M,t)^p_{13} = (M,t)^e_{23} = \varepsilon(M,t)^p_{23} \equiv 0.$$

Moreover, the boundary conditions (5.9) and (5.12) should be amended as well. There are two reasons for this. First of all, the normal vector to lines BC and AD has coordinates $(\pm 1, \ 0)$. Secondly, boundary conditions on lines AB and CD should ensure that the pipe is in a plane strain state. Finally, boundary conditions appear as follows:

$$\sigma_{11}(H,t) = -P(t); \ \sigma_{21}(H,t) = 0 \text{ on } AD,$$

$$\sigma_{11}(H,t) = 0; \ \sigma_{21}(H,t) = 0 \text{ on } BC, \tag{5.17}$$

$$\sigma_{12} = 0; \ u_2 = 0 \text{ on } AB \text{ and } CD.$$

5.3.2. Finite element solution for hardening material

In this Section the finite element solution of problem (5.1), (5.3)-(5.8), (5.16)-(5.17) is provided. In order to compare the results obtained with the ones for a plane strain problem (Section 5.2.3), a pipe made of the same piecewise linear hardening material described in Section 5.2.2 was used.

A mesh of four 8-noded isoparametric quadrilateral elements was used for this test example. Both von Mises and Hoffman calculations were performed using the same mesh. The same load steps (Table 5.2) were used.

Node	Von Mises		Hoffman	
	u_r	u_z	u_r	u_z
1	0.480714E-02	0.000000E+00	0.480714E-02	0.000000E+00
2	0.480714E-02	-0.561427E-19	0.480714E-02	-0.299395E-18
3	0.480714E-02	0.000000E+00	0.480714E-02	0.000000E+00
4	0.444380E-02	0.000000E+00	0.444380E-02	0.000000E+00
5	0.444380E-02	0.000000E+00	0.444380E-02	0.000000E+00
6	0.413414E-02	0.000000E+00	0.413414E-02	0.000000E+00
7	0.413414E-02	-0.200601E-18	0.413414E-02	0.916329E-19
8	0.413414E-02	0.000000E+00	0.413414E-02	0.000000E+00
9	0.380734E-02	0.000000E+00	0.380734E-02	0.000000E+00
10	0.380734E-02	0.000000E+00	0.380734E-02	0.000000E+00
11	0.353408E-02	0.000000E+00	0.353408E-02	0.000000E+00
12	0.353408E-02	0.139158E-19	0.353408E-02	0.118733E-18
13	0.353408E-02	0.000000E+00	0.353408E-02	0.000000E+00
14	0.322163E-02	0.000000E+00	0.322163E-02	0.000000E+00
15	0.322163E-02	0.000000E+00	0.322163E-02	0.000000E+00
16	0.297259E-02	0.000000E+00	0.297259E-02	0.000000E+00
17	0.297259E-02	0.949537E-19	0.297259E-02	0.772097E-19
18	0.297259E-02	0.000000E+00	0.297259E-02	0.000000E+00
19	0.272277E-02	0.000000E+00	0.272277E-02	0.000000E+00
20	0.272277E-02	0.000000E+00	0.272277E-02	0.000000E+00
21	0.253314E-02	0.000000E+00	0.253314E-02	0.000000E+00
22	0.253314E-02	-0.323609E-19	0.253314E-02	0.139458E-19
23	0.253314E-02	0.000000E+00	0.253314E-02	0.000000E+00

Table 5.5. Nodal displacement of the pipe (axisymmetric problem) from initial configuration in the case of hardening.

It is easy to see from Table 5.5 that the nodal displacements obtained by the developed numerical algorithm for the Hoffman material model are identical to the nodal displacements obtained by the von Mises numerical subroutines developed in HYPLAS (de Souza Neto *et al.*, 2003). The same correspondence was proved for stresses and accumulated plastic strains as well.

The results obtained are physically reasonable as $u_z = 0$ for all nodes. This fact proves that the pipe is also in a plane strain condition.

5.3.3. Finite element solution for perfectly plastic material

Analogously to the procedure described in Section 5.2.4, tests for the pipe made of perfectly plastic material were performed. The limit internal pressure (5.15) remains the same as the material has the same properties.

There were 11 load steps during the finite element computation according to Table 5.4. All calculations were made on the same mesh used in Section 5.3.2.

The following results were achieved:

4. Both the von Mises and Hoffman algorithms converged for all loads less then 99.975% of the limit pressure (5.15).
5. Displacements obtained by the developed algorithm for the Hoffman material were identical to displacements obtained by the von Mises subroutines developed in HYPLAS (de Souza Neto *et al.*, 2003).
6. As the load reached 99.8% of the limit pressure (5.15) the effective stress in all Gauss points reached the yield stress according to both algorithms.

5.3.4. Concluding remarks

By comparing results obtained by the developed algorithm for the Hoffman material and by the von Mises subroutines developed in HYPLAS one can make a conclusion that for an axisymmetric problem for an isotropic material all 5 developed subroutines (Section 2.2.4) were correct and were able to work properly together with the main body of the HYPLAS program (de Souza Neto *et al.*, 2003).

5.4. Comparing plane strain and axisymmetric problems

This Section is dedicated to comparison of results obtained by the developed algorithm for the Hoffman material both for plane strain and axisymmetric problems.

5.4.1. Comparison for von Mises material

It is worth saying that radius HG (Figure 5.2) contains nodes 1, 4, 6, 9, 11, 14, 16, 19, and 21 in the direction from H to G respectively. Node 1 is located at point H, and node 21 is located at point G. This radius is interesting as the X axis of the Cartesian coordinate system is identical to the R axis of the cylindrical

coordinate system. That is why correct solutions of plane strain and axisymmetric problems should be identical along this radius.

From Tables 5.3 and 5.5 it follows that the nodal displacements obtained as finite element solutions of plane strain and axisymmetric problems for the pipe made of isotropic material are identical at all 9 mentioned nodes located on radius HG. These displacements are represented in Figure 5.5. The same correspondence was proved for accumulated plastic strains and stresses which are represented in Figures 5.6 and 5.7. When $P(\bar{t}) = 900MPa$ the whole pipe has plastic deformations.

In the text book by Kachanov (1969) stress distribution in a steel cylindrical pipe loaded by internal pressure are shown (Figure 5.8) for the pipe which has both elastic and plastic areas. To compare with these results calculations were made for the same pipe made of von Mises material (5.13) but loaded by smaller pressure equal to $P(\bar{t}) = 700MPa$. Stress distributions are shown on Figures 5.9 and 5.10 and they look the same to results obtained by Kachanov (1969).

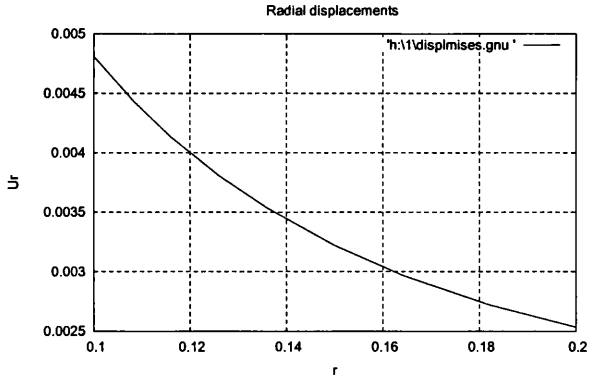

Figure 5.5. Radial displacements for the von Mises material (5.13). $P(\bar{t}) = 900MPa$.

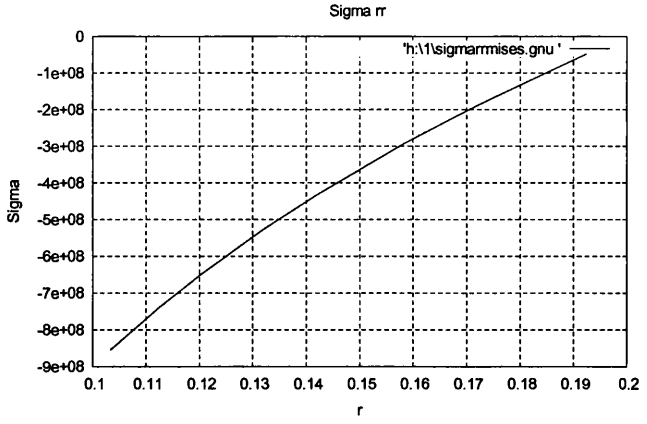

Figure 5.6. σ_{rr} for the von Mises material (5.13). $P(\bar{t}) = 900MPa$.

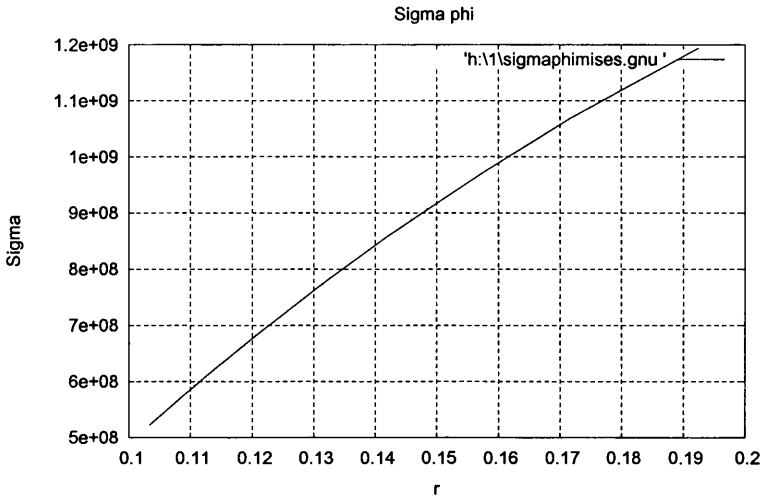

Figure 5.7. $\sigma_{\varphi\varphi}$ for the von Mises material (5.13). $P(\bar{t}) = 900MPa$.

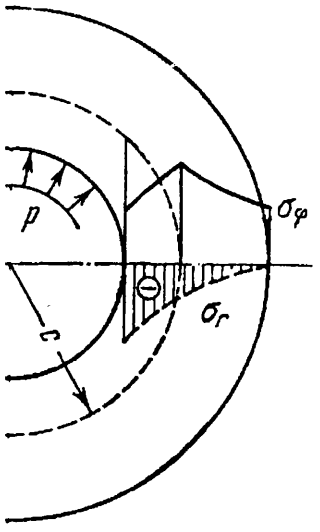

Figure 5.8. $\sigma_{\varphi\varphi}$ and σ_{rr} for a steel pipe loaded by internal pressure. The circle with radius C is a boundary between plastic (inside) and elastic areas of the pipe. (Kachanov, 1969).

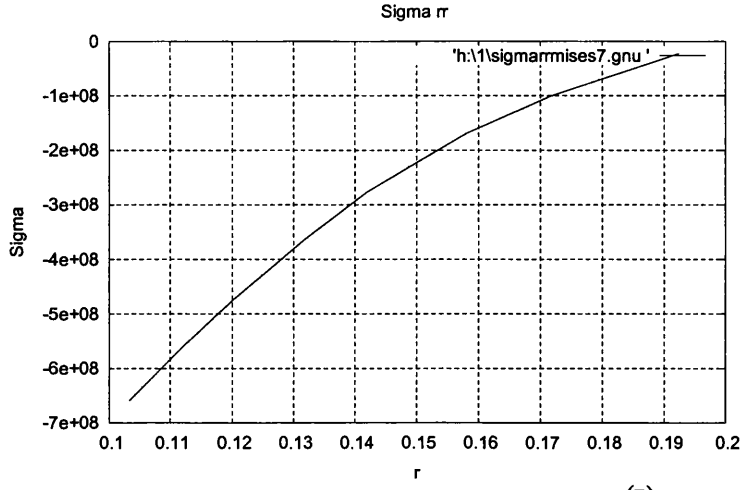

Figure 5.9. σ_{rr} for the von Mises material (5.13). $P(\bar{t}) = 700MPa$.

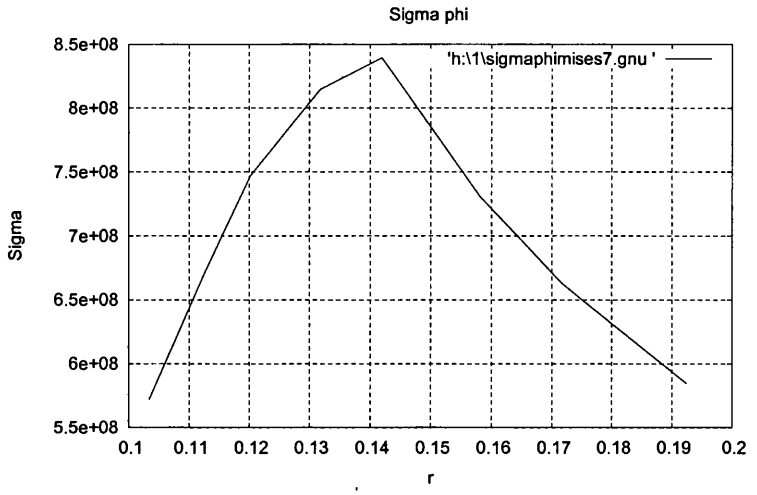

Figure 5.10. $\sigma_{\varphi\varphi}$ for the von Mises material (5.13). $P(\bar{t}) = 700MPa$.

It is evident now that the developed algorithm for the Hoffman material gives correct solutions both for plane strain and axisymmetric problem in case of a von Mises material.

5.4.2. Comparison for composite materials

Analogously to Section 5.4.2, finite element solutions of plane strain and axisymmetric problems for the anisotropic pipe has been compared. Both elastic and plastic anisotropy were taken into account.

The problem statements (5.1)-(5.9), (5.12) and (5.1), (5.3)-(5.8), (5.16)-(5.17) will remain the same for plane strain and axisymmetric cases respectively. However, material constants should be calculated according to expressions (3.7), (3.8).

Several tests were performed for different types of composite materials. The results obtained are presented below.

Comparison for elastically isotropic composites

Two tests for a pipe made of material having Young's modulus $E = 200GPa$ and Poisson ratio $\nu = 0.3$ were performed.

The first test was performed on a material whose plastic properties (5.18) are similar to the ones material 1 (Table 4.1) has. The yield surface is isotropic, but the material has different yield stresses for tension and compression:

$$\sigma_Y = 1000MPa\ ,$$

isotropic hardening occurs according to Table 5.1;

$$\begin{aligned} &\sigma_{11T_0} = \sigma_{22T_0} = \sigma_{33T_0} = 1000MPa\,, \\ &\sigma_{11C_0} = \sigma_{22C_0} = \sigma_{33C_0} = 1200MPa \\ &\sigma_{12S_0} = \sigma_{13S_0} = \sigma_{23S_0} = 500MPa\,. \end{aligned} \tag{5.18}$$

Internal pressure for the problem was equal to:

$$P(\bar{t}) = 700MPa\,. \tag{5.19}$$

There were 10 load increments, each being 10% of the total load (5.19). Nodal displacements along the pipe's radius are presented in Table 5.6 and on Figure 5.11.

It is easy to see from Table 5.6 that the nodal displacements along the pipe radius obtained by the developed algorithm for the Hoffman material model for plane strain and axisymmetric problems are identical. The same correspondence was proved for stresses and accumulated plastic strains.

Radius r, m	u_r for a plane strain problem, m	u_r for an axisymmetric problem, m
0.100000	0.768807E-03	0.768806E-03
0.116000	0.676013E-03	0.676012E-03
0.136000	0.599731E-03	0.599730E-03
0.164000	0.532593E-03	0.532593E-03
0.200000	0.481825E-03	0.481825E-03

Table 5.6. Nodal displacements along the pipe's radius for elastically isotropic material with isotropic plastic properties (5.18).

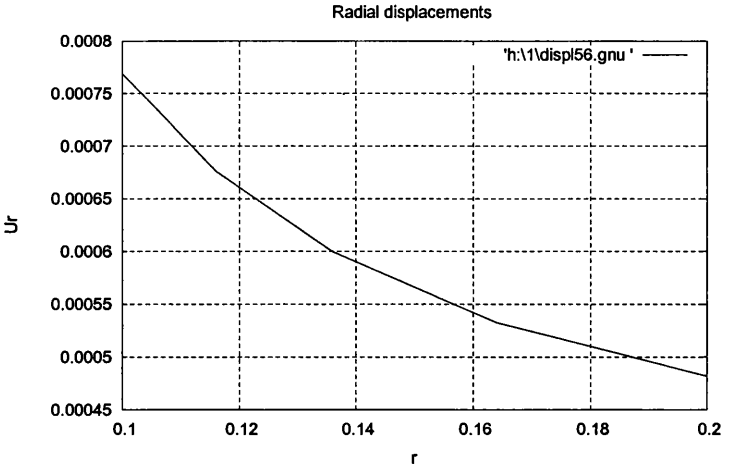

Figure 5.11. Nodal displacements along the pipe's radius for elastically isotropic material with isotropic plastic properties (5.18).

The second test was performed on a material whose yield surface is anisotropic and yield stresses for tension and compression are different (axes are defined according to Figures 5.1 and 5.4):

$$\sigma_Y = 1000MPa\ ,$$

isotropic hardening occurs according to Table 5.1;

$$\sigma_{xxT_0} = \sigma_{yyT_0} = 800MPa,\ \sigma_{xxC_0} = \sigma_{yyC_0} = 900MPa, \tag{5.20}$$

$$\sigma_{zzT_0} = 1000MPa,\ \sigma_{zzC_0} = 1200MPa,$$

$$\sigma_{12S_0} = \sigma_{13S_0} = \sigma_{23S_0} = 500MPa.$$

Internal pressure for the problem was equal to (5.19). There were 10 load increments, each being 10% of the total load (5.19). Nodal displacements along the pipe's radius are presented in Table 5.7 and Figure 5.12.

It is easy to see from Table 5.7 that the node displacements along the pipe radius obtained by the developed algorithm for the Hoffman material model for plane strain and axisymmetric problems are identical. The same correspondence was proved for stresses and accumulated plastic strains.

Radius r, m	u_r for a plane strain problem, m	u_r for an axisymmetric problem, m
0.100000	0.495480E-02	0.495485E-02
0.116000	0.436086E-02	0.436093E-02
0.136000	0.381578E-02	0.381589E-02
0.164000	0.328378E-02	0.328389E-02
0.200000	0.283764E-02	0.283775E-02

Table 5.7. Nodal displacements along the pipe's radius for elastically isotropic material with plastic properties (5.20).

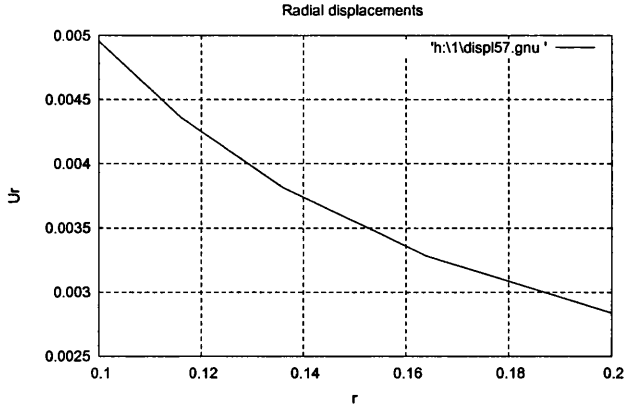

Figure 5.12. Nodal displacements along the pipe's radius for material with elastic properties (5.21) and plastic properties (5.20).

Comparison for elastically anisotropic composites

Two tests for a pipe where fibres are located along the Z axis (Figure 5.13) were performed. Elastic material properties of such a material are shown in set (5.21) with the ratio between elastic moduli $\frac{E_z}{E_x} = \frac{E_z}{E_y} = 2$. Axes used in set (5.21) were defined according to Figures 5.1 and 5.4. Different numbers of these axis and material properties used in the state update procedure for plane strain and axisymmetric problems are represented in Table 5.8.

For the plane strain case the domain shown in Figure 5.14. This domain differs from the one shown in Figure 5.2 as symmetry about the X axis has to be ensured to avoid rotation of axes while defining material properties for the anisotropic material. A very small angle EOH was used as well.

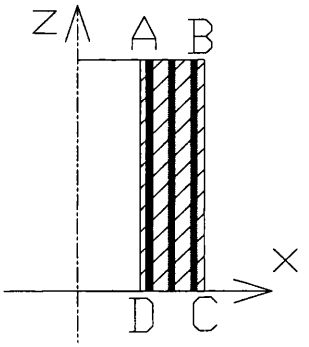

Figure 5.13. Fibres located along the Z axis.

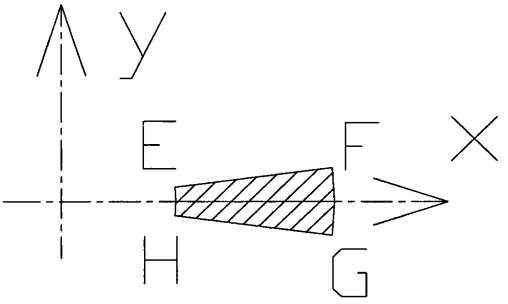

Figure 5.14. Domain for the plane strain case.

$$
\begin{aligned}
E_z &= 200GPa, \\
E_x &= E_y = 100GPa, \\
\nu_{xy} &= \nu_{yz} = \nu_{zx} = 0.3, \\
G_{xy} &= G_{xz} = G_{zy} = 15GPa;
\end{aligned}
\tag{5.21}
$$

Plastic properties in the first example are identical to von Mises with yield stress $\sigma_Y = 1000MPa$. Hardening is isotropic and occurs according to Table 5.1. Internal pressure for the example was equal to $P(\bar{t}) = 550MPa$. There were 10 load increments, each being 10% of the total load. Nodal displacements along the pipe's radius are presented in Table 5.9 and Figure 5.15.

Plane strain problem	Coordinate notation	Axisymmetric problem
1	Axis X	1
2	Axis Y	3
3	Axis Z	2
E_1	E_z	E_1
E_2	E_y	E_3
E_3	E_z	E_2
ν_{12}	ν_{xy}	ν_{13}
ν_{23}	ν_{yz}	ν_{32}
ν_{31}	ν_{zx}	ν_{21}

Table 5.8. Numbers of coordinate axes and material properties used for the plane strain and axisymmetric problems.

It is evident from Table 5.9 that the nodal displacements along the pipe radius obtained by the algorithm developed for the Hoffman material model for plane strain and axisymmetric problems are identical. The same correspondence was proved for stresses and accumulated plastic strains.

Radius r, m	u_r for a plane strain problem, m	u_r for an axisymmetric problem, m
0.100000	0.102765E-02	0.102764E-02
0.116000	0.894168E-03	0.894160E-03
0.136000	0.786130E-03	0.786123E-03
0.164000	0.688527E-03	0.688521E-03
0.200000	0.615788E-03	0.615783E-03

Table 5.9. Nodal displacements along the pipe's radius for elastically anisotropic material (5.21) with Von Mises yield surface.

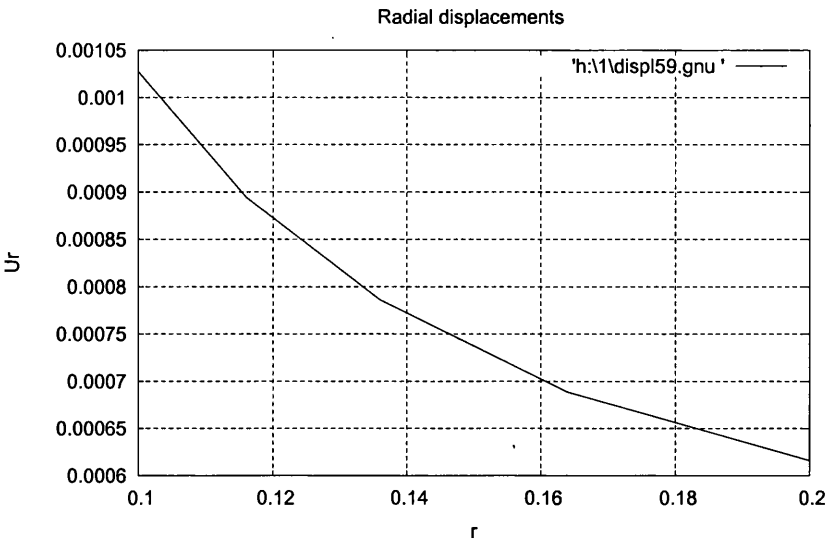

Figure 5.15. Nodal displacements along the pipe's radius for elastically anisotropic material (5.21) with Von Mises yield surface.

The second example will be performed for a fully anisotropic material having elastic properties (5.21) and plastic properties (5.20). Internal pressure for the example was equal to $P(\bar{t}) = 500MPa$. There were 10 load increments, each being 10% of the total load. Nodal displacements along the pipe's radius are presented in Table 5.10.

It is quite clear from Table 5.10 that the nodal displacements along the pipe radius obtained by the algorithm developed for the Hoffman material model for plane strain and axisymmetric problems are identical. The same correspondence was proved for stresses (Figures 5.5 and 5.6) and accumulated plastic strains.

Radius r, m	u_r for a plane strain problem, m	u_r for an axisymmetric problem, m
0.100000	0.101901E-02	0.101900E-02
0.116000	0.883682E-03	0.883675E-03
0.136000	0.774090E-03	0.774083E-03
0.164000	0.677979E-03	0.677974E-03
0.200000	0.606351E-03	0.606346E-03

Table 5.10. Nodal displacements along the pipe's radius for anisotropic material with elastic properties (5.21) and plastic properties (5.20).

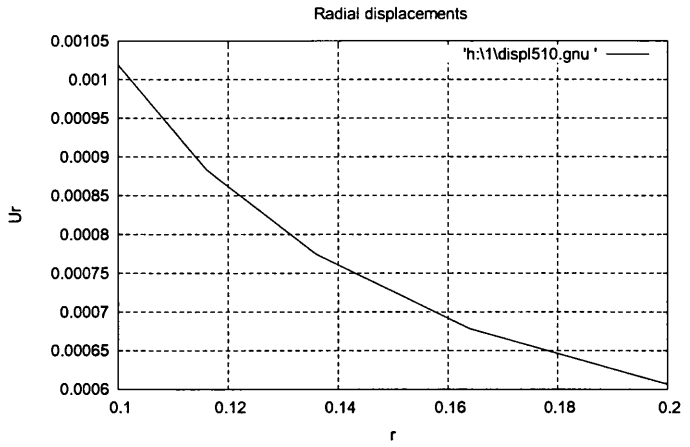

Figure 5.16. Nodal displacements along the pipe's radius for anisotropic material with elastic properties (5.21) and plastic properties (5.20).

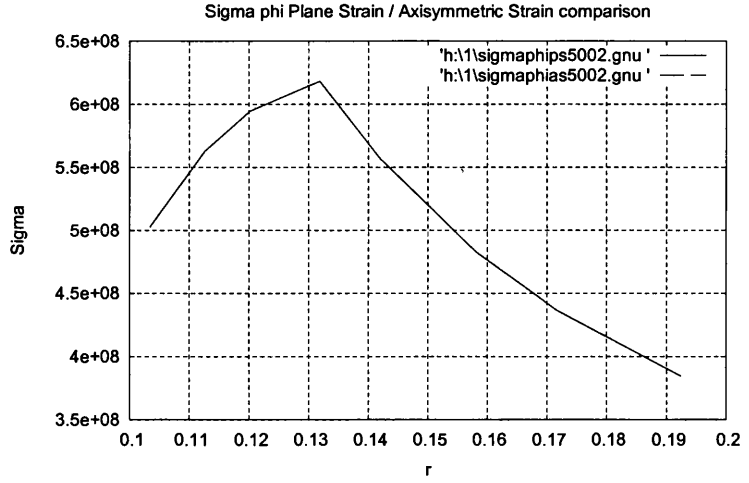

Figure 5.17. Comparison of $\sigma_{\varphi\varphi}$ for plane strain and axisymmetric problems with elastic properties (5.21) and plastic properties (5.20). Results for the plane strain problem are shown by a solid line.

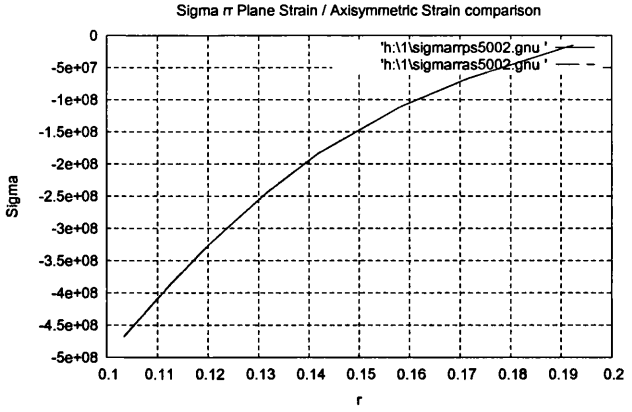

Figure 5.18. Comparison of σ_{rr} for plane strain and axisymmetric problems with elastic properties (5.21) and plastic properties (5.20). Results for the plane strain problem are shown by a solid line.

5.4.3. Concluding remarks

In Section 5.4 it was shown that finite element solutions obtained by the algorithm developed for the Hoffman material for plane strain and axisymmetric problems were identical in cases of isotropic/anisotropic elasticity and isotropic/anisotropic plasticity. For the von Mises material a comparison was also made with results given in a text book by Kachanov (1969).

Finally, one can make a conclusion that all 5 developed subroutines (Section 2.2.4) were correct and were able to work properly together with the main body of the HYPLAS program (de Souza Neto *et al.*, 2003) both for plane strain and axisymmetric cases for anisotropic material.

5.5. Further tests for different structure designs when the degree of elastic anisotropy is high

Despite correctness of all 5 developed subroutines was proved in Section 5.4, further tests have to be performed to check if the high degree of elastic anisotropy and the structure design influence the solution accuracy. These tests had to be performed since the fact that high degree of elastic anisotropy may cause significant error in iso-error maps (Section 4.1.7). On the other hand, there may be errors in the directions of smaller elastic rigidity.

Two tests for two pipes with different design have been performed. The first pipe is made of fabric material laid in the XY plane (Figure 5.19). Fibres of the second one are located along the Z axis (Figure 5.13). It is evident that the first pipe has a larger rigidity in the XY plane than the second one, whilst the first pipe has a smaller rigidity along the Z axis.

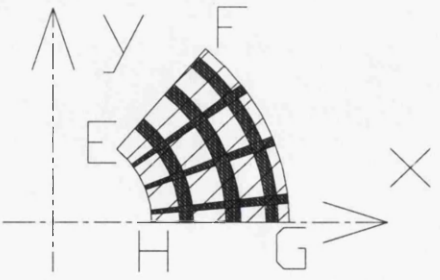

Figure 5.19. Fabric material laid in the XY plane.

In all examples plastic properties (5.20) were used, which are anisotropic with different tension and compression yield stresses.

5.5.1. Results for the pipe made of fabric laid in the XY plane

Two tests for two pipes with different ratios of elastic moduli: $\frac{E_z}{E_x}=\frac{E_z}{E_y}=\frac{1}{3}$ (elastic properties (5.22)) and $\frac{E_z}{E_x}=\frac{E_z}{E_y}=\frac{1}{5}$ (elastic properties (5.23)) were performed:

$$E_z = 66.6GPa,\ E_x = E_y = 200GPa,$$
$$\nu_{xy} = \nu_{yz} = \nu_{zx} = 0.3,\ G_{xy} = G_{xz} = G_{zy} = 15GPa; \tag{5.22}$$

$$E_z = 40GPa,\ E_x = E_y = 200GPa,$$
$$\nu_{xy} = \nu_{yz} = \nu_{zx} = 0.3,\ G_{xy} = G_{xz} = G_{zy} = 15GPa; \tag{5.23}$$

Internal pressure for both examples was equal to $P(\bar{t}) = 600MPa$. There were 10 load increments, each being 10% of the total load.

Nodal displacements along the pipe radius for the pipe having $\frac{E_z}{E_x}=\frac{E_z}{E_y}=\frac{1}{3}$ are presented in Table 5.11 and Figure 5.20. It is easy to see from this Table that the nodal displacements along the pipe radius obtained by the algorithm developed for the Hoffman material model for plane strain and axisymmetric problems are identical. As for the stresses, they are also identical (in Figures 5.21 and 5.22, results for the plane strain problem are shown by a solid line). Accumulated plastic strains are identical too.

Radius r, m	u_r for a plane strain problem, m	u_r for an axisymmetric problem, m
0.100000	0.835277E-03	0.835076E-03
0.116000	0.737530E-03	0.737437E-03
0.136000	0.656047E-03	0.656032E-03
0.164000	0.587539E-03	0.587545E-03
0.200000	0.536545E-03	0.536551E-03

Table 5.11. Nodal displacements along the pipe's radius for material with elastic properties (5.22) and plastic properties (5.20).

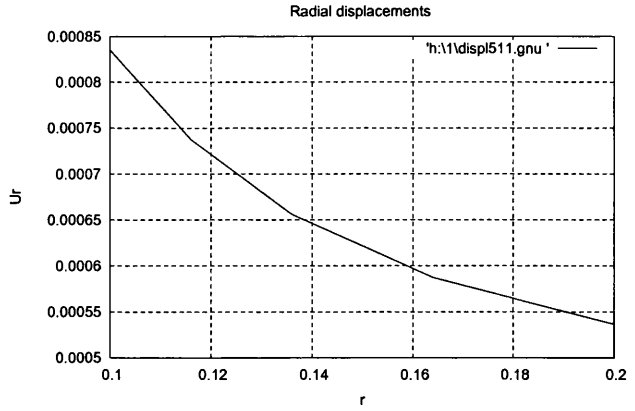

Figure 5.20. Nodal displacements along the pipe's radius for material with elastic properties (5.22) and plastic properties (5.20).

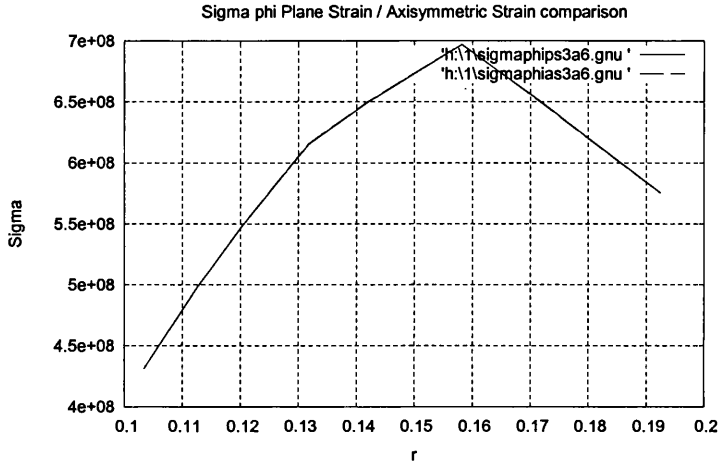

Figure 5.21. Comparison of $\sigma_{\varphi\varphi}$ for plane strain and axisymmetric problems with elastic properties (5.22) and plastic properties (5.20). Results for the plane strain problem are shown by a solid line.

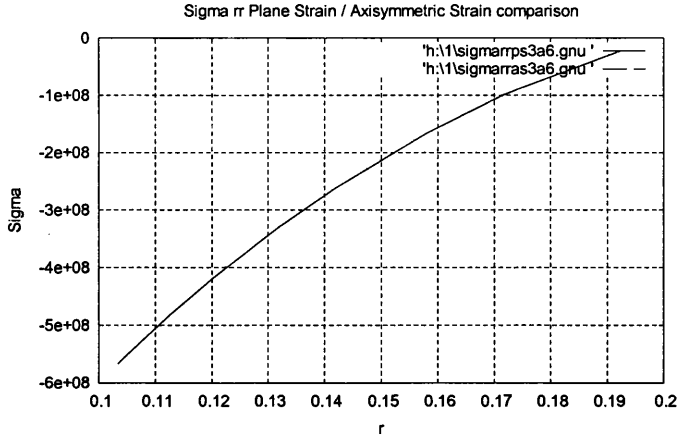

Figure 5.22. Comparison of σ_{rr} for plane strain and axisymmetric problems with elastic properties (5.22) and plastic properties (5.20). Results for the plane strain problem are shown by a solid line.

Nodal displacements along the pipe radius for the pipe with $\frac{E_z}{E_x}=\frac{E_z}{E_y}=\frac{1}{5}$ are presented in Table 5.12 and Figure 5.23. It is quite clear from this Table that the nodal displacements along the pipe radius obtained by the algorithm developed for the Hoffman material model for plane strain and axisymmetric problems are identical. As for the stresses, they are also identical (Figures 5.24 and 5.25, results for the plane strain problem are shown in a solid line). Accumulated plastic strains are identical too.

Radius r, m	u_r for a plane strain problem, m	u_r for an axisymmetric problem, m
0.100000	0.820963E-03	0.820778E-03
0.116000	0.732724E-03	0.732651E-03
0.136000	0.658979E-03	0.658976E-03
0.164000	0.595892E-03	0.595898E-03
0.200000	0.546612E-03	0.546619E-03

Table 5.12. Nodal displacements along the pipe's radius for material with elastic properties (5.23) and plastic properties (5.20).

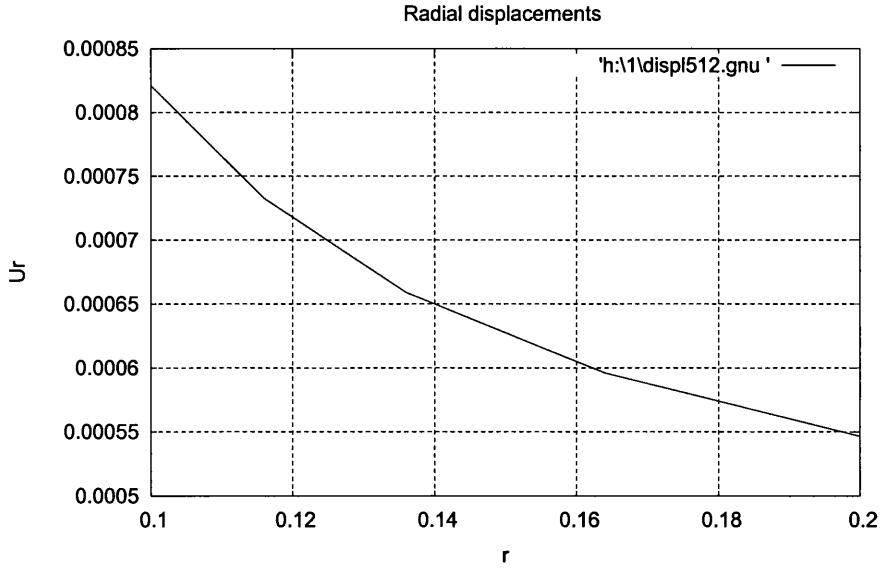

Figure 5.23. Nodal displacements along the pipe's radius for material with elastic properties (5.23) and plastic properties (5.20).

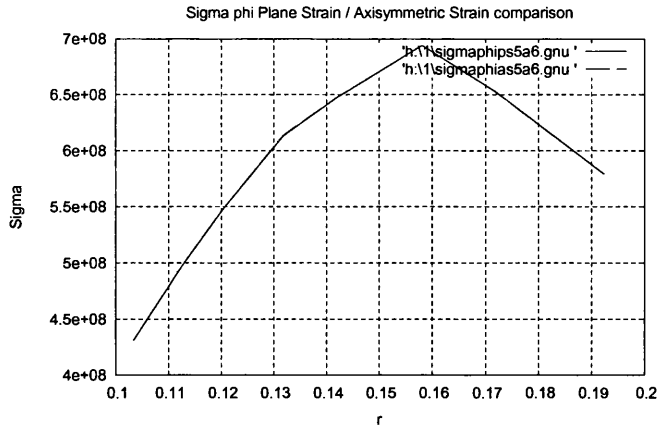

Figure 5.24. Comparison of $\sigma_{\varphi\varphi}$ for plane strain and axisymmetric problems with elastic properties (5.23) and plastic properties (5.20). Results for the plane strain problem are shown by a solid line.

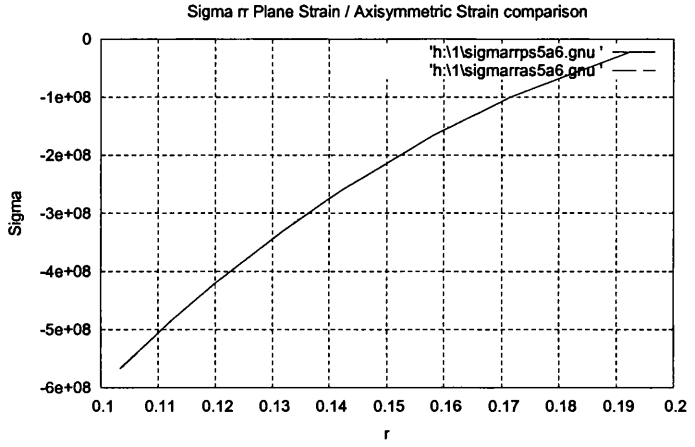

Figure 5.25. Comparison of σ_{rr} for plane strain and axisymmetric problems with elastic properties (5.23) and plastic properties (5.20). Results for the plane strain problem are shown by a solid line.

5.5.2. Results for the pipe with fibres located along the Z axis

Two tests for two pipes with different ratios of elastic moduli: $\frac{E_z}{E_x}=\frac{E_z}{E_y}=3$ (elastic properties (5.24)) and $\frac{E_z}{E_x}=\frac{E_z}{E_y}=5$ (elastic properties (5.25)) were performed:

$$E_z=200GPa,\ E_x=E_y=66.6GPa,$$
$$\nu_{xy}=\nu_{yz}=\nu_{zx}=0.3,\ G_{xy}=G_{xz}=G_{zy}=15GPa; \tag{5.24}$$

$$E_z = 200GPa,\ E_x = E_y = 40GPa,$$
$$\nu_{xy} = \nu_{yz} = \nu_{zx} = 0.3,\ G_{xy} = G_{xz} = G_{zy} = 15GPa; \tag{5.25}$$

Internal pressure for both examples is equal to $P(\bar{t}) = 500MPa$. There were 10 load increments, 10% of the mentioned total load each.

Nodal displacements along the pipe radius for the pipe with $\frac{E_z}{E_x} = \frac{E_z}{E_y} = 3$ are presented in Table 5.13 and Figure 5.26. It is quite clear from this Table that the nodal displacements along the pipe radius are identical. As for the stresses, they are also identical (Figures 5.27 and 5.28). Accumulated plastic strains are identical too.

Radius r, m	u_r for a plane strain problem, m	u_r for an axisymmetric problem, m
0.100000	0.144346E-02	0.144345E-02
0.116000	0.124189E-02	0.124189E-02
0.136000	0.107364E-02	0.107363E-02
0.164000	0.926391E-03	0.926387E-03
0.200000	0.817479E-03	0.817475E-03

Table 5.13. Nodal displacements along the pipe's radius for material with elastic properties (5.24) and plastic properties (5.20).

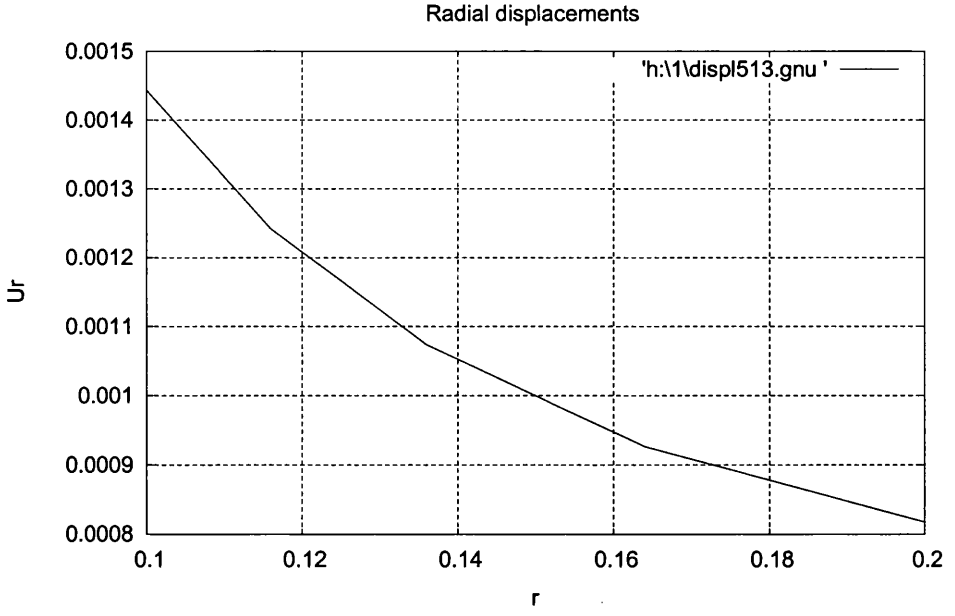

Figure 5.26. Nodal displacements along the pipe's radius for material with elastic properties (5.24) and plastic properties (5.20).

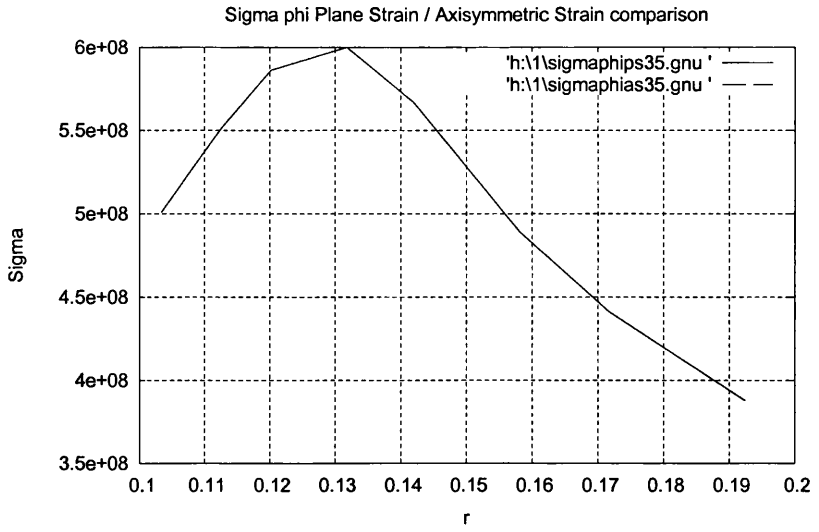

Figure 5.27. Comparison of $\sigma_{\varphi\varphi}$ for plane strain and axisymmetric problems with elastic properties (5.24) and plastic properties (5.20). Results for the plane strain problem are shown by a solid line.

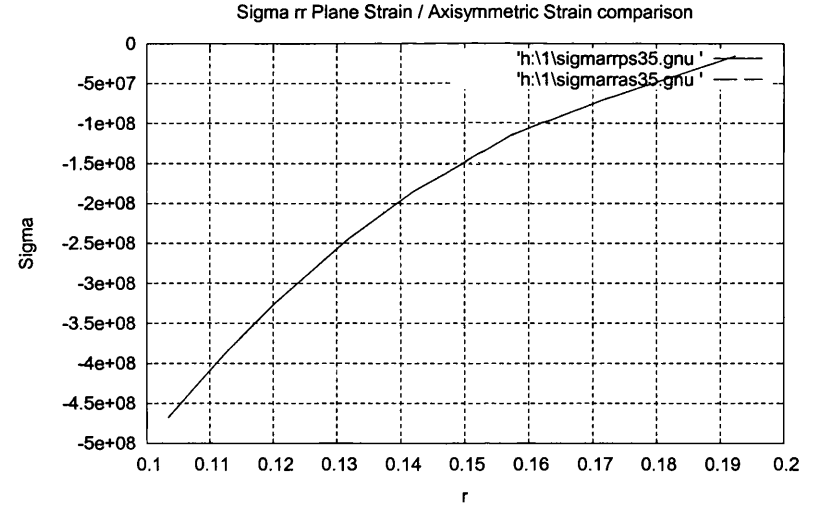

Figure 5.28. Comparison of σ_{rr} for plane strain and axisymmetric problems with elastic properties (5.24) and plastic properties (5.20). Results for the plane strain problem are shown by a solid line.

Nodal displacements along the pipe radius for the pipe with $\frac{E_z}{E_x}=\frac{E_z}{E_y}=5$ are presented in Table 5.14 and Figure 5.29. It is quite clear from this Table that the nodal displacements along the pipe radius are identical. As for the stresses, they are also identical (Figures 5.30 and 5.31). Accumulated plastic strains are identical too.

Radius r, m	u_r for a plane strain problem, m	u_r for an axisymmetric problem, m
0.100000	0.215039E-02	0.215039E-02
0.116000	0.182628E-02	0.182628E-02
0.136000	0.153989E-02	0.153989E-02
0.164000	0.127787E-02	0.127787E-02
0.200000	0.108502E-02	0.108502E-02

Table 5.14. Nodal displacements along the pipe's radius for material with elastic properties (5.25) and plastic properties (5.20).

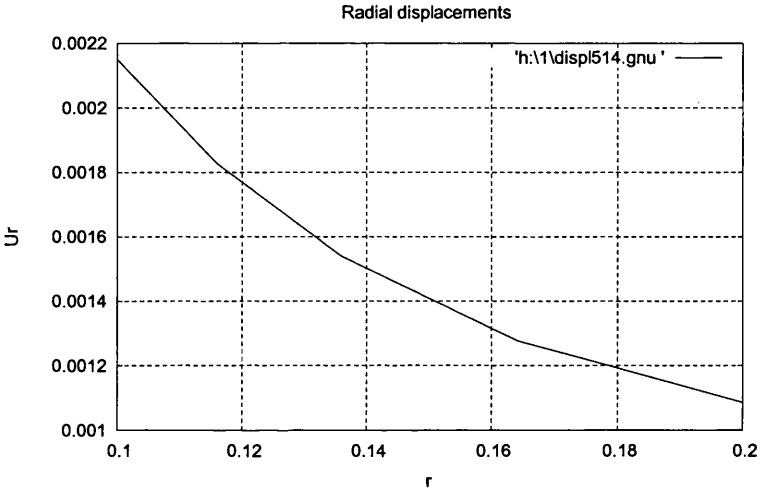

Figure 5.29. Nodal displacements along the pipe's radius for material with elastic properties (5.25) and plastic properties (5.20).

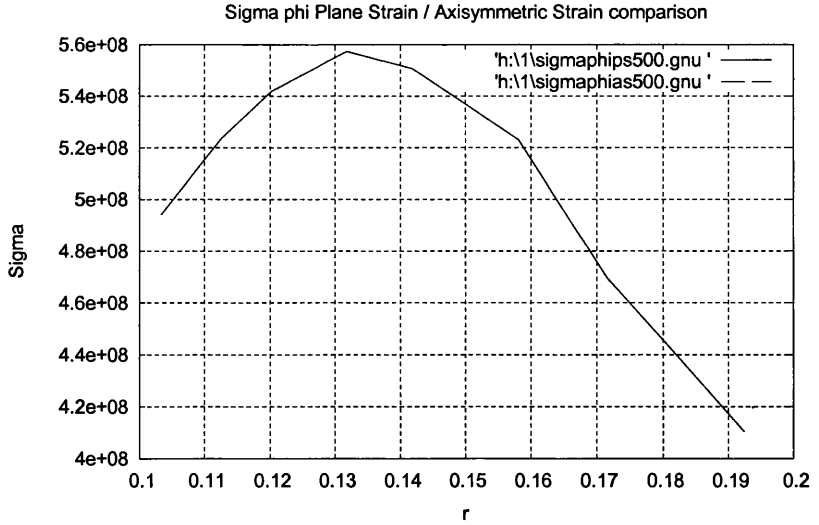

Figure 5.30. Comparison of $\sigma_{\varphi\varphi}$ for plane strain and axisymmetric problems with elastic properties (5.25) and plastic properties (5.20). Results for the plane strain problem are shown by a solid line.

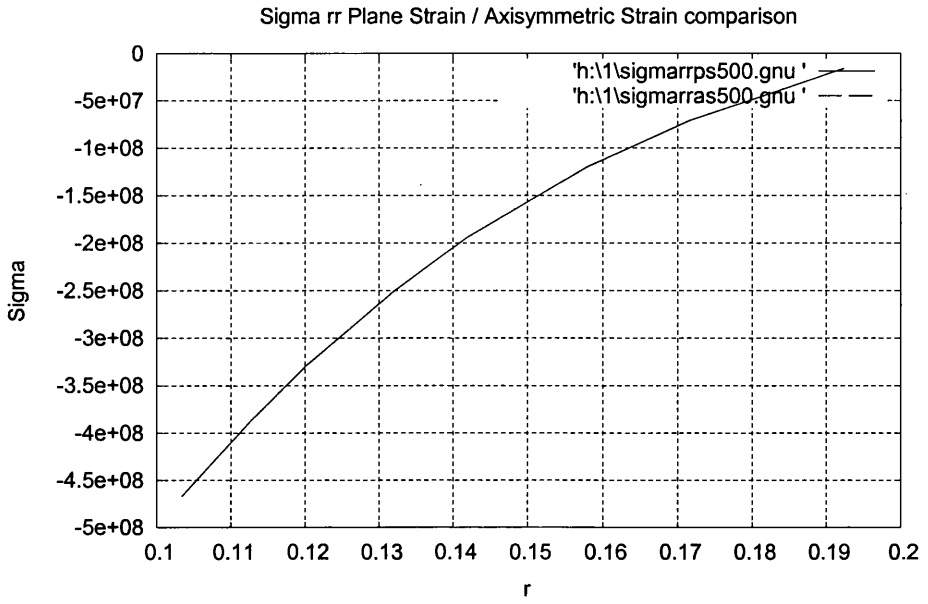

Figure 5.31. Comparison of σ_{rr} for plane strain and axisymmetric problems with elastic properties (5.25) and plastic properties (5.20). Results for the plane strain problem are shown by a solid line.

5.5.3. Concluding remarks

In Section 5.5 it was shown that finite element solutions obtained by the algorithm developed for the Hoffman material for plane strain and axisymmetric problems were identical for two pipes with fibres laid in the XY plane and along the Z axis respectively in case of high rates of elastic anisotropy.

5.6. Checking of solution's convergence

Since the integration algorithm is first order accurate it is quite easy to check its convergence. So, solutions of the same problem obtained with 10 and 1000 load steps respectively have to be compared. A problem solved in Section 5.5.2 for a pipe made of material with elastic properties (5.25) and plastic properties (5.20) was chosen.

Nodal displacements along the pipe radius are presented in Table 5.15.

A comparison between Tables 5.14 and 5.15 (i.e. solutions obtained with 10 and 1000 load steps) is presented in Figure 5.32. Comparison of stresses obtained with 10 and 1000 load steps are presented in Figures 5.33 and 5.34. The mentioned results are nearly identical which means that an accurate solution was obtained using 10 load steps.

Radius r, m	u_r for a plane strain problem, m	u_r for an axisymmetric problem, m
0.100000	0.214175E-02	0.214175E-02
0.116000	0.181991E-02	0.181991E-02
0.136000	0.153502E-02	0.153502E-02
0.164000	0.127390E-02	0.127390E-02
0.200000	0.108165E-02	0.108165E-02

Table 5.15. Nodal displacements along the pipe's radius for material with elastic properties (5.25) and plastic properties (5.20) calculated with 1000 load steps.

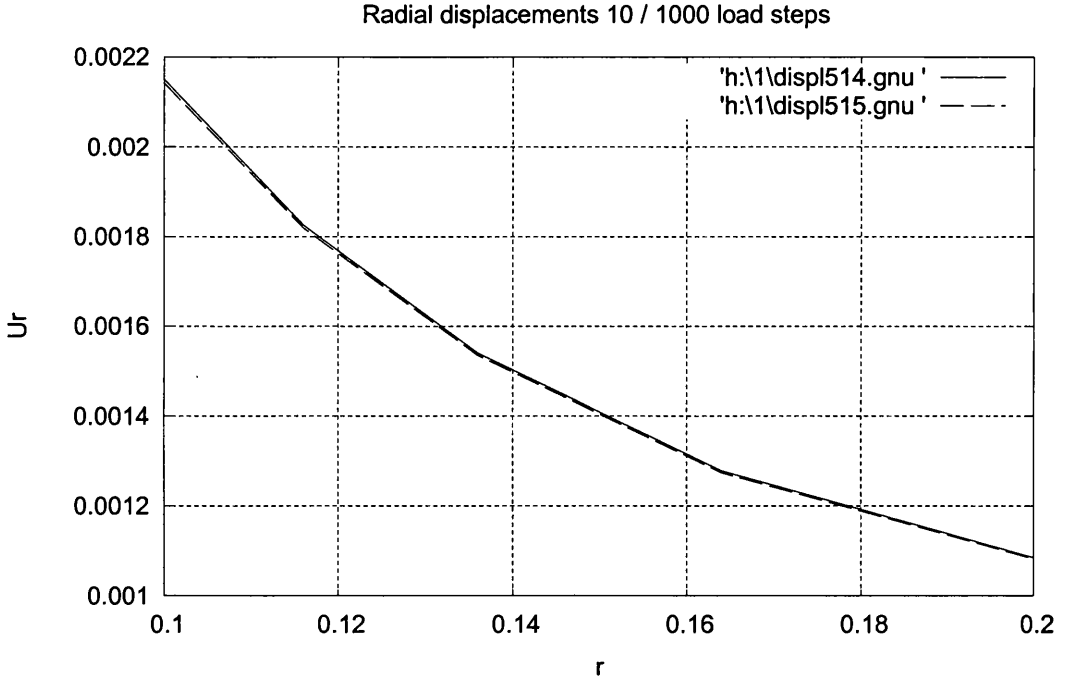

Figure 5.32. Comparison of nodal displacements along the pipe's radius obtained with 10 (solid line) and 1000 load steps for pipes made of material with elastic properties (5.25) and plastic properties (5.20).

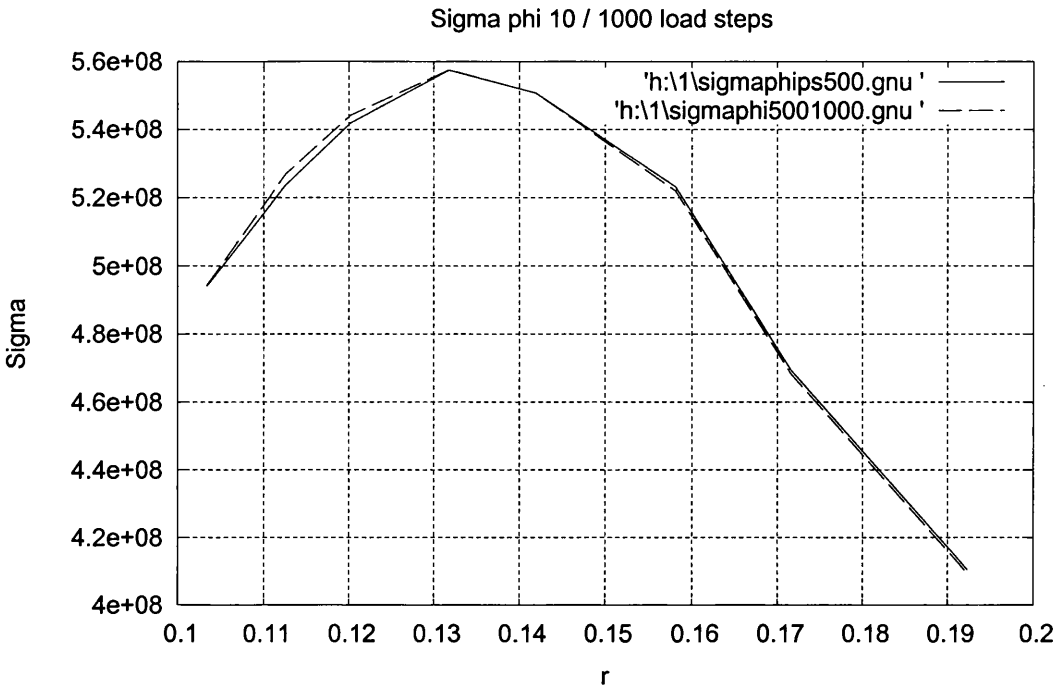

Figure 5.33. Comparison of $\sigma_{\varphi\varphi}$ obtained with 10 (solid line) and 1000 load steps for problems with elastic properties (5.25) and plastic properties (5.20).

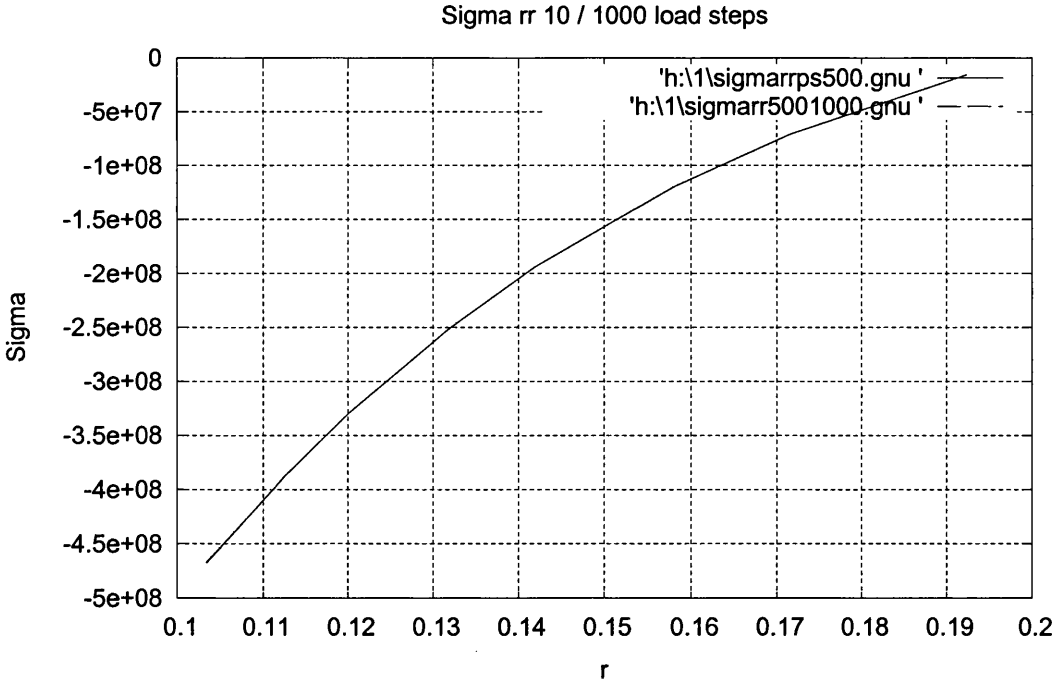

Figure 5.34. Comparison of σ_{rr} obtained with 10 (solid line) and 1000 load steps for problems with elastic properties (5.25) and plastic properties (5.20).

5.7. Checking the rate of the solution convergence

To ensure the quadratic rate of asymptotic convergence of an iterative solution scheme based upon Newton's method, the tangent operator consistent to the integration algorithm employed in the solution of the incremental problem has to be used.

So, showing that the tangent operator provides the quadratic rate of convergence is one more (apart from results presented in Section 4.2.3) proof of correctness of the CTHF routine.

Such convergence is demonstrated below for axisymmetric and plane strain problems for the pipe examined before. Results are provided for two following materials having isotropic hardening that occurs according to Table 5.1:

1. Anisotropically elastic material (5.24) with the Hill yield surface (5.26), $P(\bar{t}) = 500MPa$;
2. Anisotropically elastic material (5.24) with the Hoffman yield surface (5.20), $P(\bar{t}) = 500MPa$.

$$\begin{gathered} \sigma_Y = 1000MPa\ , \\ \sigma_{xxT_0} = \sigma_{yyT_0} = \sigma_{xxC_0} = \sigma_{yyC_0} = 800MPa\ , \\ \sigma_{zzT_0} = \sigma_{zzC_0} = 1000MPa\ , \\ \sigma_{12S_0} = \sigma_{13S_0} = \sigma_{23S_0} = 500MPa\ . \end{gathered} \tag{5.26}$$

The convergence rate was assessed via considering a relative residual norm in percent for equation (2.15) during the last load step that is equal to 10% of the total load. The results are presented below in Tables 5.16-5.17. It is quite clear from these Tables that the rate of convergence is quadratic which means that the tangent modulus is consistent to the integration algorithm, i.e. it was obtained correctly.

Iteration number	Relative residual norm, % plane strain problem	Relative residual norm, % axisymmetric problem
1	0.343621	1.49886
2	0.732665E-03	0.278609E-02
3	0.832604E-06	0.159354E-05
4	0.191147E-10	0.646178E-09

Table 5.16. Relative residual norm, for material with elastic properties (5.24) and plastic properties (5.26).

Iteration number	Relative residual norm, % plane strain problem	Relative residual norm, % axisymmetric problem
1	0.138319E-01	1.22917
2	0.152500E-02	0.708428E-01
3	0.388614E-04	0.118858E-03
4	0.993903E-08	0.539122E-06
5		0.284289E-09

Table 5.16. Relative residual norm, for material with elastic properties (5.24) and plastic properties (5.20).

Chapter 6. Conclusions

The aim of this work was to develop a finite element procedure for the numerical simulation for plastic flow of orthotropic composites governed by the Hoffman yield criterion. The criterion overcomes the restriction of the Hill criterion as it allows taking into account of different tensile and the compressive yield stresses.

All algorithms were implemented within the HYPLAS finite element code which is supplied with a text book by de Souza Neto *et al.,* (2003). This software is used for implicit small and large strain analysis of hyperelastic and elasto-plastic solids in plane stress, plane strain and axisymmetric states.

Hence, all numerical procedures were developed for plane strain and axisymmetric states. Strains were considered infinitesimal and thermal effects were ignored. This loading was assumed to be quasi-static. It was also assumed that no fracture or debonding occurred. The hardening behaviour was isotropic. Both elastic and plastic anisotropy were taken into account.

In order to implement these numerical algorithms within the HYPLAS structure the following subroutines for the Hoffman material were coded:

1. State update procedure which calculates new stresses, algorithmic and state variables at the end of the load increment for each Gauss point.
2. Tangent computation procedure which calculates the consistent tangent operator using converged values of stresses, algorithmic and state variables for each Gauss point.
3. Switching / initialisation subroutine which is used for the initialisation of variables as well as switching between current and converged values in material specific routines.
4. Data input procedure that reads all material model/algorithm-related data and stores them in the appropriate HYPLAS arrays.
5. Output subroutine that writes the results to a result file.

The strategy used for the numerical simulation of the Hoffman material model was based on implicit displacement finite element procedures. The full Newton-Raphson algorithm is used in HYPLAS to solve the nonlinear system of finite element equations during the global system iteration.

An operator split methodology and fully implicit backward Euler elastic predictor / plastic corrector algorithm were used to find an appropriate stress state at the Gauss point. During the plastic corrector phase of this algorithm the full Newton-Raphson method was used to solve the corresponding nonlinear equations. A line search algorithm based on dichotomy concept was developed to find an improved initial guess for the Newton-Raphson method in order to obtain a physically sensible solution for materials with high degree of elastic anisotropy. The tangent modulus consistent to the state update algorithm was obtained to ensure the quadratic rate of convergence of the global system iteration.

The objective of this work was successfully achieved. Validation of the algorithms developed was carried out separately for both state update and tangent computation procedures. Moreover, a number of model boundary value problems for different materials were solved. Solutions of certain plane strain and axisymmetric problems were compared and their results were in good agreement. The results obtained in this thesis were compared to results obtained by other authors where possible.

It was also shown that when the degree of anisotropy is very high the load steps should be very small as the state update procedure gives a less accurate solution in this case.

6.1. Suggestions for future research

There is still much scope for future work in this project.

One aspect is the extension of the technique to three-dimension problems. This will require extension of the developed algorithms.

The second possible extension is to consider an anisotropic hardening described in the article by Hashagen and de Borst (2001). As in this article there were no examples with anisotropic elasticity provided, it will be interesting to find out how the degree of elastic anisotropy influences the accuracy of the algorithm.

Bibliography

Abovskiy, N.P., Andreev, N.P., and Deruga, A.P. 1978. Variational principles and elasticity theory and shells theory. (in Russian). Moscow, Nauka.

Amosov, A.A., Dubinskiy, Yu.A., and Kopchionova, N.V. 1994. *Numerical methods for engineers.* (in Russian). Moscow, Vicshaya shkola.

Argyris, J.H., and Kelsey S. 1955. Energy theorems and structural analysis. *Aircraft Engng.,* **26** (part 1), **27** (part 2).

Bahvalov, N.S., Gidkov, N.P., and Kobelkov, G.M. 2000. *Numerical methods* (in Russian). Moscow, Laboratoriya bazovih znaniy.

Bathe, K.J. 1996. *Finite element procedures.* Upper Saddle River, New Jersey, Prentice Hall.

Belytschko, T., Liu, W.K., and Moran, B. 2001. *Nonlinear finite elements for continua and structures.* Chichester, John Wiley & Sons.

Bonet, J., and Wood, R.D. 1997. *Nonlinear continuum mechanics for finite element analysis.* Cambridge, Cambridge University Press.

Borisenko, A.I., and Tarapov, I.E. 1968. *Vector and tensor analysis with applications.* Revised English edition. Translated and edited by R.A. Silverman. Englewood Cliffs, N.J., Prentice-Hall.

Calcote, L.R. 1969. *The analysis of laminated composite structures.* New York, Van Nostard Reinhold Company.

Cheney, W., and Kincaid, D. 1980. *Numerical mathematics and computing.* Monterey, Brooks/Cole Publishimg Comp.

Clough, R.W. The finite element in plane stress analysis. *Proc. 2nd ASCE Conf. On. Electronic computation.* Pittsburgh, Pa., Sept. 1960.

Curiel Sosa, J.L. 2002. *Testing, finite element analysis and asymptotic expansion homogeneization of laminated glass reinforced plastic materials.* Thesis submitted to the University of Wales in candidature for the degree of Master of Research.

de Borst, R. 1987. Integration of plasticity equations for singular yield functions. *Computers & Structures,* **26**, pp. 823-829.

de Souza Neto, E.A. 1994. *Aspects of continuum modelling and numerical simulation of internal and surface damage in finitely deformed solids.* Thesis submitted to the University of Wales in candidature for the degree of Doctor of Philosophy.

de Souza Neto, E.A., Perić, D., and Owen, D.R.J. *Computational plasticity: small and large strain finite element analysis of elastic and inelastic solids.* 2003, in press.

Dimitrienko, Yu.I. 1997. *Mechanics of composite materials at high temperatures.* (in Russian). Moscow, Mashinostroenie.

Dimitrienko, Yu.I. 2001. *Tensor analysis.* (in Russian). Moscow, Vicshaya shkola.

Dutko, M., Perić, D., and Owen, D.R.J. 1993. Universal anisotropic yield criterion based on superquadratic functional representation. Part 1. Algorithmic issues and accuracy analysis. *Comp. Meth. Appl. Mech Engng.,* **109**, pp. 73-93.

Feodosief, V.I. 1972. *Strength of materials* (in Russian). Moscow, Nauka.

Gürdal, Z., Haftka. R.T., and Hajela, P. 1999. *Design and optimization of laminated composite materials.* New York, John Wiley & Sons.

Han, W., and Reddy, B.D. 1999. *Plasticity. Mathematical theory and numerical analysis*. New York, Springer.

Hashagen, F., and de Borst, R. 2001. Enhancement of the Hoffman yield criterion with an anisotropic hardening model. *Computers & Structures,* **79**, pp. 637-651.

Hearmon, R.F.S. 1961. *An introduction to applied anisotropic elasticity.* Oxford University Press.

Henwood, D., and Bonet, J. 1996. *Finite elements. A gentle introduction.* Basingstoke, Macmillan.

Hill, R. 1947. A theory of the yielding and plastic flow of anisotropic materials. *Proc. R. Soc.,* **A193**, pp. 281-297.

Hill, R. 1950. *The mathematical theory of plasticity.* London, Oxford Univ. Press.

Hinton, E., and Owen, D.R.J. 1977. *Finite element programming.* London, Academic Press.

Hinton, E., and Owen, D.R.J. 1985. *An introduction to finite element computation.* Swansea, Pineridge Press Ltd.

Hirsch, M.W., and Smale, S. 1974. *Differential equations, dynamical systems, and linear algebra.* New York, Academic Press.

Hoffman, O. 1967. The brittle strength of orthotropic materials. *J. Composite materials,* **1**, pp 200-206.

Hrenikof, A. 1941. Solutions of problems in elasticity by the framework method. *J. Appl. Mech.*, **A8**, pp 169-175.

Hou, J.P., Petrinic, N., and Ruiz C. 2001. A delamination criterion for laminated composites under low-velocity impact. *Composites Science and Technology,* **61**(14), pp 2069-2074.

Ilushin, A.A. 1971. *Continuum mechanics.* (in Russian). Moscow, Moscow State University Press.

Kachanov, L.M. 1969. *Fundamentals of the theory of plasticity.* (in Russian). Moscow, Nauka.

Kardestuncer, H., and Norrie, D.H. 1987. *Finite element handbook.* McGraw-Hill, New York.

Kaw, A.K. 1997. *Mechanics of Composite Materials.* Boca Raton, CRC Press.

Kelley, C.T. 1995. *Iterative methods for linear and nonlinear equations.* Philadelphia SIAM.

Kiselyov, V.A. 1976. *Plane problem of elasticity.* (in Russian). Moscow, Vicshaya shkola.

Koh, C.G., Owen, D.R.J., and Perić, D. 1995. Explicit dynamic analysis of elasto-plastic laminated composite shells: implementation of non-iterative stress update schemes for the Hoffman yield criterion. *Computational mechanics,* **16,** pp. 307-314.

Krieg, R.D., and Krieg, D.B. 1977. Accuracies of numerical solution methods for the elastic-perfectly plastic model. *J. Pressure Vessel Tech,* **Nov,** pp. 510-515.

Kuvirkin, G.N. 1995. *Basic correlations of continuum mechanics.* (in Russian). Ed. by Zarubin V.S. Moscow, Bauman Moscow State Technical University Press.

Lekhnitskii, S.G. 1963. *Theory of elasticity of an anisotropic plastic body.* San Francisco. Holden-Day, Inc.

Lourenco, P.B., de Borst, R, and Rots, J.G. 1997. A plane stress softening plasticity model for orthotropic materials. *Int. J. Num. Meth. Engng.,* **40,** pp. 4033-4057.

Malinin, N.N. 1968. *Applied theory of plasticity and creep.* (in Russian). Moscow, Mashinostroenie.

Maron, M.J. 1987. *Numerical analysis. A practical approach.* 2nd ed. New York, Macmillan Publ. Comp; London, Collier Macmillan Publ.

Massonnet, C, Olszak, W, and Phillips, A. 1979. *Plasticity in structural engineering. Fundamentals and applications.* Wien – New York, Springer.

Matthews, F.L., and Rawlings, R.D. 1994. *Composite materials: engineering and science.* London, Chapman & Hall.

McHenry, D. 1943. A lattice analogy for the solution of plane stress problems analysis. *J. Inst. Civ. Eng.*, **21**, pp 59-82.

Mikhlin, S. G. 1964. *Variational methods in mathematical physics* / translated from the Russian by T. Boddington; editorial introduction by translation editor L.I.G. Chambers, Pergamon.

Nanney, T.R. 1981. *Computing. A problem solving approach with FORTRAN 77.* Englewood Cliffs, New Jersey, Prentice-Hall Inc.

Newmark, N.M. 1949. Numerical methods of analysis in bars, plates and elastic bodies, in *Numerical methods in Analysis in Engineering* (ed. L.E. Grinter). Macmillan, 1949.

Noor, A.K. 1991. Bibliography of books and monographs on finite element technology. *Appl. Mech. Rev*, **44**(6), pp 307-317.

Norrie, D.H., and de Vries, G. 1973. *The finite element method: fundamentals and applications*. New York, Academic Press.

Owen, D.R.J., and Hinton, E. 1980. *Finite elements in plasticity: Theory and practice.* Swansea, Pineridge Press Ltd.

Owen, D.R.J., and Hinton, E. 1980. *A simple guide to finite elements.* Swansea, Pineridge Press Ltd.

Perry, W.L. 1988. *Elementary linear algebra.* New York, McGraw-Hill.

Prager, W. 1959. *An introduction to plasticity.* Reading, Mass., London, Addison-Wesley.

Press, W.H., Teukolsky, S.A., Vetterling, W.T., and Flannery, B.P. 1992. *Numerical recipes in FORTRAN. The art of scientific computing.* 2nd ed. Cambridge Univ. Press.

Rabotnov, Yu. N. 1988. *Mechanics of deformable solid body* (in Russian). Moscow, Nauka.

Reddy, J.N., and Miravete, A. 1995. *Practical analysis of composite laminates.* Boca Raton, CRC Press.

Schellekens, J.C.J., and de Borst, R. 1990. The use of the Hoffman yield criterion in finite element analysis of anisotropic composites. *Computers & Structures,* **37** (6), pp. 1087-1096.

Selivanov, V.V., Zarubin, V.S., and Ionov V.N. 1994. *Analytical methods of continuum mechanics.* (in Russian). Moscow, Bauman Moscow State Technical University Press.

Simo, J.C., and Hughes, T.J.R. 1987. General return mapping algorithms for rate-independent plasticity. *In* Desai C.S. *et al.* (ed), *Constitutive laws for engineering materials: Theory and applications*. Elsevier. pp. 221-231.

Simo, J.C., and Hughes, T.J.R. 1998. *Computational Inelasticity*. New York, Springer.

Simo, J.C., and Taylor, R.L. 1985. Consistent tangent operators for rate independent elastoplasticity. *Comp. Meth. Appl. Mech. Engng.*, **48**, pp. 101-118.

Strang, G. 1976. *Linear algebra and its applications*. New York, Academic press.

Tikhonov, A.N., and Samarskii A.A. 1964-67. *Partial differential equations of mathematical physics.* translated from Russian by S. Radding. San Francisco, Holden-Day.

Timoshenko, S.P., and Goodier, J.N. 1970. *Theory of elasticity*. New York, McGraw-Hill.

Turner, M.J., Clough, R.W., Martin H.C., and Topp L.J. 1956. Stiffness and deflection analysis of complex structures. *J. Aero. Sci.*, **23**, pp. 805-23.

Van'ko, V.I., Ermoshina, O.V., and Kuvirkin, G.N. 1999. *Variational calculus and optimal control.* (in Russian). Moscow, Bauman Moscow State Technical University Press.

Washizu, K. 1982. *Variational methods in elasticity and plasticity.* 3rd ed. Oxford, Pergamon Press.

Xikui, L., Duxbury, P.G., and Lyons, P. 1994. Considerations for the application and numerical implementation of strain hardening with the Hoffman yield criterion. *Computers & Structures,* **52** (4), pp. 633-634.

Zarubin, V.S. 1983. *Engineering methods for solving heat problems.* (in Russian). Moscow, Energoatomizdat.

Zarubin, V.S. 1985. *Applied problems of structures' elements' thermostrength.* (in Russian). Moscow, Mashinostroenie.

Zarubin, V.S., and Savichev V.V. 1990. *Methods for solving nonlinear thermoelasticity problems.* (in Russian). Moscow, Bauman Moscow State Technical University Press.

Zarubin, V.S., and Selivanov V.V. 1993. *Variational and numerical methods of continuum mechanics.* (in Russian). Moscow, Bauman Moscow State Technical University Press.

Zienkiewicz, O.C., and Cheung Y.K. The finite element method for analysis of elastic isotropic and orthotropic slabs. *Proc. Inst. Civ. Eng.,* **28**, pp 471-488.

Zienkiewicz, O.C., and Morgan, K. 1993. *Finite elements and approximation.* New York, John Wiley & Sons.

Zienkiewicz, O.C., and Taylor, R.L. 2000a. *The finite element method. Vol. 1. The basics.* 5th ed. Oxford, Butterworth Heinmann.

Zienkiewicz, O.C., and Taylor, R.L. 2000b. *The finite element method. Vol. 2. Solid mechanics.* 5th ed. Oxford, Butterworth Heinmann.